BEHAVIOR OF TWO-WAY SLABS REINFORCED WITH GFRP BARS

EHAB EL TOM

BEHAVIOR OF TWO-WAY SLABS REINFORCED WITH GFRP BARS

by

©Ehab El Tom, B.Sc. (Eng)

A thesis submitted to the
School of Graduate studies
in partial fulfillment of the
requirement for the degree of
Master of Engineering

Faculty of Engineering and Applied Science
Memorial University of Newfoundland

May 2007

St.John's Newfoundland Canada

Abstract

In this thesis, the performance of GFRP bars used as the main reinforcement for high strength concrete two-way slabs is investigated. A total of six interior slab-column connections, were cast and tested to failure at the structural laboratory of MUN. The dimensions of the simply supported tested slabs were 1900 ×1900 mm square and the thicknesses were 150 and 200 mm.

The reinforcement ratio and the clear concrete covers were the main variables in this investigation. A transverse central load was applied to the slabs through a central column stub. The structural behavior of the test specimens was investigated in terms of load-deflection, crack pattern and spacing, deflection profile, concrete and GFRP strains, failure mode and ultimate carrying capacity. Six slabs made of high strength concrete were constructed and reinforced with 16 mm GFRP bars. One slab was cast as a reference specimen using high strength concrete reinforced with traditional steel rebars.

The test results revealed that the slabs reinforced with GFRP bars exhibit higher deflection and wider crack width compared to similar slabs with conventional steel rebars. The load carrying capacity of the tested slabs was lower than the reference slab reinforced with steel rebars. However, slab performance can be improved by increasing slab depth.

The use of high strength concrete improved the slab ultimate load capacity and reduced the total deflection of the slab. High strength two-way slabs reinforced with GFRP show more ductility than the slabs reinforced with tradition steel; however, in terms of energy absorption, the slab reinforced with steel rebars shows higher values than the GFRP slabs.

The existing code limitations for serviceability limit state for crack width and spacing expressions were compared with the experimental results to verify their applicability in predicting crack width and spacing.

An existing numerical model and related expressions to calculate the crack width and spacing were adopted and modified to account for the low modulus of elasticity and weak bond properties associated with the use of GFRP rebars. The modified model and expression results were compared to the experimental recorded data. The modified crack model and expressions provide excellent agreement with the experimental results.

Finally, a finite element ABAQUS model was modified and adapted to predict the structural behaviour of high strength two-way slabs reinforced with GFRP. The finite elements model provides useful agreement with the experimental results in terms of ultimate load and maximum deformations.

Acknowledgements

The author would like to express his gratitude to his supervisor Dr. H. Marzouk, Professor of Civil Engineering, Memorial University of Newfoundland, for his financial support, keen supervision and guidance.

The author also would like to thank NSERC for supporting this research.

Sincere thanks are due to the technical staff of the structural engineering laboratory at Memorial University of Newfoundland, especially S. Organ, and M. Curtis. I also express my appreciation to M. Hossin, T. Sabrah, Y. Ebrahim, E. Rizk, and N. Dawood for their assistance during the laboratory work.

Finally, warm appreciation goes to my family and friends for their support.

Table of Contents

List of Tables

List of Figures

Chapter 1

1 Introduction

1.1 General

The use of fiber-reinforced polymer (FRP) materials as new construction materials to overcome the problem of corrosion has recently been accomplished. Several researches have been conducted to investigate the behavior of high strength concrete slabs reinforced using Glass Fiber-Reinforced Polymer rods (GFRP). In the meantime, the cracking of high strength concrete has been given considerable attention.

In spite of the use of high strength concrete reinforced with GFRP, there still exists insufficient information regarding the design philosophy for the identification of the behavior of high strength concrete reinforced with GFRP used in two-way slabs, such as cracking criteria and the punching shear. Most of the relevant codes extend the methodologies of the formulas of the normal strength concrete and apply them to the high performance concrete. This is expeeted to lead to uneconomical design and the failure criteria of such structures.

Due to high resistance to corrosion, non conductivity, high tensile strength, and light weight of the FRP, FRP rebars are the suitable alternative for traditional steel reinforcement. The cost of GFRP is relatively higher than conventional steel rebars; however, it can represents the best solution if corrosion is the primary concern.

1.2 Problem Definition

Generally, concrete structures were designed for strength and serviceability. The strength of a structure can be defined as the ability of the structure to resist the ultimate design load without collapsing. The serviceability is the ability of the structure to resist the working load conditions, in terms of deformation. The main concern at the serviceability limit state for designers and engineers will be deflection and cracks control.

GFRP rebars have different mechanical properties than traditional steel bars. The lower modulus of elasticity and bond properties are major drawbacks for the GFRP as a material that can be used in reinforced concrete structures.

The lower modulus of elasticity for GFRP as reinforcing material for concrete members will result in higher deflections compared to the ones reinforced with the conventional steel rebars. The lower bond properties will affect cracking behavior and crack width for structural members reinforced with GFRP.

It is vital to evaluate the behavior of concrete reinforced with GFRP at the serviceability limit state.

1.3 Scope and Objectives

The primary objective of this investigation is to study the behavior of high strength concrete (HSC) reinforced with glass fiber reinforced polymer (GFRP), the flexural cracking behavior of concrete slabs, deflection and ultimate load.

In this study, high strength two-way slabs reinforced with GFRP are tested up to the failure. The most important variable that would affect the flexural and the cracking behavior are considered and examined. The reinforcement ratio and the clear concrete cover are the main variables in this investigation. The performance of the high strength two-way slabs reinforced with GFRP in terms of ultimate load, crack pattern and width, type of failure, concrete strain, GFRP strain and the load-deflection relation are investigated with more attention to the cracking behavior.

The scope of this study is limited to one type of GFRP material, the glass fiber reinforced polymer (GFRP), commercially known as Aslan 100 Vinly Ester Matrix GFRP Rebars. Furthermore, only the interior slabs under central load are investigated.

1.4 Thesis Outline

Chapter 2 contains the literature review that is relevant to this investigation. In this chapter, some of the previous work concerning the cracking behavior of concrete, models and expressions developed to estimate the crack width are presented. FRP properties as a new construction material and previous work and code limitations for FRP use in concrete design are discussed.

Chapter 3 explains the experimental program in detail. Details of the setup, loading, specimen preparation, material used and concrete mix design, instrumentation and the data acquisition system are provided.

Chapter 4 contains the test results and observations obtained from the experimental program. Load-deflection relationship, crack width, cracks spacing, concrete strain, and GFRP strain are presented at the serviceability limit state and failure.

Chapter 5 contains the numerical verifications for the test results. An existing model to calculate the crack width and existing code expression to estimate the crack spacing are adopted and modified to account for GFRP's different performance. Also, a finite element model is adopted and modified to verify the ultimate capacity and the maximum deflection of the tested specimens.

Chapter 6 summarizes the findings from this investigation and presents recommendations for future research.

Chapter 2

2 Literature Review

2.1 Introduction

Recently, the use of Fiber Reinforced Plastics (FRP) composite material in construction has been growing to solve traditional civil engineering problems, such as corrosion of steel. The use of Glass Fiber Reinforced Plastics (GFRP), one of the most common types of FRP composite material, is not only limited to reinforcing concrete structures in a aggressive environment, but it can also be used in strengthening existing concrete and masonry structures. The non-corrosive, high strength, and light weight of the GFRP bars would be beneficial to concrete structures such as bridges, marine structures, and parking structures.

Cracks in reinforced concrete structures are expected to occur due to concrete's weakness in tension at low stresses. Since cracks would affect the stiffness of concrete structure members, contribute to reinforcement's corrosion, and the structure serviceability

purposes, the cracking behavior of concrete structure and crack controlling are vital in design.

Cracks can be induced by either external or internal forces. Concrete cracks when the tensile strength of concrete is exceeded. In order to control the crack width due to external loads, reinforcement can be placed on the tension side and by implementing code minimum requirements. However, in the case of high strength concrete (HSC) reinforced with fiberglass reinforced polymer (GFRP), very little information is available.

Due to movement restrictions, internal forces, temperature, shrinkage, and the settlement of supports, reinforced concrete structural members develop micro cracks; however, it is not the focus of this study.

2.2 Concrete Cracking Behavior

Concrete structural members that are subjected to loading develop different types of cracks, which are mainly due to direct tension, flexure, and shear. In this thesis, flexural crack behavior will be the main focus.

2.2.1 Flexural Cracking Mechanism

Two types of stresses act on the tension side of reinforced concrete slab members: longitudinal and lateral sets of stresses. As the longitudinal stresses act, the tensile zone undergoes a lateral contraction before cracking, resulting in lateral compression between the concrete and reinforcing bars.

When the concrete stresses reach the tensile strength, the tensile stress is just enough to form the first crack. To maintain the equilibrium of the section, as shown in Figure 2-1, the biaxial lateral compression has to disappear because the tension stress at the crack location is assumed to be zero.

All of the tension forces have to transfer from the concrete to the reinforcement, which will cause a jump in steel stress and slippage. This will affect the bond between the reinforcement and surrounding concrete and will bring the bond stresses to zero at the crack location.

This process will continue until no further cracks can be formed, and can be referred to as a stabilized crack section. The relationship between the crack spacing and the crack width can be demonstrated by the graph shown in Figure 2-2. This is a typical concrete member's behavior acting in one-way or beam action. However, according to Nawy's work in 1971, two-way slabs and plates would behave completely different than beams.

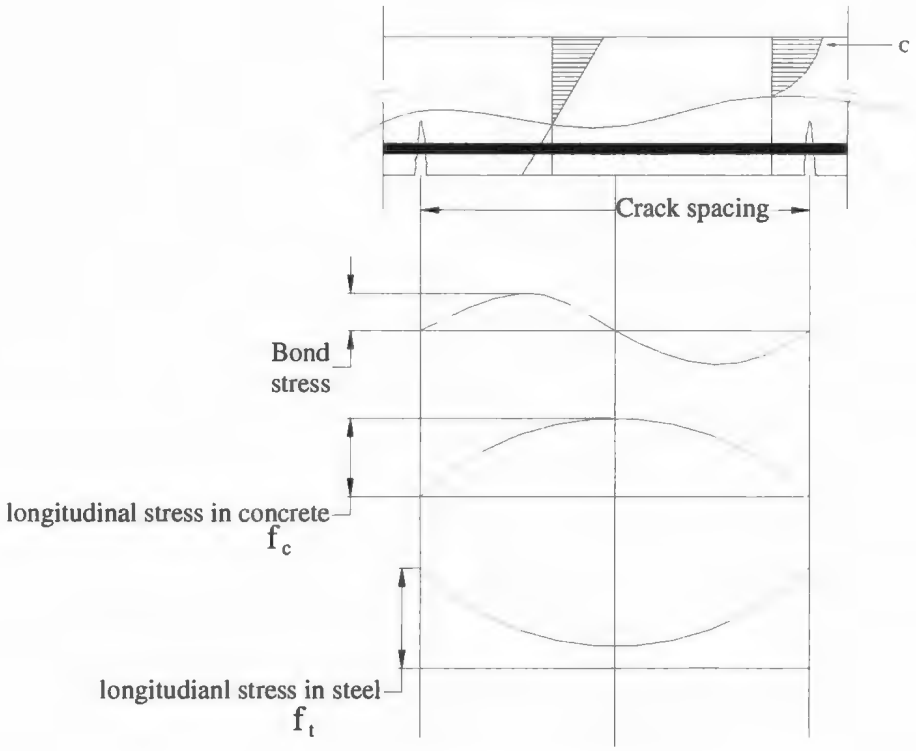

Figure 2-1 Crack section analysis

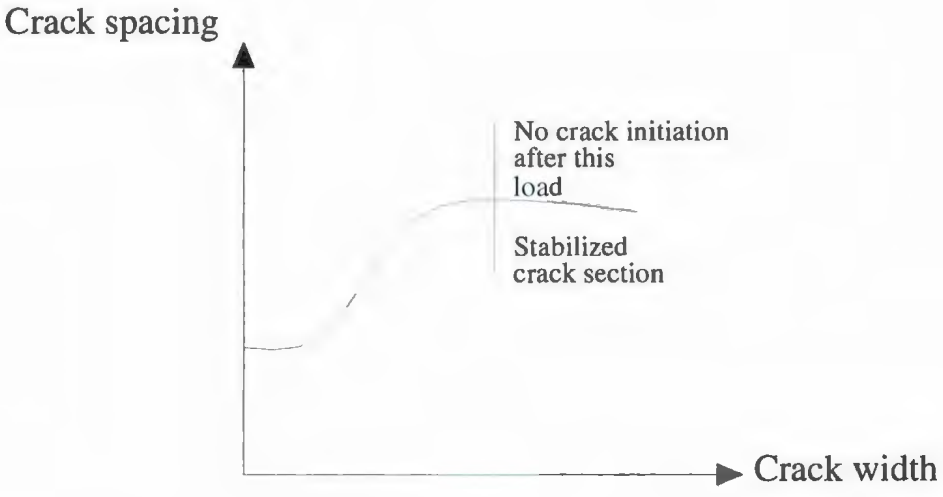

Figure 2-2 Crack width vs. Crack spacing relationship for Two- way slabs

Excessive cracking is the most common cause of damage in structures, and besides the fact that prediction of crack width is not possible; many studies have been conducted in order to develop expressions to determine the crack width and crack spacing, merely empirical or semi empirical in nature.

A different approach to estimate the cracking behavior problem is to develop a numerical model using concrete fracture mechanism. In this thesis, both approaches will be discussed.

2.3 Empirical Cracking Formulas

2.3.1 Gergely and Lutz (1968)

Gergely and Lutz derived the following equation to estimate maximum crack widths based on a statistical analysis of crack widths measured on the tension face of steel-reinforced concrete beams and one way slabs.

$$w_{max} = 11\times10^{-6}\frac{h_2}{h_1}z = 11\times10^{-6}\frac{h_2}{h_1}\sigma_{sr}\sqrt[3]{d_c A} \qquad (2.1)$$

where h_1 is the distance from the extreme tension surface to the neutral axis, h_2 is the distance from the tension reinforcement centroid to the neutral axis, σ_{sr} is the steel stress

at the crack, d is the concrete cover measured from the centroid of the tension reinforcement to the extreme tension surface, and A is the effective concrete area in tension surrounding the reinforcement having the same centroid as the reinforcement divided by the number of bars, as demonstrated in the Figure below:

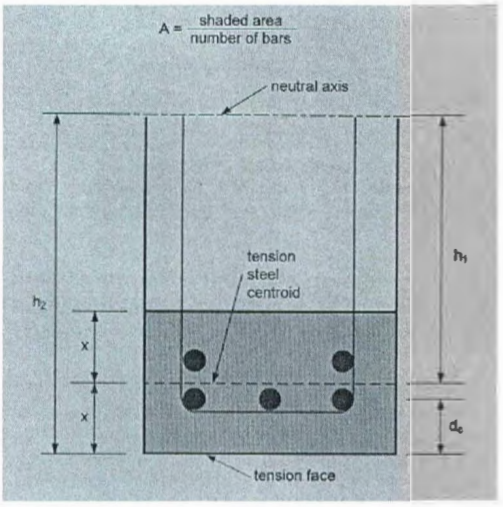

Figure 2-3: Crack width parameters

According to their extensive statistical evaluation, Gergely and Lutz conclude the following;

- The reinforcing steel stress is the most important variable
- The thickness of the concrete cover is an important variable
- The area of the concrete surrounding the reinforcing steel is also an important geometric variable.

In their study, Gergely and Lutz conclude that steel stress is the most important variable, though the expression does not include the bar diameter size affect, and the bond stresses between the reinforcement and the surrounding concrete. Due to lower bond characteristics for the GFRP, the bond stresses should be one of the variables that must be considered in such expressions.

2.3.2 Broms Method

Based on the experimental testing of 37 tension members and 10 flexural members, Broms concludes that the concrete cover is the most important factor in concrete cracking behavior. He developed the following equation for predicting crack width and spacing:

$$S_{ave} = 2t \tag{2.2}$$

$$W_{ave} = S_{ave} \times \varepsilon_s = 2t\varepsilon_s \tag{2.3}$$

where,

W_{ave} = average crack width at the reinforcement level, in.

t = concrete cover thickness, in.

S_{ave} = average crack spacing, in.

ε_s = steel strain

The relationship introduced by Broms for predicting crack width and spacing is valid only when the steel stress exceeds 138 to 207 MPa (20,000 to 30,000 psi), and when the concrete cover thickness ranges from 38.1 to 76.2 mm (1.5 to 3.0 in). To coincide with the test results, Broms has changed the expression from $W_{ave} = 1.5t$ to $W_{ave} = 2t$.

In order to obtain the crack width at the extreme concrete tension fibers, Broms assumed that the elongation at any particular level will be proportional to the distance from the neutral axis. Based on the "flexural theory", the plane cross sections will remain plane. Hence, if the depth to the reinforcement and the bottom of the concrete are h1 and h2 from the neutral axis, the average crack spacing at the concrete tension surface level is equal to:

$$W_{ave.conc} = 2t\varepsilon_s \times \frac{h_2}{h_1} \qquad (2.4)$$

The method that was presented by Broms has its own limitations. It is only valid at certain levels of steel stresses and particular ranges of concrete cover. Also, the expression does not include any other variables, such as bond stresses, which might affect cracking behavior.

2.3.3 Relation between Crack Spacing, Crack Width and Steel Stress

The cracking behavior of concrete members subjected to pure tension in the presence of transverse reinforcements has been studied; Rizkalla et al. (1982) tested 16 concrete specimens, which were divided into two groups with different concrete covers. In each group, all of the specimens were identical except for the transverse steel spacing. Also, as a part of this experimental program, 18 specimens were tested to investigate existing expressions presented by Beeby (1972) and (1979).

Leonhardt (1977) presented expressions for crack width and spacing, including all important variables that affect concrete cracking behavior, such as steel stress, bar diameter, concrete cover and thickness. Leonhardt assumed the minimum possible crack spacing can be found from:

$$S_L = 0.5L_o + L_t \qquad (2.5)$$

where,

L_o = the region of lost bond, calculated according to Equation (2.6)

$$L_o = \frac{f_{S2.cr} \times d}{45} \qquad (2.6)$$

where,

$f_{s2,cr}$ = the stress in the steel at the crack at the crack immediately after cracking

L_t = the transfer length, which represents the length of the active bond stresses

d = the reinforcement diameter

$$L_t = k_1(a,c) + 0.1\frac{d}{\rho} \tag{2.7}$$

k_1 = is a factor that depends on concrete cover c and longitudinal bar spacing a.

ρ = the percentage of reinforcement ratio

Then the crack width in a fully stabilized cracked section can be calculated as

$$W_{mL} = L_o\varepsilon_{s_2} + L_t\varepsilon_m \tag{2.8}$$

$$\varepsilon_m = \varepsilon_s\left[1 - \left(\frac{f_{S2,cr}}{f_{S2}}\right)^2\right] \tag{2.9}$$

where,

$f_{s2,cr}$ = the steel stress at the crack immediately after cracking

f_{s2} = the steel stress at the crack.

ε_{s_2} = the steel strain at the cracked section

ε_m = the average gross strain measured over the cracks including the concrete contribution within the transfer length calculated according to Equation (2.9)

In the same manner, Beeby (1972) and (1979) suggests the following expressions

$$S_b = 1.33c + 0.08\frac{d}{\rho} \qquad (2.10)$$

$$W_{mb} = S_b \times \varepsilon_m \qquad (2.11)$$

where,

W_{mb} = the average crack width, and

S_b = the average crack spacing as per Equation (2.10)

ε_m = the average strain measured over the cracks including the concrete contribution within the transfer length, calculated according to Equation (2.12) below:

$$\varepsilon_m = \varepsilon_s - \frac{kf_t' f_{s2,cr}}{E_s \rho f_{s2}} \qquad (2.12)$$

where,

k = a constant that depends on the type of reinforcement

f_t' = the concrete tensile strength

E_s = the modulus of elasticity of steel.

Rizkalla, in his study, concludes that Beeby's expression shows an underestimation when compared to the measured values. On the other hand, Leonhardt was showing an overestimation; hence, the investigator introduced a refined expression based on the experiment results.

$$L_{om} = 10(d - 7.5) \qquad (2.13)$$

where,

L_{om} = the modified almost no bond length equivalent to L_o defined in Equation (2.6)

d = the reinforcement diameter in mm.

And the average crack spacing in a fully developed cracked section is

$$S_m = 0.5L_{om} + S_b \qquad (2.14)$$

where,

S_b = is the same expression that was introduced by Beeby

$$S_m = 5(d - 7.5) + 1.33c + 0.08\frac{d}{\rho} \qquad (2.15)$$

And in the presence of transverse steel

$$S_c = \beta S_m \qquad (2.16)$$

$$\beta = \frac{0.96}{R^{0.02}} \qquad (2.17)$$

$$R = \frac{S_r}{S_m}$$

where,

R = a dimensionless parameter representing the ratio of the transverse reinforcement spacing to the average crack spacing

S_r = the spacing of the transverse reinforcement

Rizkalla proposes the following equations to relate both the minimum and maximum crack width to the average crack width:

$$W_{min} = 0.67 W_{ave} \qquad (2.18)$$

$$W_{max} = 1.55 W_{ave} \qquad (2.19)$$

Rizkalla's investigations lead to the conclusion that crack spacing is influenced by the presence of the transverse reinforcement, which is the same as previous studies by Beeby (1972 and 1979), Nawy and Blair (1971), and McGregor et al. (1980).

2.3.4 Cracking Formula for Glass Reinforcing Rods (GFRP)

In a very extensive experimental program carried out by Nawy in 1977 to study the behavior of normal strength concrete reinforced with glass reinforcing rod, twelve square slabs fully restrained in all four boundaries were tested to failure; in addition, fourteen simply supported beams were investigated and tested to failure. At that time, little information was available about fiberglass reinforcement and its feasibility as main reinforcement.

The test results indicate that the behavior of fiberglass reinforced slabs and beams regarding to cracking, ultimate load, and deflection could be predicted with the same accuracy used in current structural practice for concrete reinforced with steel.

A mathematical model was proposed by Nawy for predicting the crack pattern in steel reinforced concrete two-way slabs and plates. The model defines the crack width, w, in terms of the crack spacing, a_c and the reinforcement strain ε_s, giving

$$w = \alpha' a_c^{\beta'} \varepsilon_s^{\gamma'} \qquad (2.20)$$

The above general expression for crack width can be redefined in the same manner as a function of the geometric properties of the slab or plate, the strain in the reinforcement and the grid index I

$$w = \alpha_s R(I)^{\beta'} \varepsilon_s^{\gamma'} \qquad (2.21)$$

where,

R = cover ratio= distance from the neutral axis to tensile face / distance from the neutral axis to the center of gravity of the reinforcement 1

ε_s =unit strain in the reinforcement at the various level; and α, β, γ = constants to be evaluated from test results.

The grid index is calculated according the following expression:

$$I = \frac{d_{b1} s_2}{\rho_{t1}} = \frac{s_1 s_2}{d_{b1}} \frac{8}{\pi} \qquad (2.21)$$

where,

ρ_{t1} = active steel ratio

s_1, s_2 = spacing of reinforcement in direction 1 and 2 respectively.

The same approach and expression developed by Nawy to calculate the crack width reinforced with traditional steel, were used in fiberglass reinforced concrete slabs specimens; a statistical regression analysis was performed in order to obtain the constants. Hence, the maximum crack width can be expressed as

$$w = 2.8 \times 10^{-4} R \sqrt{I} f_f \qquad (2.22)$$

in which f_f = the stress level, in the fiberglass reinforcement.

From test observation, Nawy reported that the cracking in two-way slabs consisted of orthogonal cracking which followed the reinforcement spacing in both directions.

For concrete beams reinforced with fiberglass, Nawy readjusted the ACI 381-71 developed from Gergely and Lutz's work, considering the difference in the young's modulus of the two materials; in the case of the fiberglass reinforcement, the crack width is

$$w = 0.002 f_f \sqrt[3]{d_c A} \qquad (2.23)$$

2.4 Semi-empirical Expressions

Some investigators adopted different approaches aimed at solving the cracking problem by introducing physical models. Some of the previous work will be presented in this thesis.

2.4.1 Robert J. Frosch (1999)

Frosch (1999) presented the following model, giving an expression to calculate crack width at both the steel and concrete level,

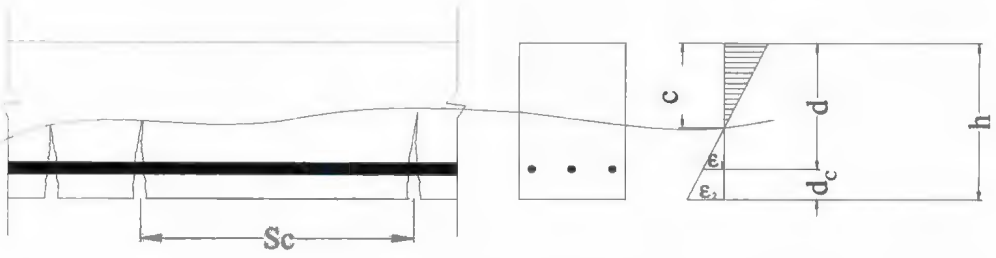

Figure 2-4: Cracked section, Strain gradient

$$W_c = \varepsilon_s S_c \qquad (2.24)$$

where,

W_c = crack width

ε_s = reinforcement strain

fs = reinforcing steel stress

Es = reinforcing steel young's modulus

S_c = the crack spacing

The above expression calculates crack width at the steel level. In order to obtain the crack width at bottom of the concrete, the strain gradient factor β was introduced.

$$\beta = \frac{\varepsilon_1}{\varepsilon_2} = \frac{h-c}{d-c}$$

The crack spacing S_c in equation (2.24) should be calculated from the following expression:

$$S_c = \psi \times d^* \qquad (2.25)$$

where,

d^* = is the controlling cover distance

ψ = is the crack spacing factor (= 1.0 for minimum, 1.5 for average, and 2.0 for maximum crack spacing).

d^* = is calculated as illustrated in the Figure 2-4 below according to the expression;

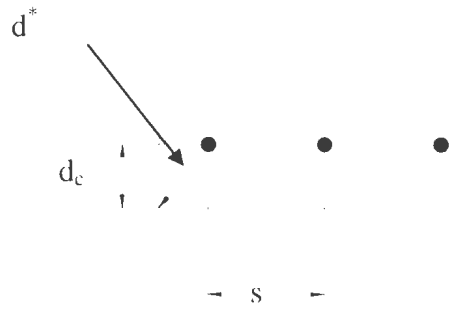

Figure 2-5: Controlling cover distance calculation

$$d^* = \sqrt{d_c^2 + \left(\frac{s}{2}\right)^2} \qquad (2.26)$$

In his expression, Frosch relates crack width to reinforcement spacing; thus, crack controlling can be achieved by limiting reinforcement spacing in concrete members, and he suggests the following design recommendations which have been adopted by the ACI code (1999).

$$S = 12\alpha_s\left[2 - \frac{d_c}{3\alpha_s}\right] \leq 12\alpha_s \qquad (2.27)$$

$$\alpha_s = \left(\frac{36}{f_s}\right)\gamma \qquad (2.28)$$

where,

γ = the reinforcing coating factor = 1.0 for uncoated bars, 0.5 for epoxy coated bars.

2.4.2 R.I. Gilbert (2004)

In his study, Gilbert adopts the tension chord model of Marti et al. (1998) to develop an expression for crack width and spacing for both instantaneous and sustained service loads. For flexure members, the concrete and steel stresses can be expressed as follows:

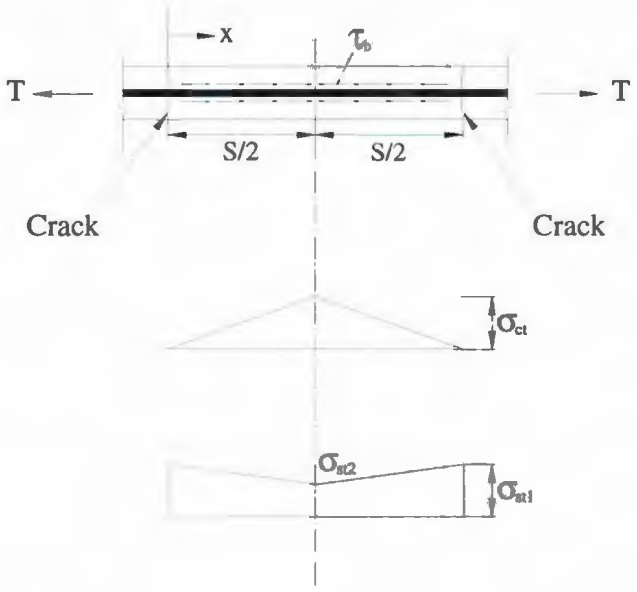

Figure 2-6: Cracked section, concrete and steel stresses after cracking

$$\sigma_{st} = \frac{T}{As} - \frac{4t_b x}{\phi} \tag{2.29}$$

$$\sigma_{cx} = \frac{4t_b \rho x}{\phi} \tag{2.30}$$

where,

t_{bx} = Bond stress

$\rho = \frac{A_{st}}{A_{ct}}$

ϕ = Bar diameter

when,

$x = \frac{s}{2}$

$$\sigma_{st} = \frac{T}{A_s} - \frac{2t_b s}{\phi} \tag{2.31}$$

$$\sigma_{cx} = \frac{2t_b \rho s}{\phi} \tag{2.32}$$

The maximum crack spacing is equal to

$$S_{max} = \frac{f_{ct}\phi}{2t_b \rho} \tag{2.33}$$

when,

$\sigma_{cx} = f_{ct}$

Gilbert defines crack width as the difference between the elongation of the steel and the elongation of the concrete between the cracks.

$$w = \frac{s}{E_s}\left[\frac{T}{A_s} - \frac{t_b s}{\phi}(1+n\rho)\right] \qquad (2.34)$$

The researcher includes in his expression the factors necessary to predict crack width, including those which affect the cracks in a reinforced concrete member, such as steel stresses, bond stresses, bar diameter and reinforcement ratio, which are agreed upon by most of investigators. Bond stresses would be one of the important variables in the case of using GFRP as main reinforcement.

2.4.3 The Tension Chord Model

This model is set up in terms of a simple yet complete formulation of the deformation process undergone by a reinforced concrete member by integrating the actual steel and concrete strains between cracks. Earlier formulations of the procedure were presented by Leonhardt (1977). Concepts from these procedures constitute the basis of the crack width calculation design rules for reinforced concrete members in CEB/FIP MC 90. The model has lately been the subject of considerable refinement and simplification by Sigrist and Marti (1994), Alvarez (1998), and Marti et al. (1998), who developed the "Tension Chord Model" name.

One major feature of the tension chord model is the bond-slip constitutive relationship for steel. Acknowledging that the exact distribution of stresses in concrete and steel is not of primary interest as long as the resulting steel stresses and overall member strains reflect governing influences and match experimental data, Marti et al. (1998) used a rigid perfectly plastic bond-slip relationship with a stepped descending branch that depends on the yielding of steel.

Since the amount of slip in steel-reinforced concrete members is not significant at service load levels, CEB/FIP MC90 proposes a rigid-perfectly plastic bond-slip relationship for the serviceability design of steel-reinforced concrete members:

$$\tau_b = 1.8 f_{ctm} \tag{2.35}$$

where,

f_{ctm} = is defined as the mean tensile strength of concrete.

The model assumes that if the concrete stresses between cracks under maximum crack spacing conditions reach f_{ct}, a new crack will form midway between those spaced at s_{max}. As a result, the mean crack spacing in the stabilized crack formation stage is bounded by the following limits:

$$(s_{min} = \frac{s_{max}}{2}) \leq s_m \leq s_{max}$$

or

$$0.5 \leq \lambda = \frac{s_m}{s_{max}} \leq 1.0$$

where λ is defined as a parameter introduced by Marti et al. (1998)

The mean crack spacing is

$$s_m = \lambda s_{max} = \frac{\lambda f_{ct} \phi_b}{2\tau_{b0}} \left[\frac{1-\rho_s}{\rho_s} \right], 0.5 \leq \lambda \leq 1.0 \qquad (2.36)$$

The tension chord model overcomes this problem by assuming that the mean crack width in the stabilized cracking stage can be calculated as

$$w_m = s_m(\varepsilon_{sm} - \varepsilon_{cm}) \qquad (2.37)$$

where s_m is the mean crack spacing, ε_{sm} is the mean steel strain, both at the given load level, and ε_{cm} is the mean concrete strain at the end of the single crack formation phase.

Based on the concrete stress distributions the mean concrete strain is

$$\varepsilon_{cm} = \frac{\lambda}{2} \frac{f_{ct}}{E_c} \qquad (2.38)$$

That leads to

$$w_m = s_m\left[\varepsilon_{sr} - \frac{\lambda}{2}\frac{f_{ct}}{E_s}\frac{(1+\rho_s(n-1))}{\rho_s}\right] \tag{2.39}$$

The above equation evaluates the crack width at the reinforcement level. However, for slab sections, the cracks that matter are those at the tension face. These crack widths can be obtained by multiplying the same equation by $\left[\frac{h-x_d}{d-x_d}\right]$ (as recommended by Broms, 1965), where x_d is the neutral axis depth, as shown in Figure 2-7.

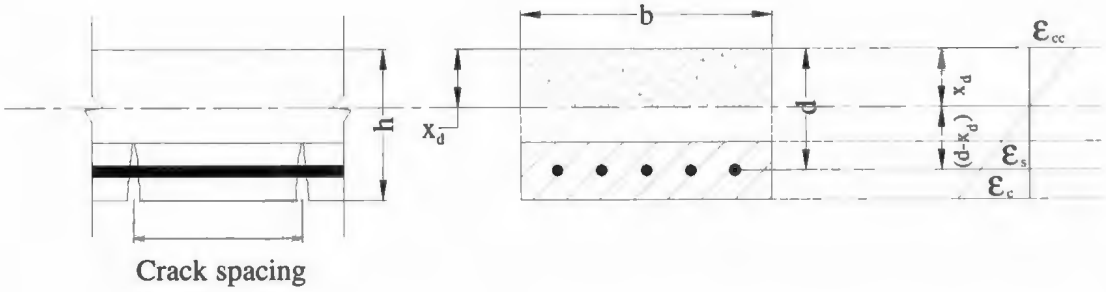

Figure 2-7: Concrete cracked section

2.5 Concrete Fracture Mechanics Approach

Investigators and scientists use this approach mainly in developing expressions for crack width and spacing for reinforced and plain concrete members subjected to tension cracks. This approach is mainly used for tensile cracking, in general the cracks that are formed on reinforced or plain concrete specimens can be characterized by the stress- deformation curve which exhibits linear and non-linear paths before the peak stress, and a nonlinear strain-softening branch after peak stress.

The accurate definition of this curve is very important and difficult to obtain experimentally, especially the softening part of the curve. In all previous work, investigators have been agreed upon defining not only the fracture energy G_f, but also the characteristic length l_c for both normal and high strength concrete, with a very slight difference in some of the fracture mechanics properties, such as concrete brittleness.

2.6 Tension Stiffening Models for High Strength Concrete

Forty plain concrete specimens with different w/c ratios varying from 0.3 to 0.6 were tested by Phillips and Binsheng (1993), in order to examine different factors that might

affect the plain concrete behavior under direct tension. The total deformation of the specimen can be expressed as

$$\delta = \delta_e + \delta_o + w \qquad (2.40)$$

Where δ_e and δ_o are defined as the elastic deformations, and w is the crack width. Also, a relationship between f_{cu} and f_t was obtained from the test results as

$$f_t = 0.45 f_{cu}^{\frac{1}{2}} \qquad (2.41)$$

Form this set of tested specimens, a full stress-deformation curve has been developed, which can be divided clearly to four different stages: linear, nonlinear strain-stiffening, rapid strain-softening and slow strain-softening. These stages can be represented with four characteristic points: the nonlinear point, the cracking point, the strain-softening characteristic point, and the failure point. In this study, a brittleness parameter B' is proposed which can be expressed as the ratio of the maximum elastic deformation δ_e to the total deformation at failure δ_F, for a specified length L where a crack has been formed:

$$B' = \eta_1 L f_t^2 / E G_f - \eta_2 B \qquad (2.42)$$

The brittleness parameter will increase with the strength and the length, and this coincides with the fact that high strength concrete is very brittle material.

In a unique test setup conducted by Marzouk and Chen (1995), consisting of a strain-controlled mode through a close-loop testing machine, plain high strength concrete was tested under direct uniaxial tension. A total of 48 specimens with dimensions of $20\times75\times300\,\text{mm}$ were tested to determine the fracture energy, and characteristic length. Load-deformation curves, a relationship between tensile and compressive strength, and a softening model for high strength concrete were presented.

The softening model proposed by Marzouk and Chen (1993) describes a constitutive relationship for plain high strength concrete in uniaxial tension governed by the following expression:

$$y = 2x - x^2, x \le 1.0$$
$$y = \frac{x}{\alpha(x-1)^{\beta} + x}, x \ge 1.0 \qquad (2.43)$$

where,

y = relative stress $f_t/f_t^{'}$

x = relative strain $\varepsilon_t/\varepsilon_p$

The high strength concrete load deformation curves clearly show the brittleness of the material, very high strength before cracking, relatively high young modulus, and sharp descending portion after the high tensile strength was reached and the specimens started to crack. The tensile strength of high strength concrete is 4% of the maximum compressive strength reported by the investigator.

A value of 3.5 MPa was reported for the tensile strength for plain high strength concrete, which will be adopted in this current study for crack width calculations.

2.7 Code Restrictions for Crack Estimation

2.7.1 CSA A23.3-04

The CSA A23.3-04 method is based on the Gergely and Lutz research investigation. CSA A23.3-04 does not limit the crack width directly. Instead, it limits the magnitude of the term z. For thin one-way slabs, the maximum z values are 30000 and 25000 N/mm for interior and exterior exposure, respectively. These limits correspond to crack widths of 0.4 and 0.33 mm, respectively. The term σ_{sr} is calculated based on the naked steel response or is assumed to be equal to 60 % of steel yield strength.

2.7.2 ACI 318-99

Crack control provisions in ACI 318-99 vary a little from the Gergely-Lutz approach that was adopted in previous code versions. The maximum bar spacing is now specified directly as a function of the concrete cover and the level of stress in the steel reinforcement. The new provisions are intended to control surface cracks to a width that is generally acceptable in practice but may vary widely in a given structure. ACI 318- 05 has also abandoned the distinction between interior and exterior exposure conditions.

2.7.3 ISIS M04-00 (2001)

The majority of design provisions to calculate crack widths in members with FRP are based on modifications made to the Gergely-Lutz equation. The expression that ISIS M04-00 (2001) recommends the following expression to be used for calculating crack width for concrete members reinforced with FRP

$$w = 11\times10^{-6}\sigma_{fr}K_b\frac{h_2}{h_1}\sqrt[3]{d_c A} \qquad (2.44)$$

where,

K_b = is a bond coefficient, taken as 1.0 for GFRP bars with bond properties similar to those of steel, greater than 1.0 for GFRP bars with inferior bond quality, and less than 1.0 for GFRP bars with superior bond quality.

2.7.4 CSA S806–02

The Canadian Standard for the design of GFRP-reinforced concrete structures, CSA S806-00, controls crack widths by limiting a factor, z, which is defined as

$$z = K_b \frac{E_s}{E_f} \sigma_{fr} \sqrt[3]{d_c A} \qquad (2.45)$$

The maximum values for z are 45000 and 38000 N/mm, for interior and exterior exposure, respectively, E_f is FRP modulus of elasticity, and K_b is a bond coefficient equal to 1.2 for deformed FRP bars. These z values are equivalent to maximum allowable crack widths of about 1.5 times greater than those allowed for both interior and exterior exposure conditions by CSA A23.3-04 for the design of steel-reinforced concrete members. The increase in the allowable crack width limits for GFRP-reinforced concrete members has been driven by the superior corrosion resistance of GFRP reinforcement.

2.8 Bond between GFRP Bars and Concrete

In general, reinforced concrete members resist loading in such a way that compression will be resisted by concrete and tension will be taken by the reinforcement bars. In order for this process to be completed, a force transfer must exist: the bond. For flexure concrete members, bond stresses are the transfer media between concrete and rebars. If the bond stresses vanish or disappear, the tension in reinforcement drops to zero and the bars pull out and, as a result, the member will fail.

Bond stress develops in the surrounding surface area of the bar embedded in concrete by chemical adhesion, friction and mechanical interaction between concrete and deformed bars (ribs).

In comparison between steel deformed bars and GFRP, beside the lower GFRP modulus of elasticity, the deformations in rebars play a major role in bond stresses. Since the GFRP bars have no deformation ribs, bond stresses mainly depend on chemical adhesion and friction. This will result in lower bond stresses, which might affect the cracking behavior of concrete members reinforced with GFRP.

2.8.1 GFRP Bond Influential Parameters

The most influential parameters on the bond interaction between FRP and concrete are:

1) Cross-sectional shape of GFRP reinforcement
2) GFRP's elastic modulus in both axial and transverse directions
3) Bar diameter or cross-sectional size
4) Surface conditions
5) Resin type
6) Concrete strength
7) Confinement conditions
8) Poisson's ratio of GFRP
9) Position of the bar in the structural member's cross-section
10) Concrete cover

2.8.2 Bond of GFRP Relative to Steel

The bond strength of FRP is expected to be less than that of conventional steel because:

i) The modulus of elasticity of GFRP in both radial and longitudinal directions is lower than that of steel.
ii) The resin matrix has a lower shear strength, and
iii) The shear stiffness of GFRP is lower than that of steel.

In order to measure the bond stresses in a reinforced concrete member, two different types of test can be conducted: the pull out test and the beam test.

The pull out test has been used extensively to determine bond strength. In this test, a tensile force is applied to the bars to pull out of concrete. The concrete will be in compression and does not crack. The results obtained using the pull out test does not simulate the actual behavior of flexural concrete members. Engineers and scientists have found that the beam test is more representative to the actual behavior of reinforced concrete members in flexure.

Tastani and Pantazopoulou (2002) designed a new way to test the bond of GFRP bars; in the new test, the concrete is under tension, which reflects the real behavior of reinforced concrete and simulates the real force developed in the bars and the surrounding concrete.

There exists a limited amount of research in FRP bond properties, and all investigators have agreed on the expression below to obtain the bond strength for concrete members reinforced with FRP:

$$\mu = \frac{T}{\pi . d_b . l} \qquad (2.46)$$

where,

μ = bond strength in MPa.

T = applied load

d_b = bar diameter

l = embedded length

The expression above can be used in both pullout and beam tests. Tastani and Pantazopoulou (2002) report a 5 MPa value for bond strength. Ehsani (1996) reports a value of 4.9 MPa from both beam and pullout tests. Benmokrane (1993) reports a value of 7.3 MPa, obtained from the beam test, as a maximum bond strength of 15.9 mm GFRP bars, which is considered a very high value for bond strength for GFRP.

2.9 Tension Stiffening Effect in FRP-reinforced Concrete Members

According to the tension chord model fundamentals, the strain correction due to concrete's tension stiffening is highly influenced by the amount of reinforcement and the elastic modulus of the reinforcement. The effect of these variables in members with GFRP could be more influential than in steel-reinforced concrete members. If the tension stiffening effect is important in the context of steel-reinforced concrete members, it does not seem sensible to neglect it for the serviceability design of GFRP-reinforced concrete members.

2.10 GFRP Reinforcement for Concrete Structures

Recently, GFRP became the center of the attention of scientists and engineers both as a new material used in reinforcing concrete, and as an alternative for conventional steel in corrosive environment. GFRP is a non-corrosive and non-magnetic material.

Glass Fiber Reinforced Plastics (GFRP) are the most common type of FRP and other types of FRP were examined, like carbon (CFRP) and Aramid (AFRP). Compared to conventional steel reinforcement rebars, GFRP has different physical properties. The lower modulus of elasticity is a major draw back in using GFRP as a reinforcing material.

The use of FRP is limited to corrosive, non-magnetic environments, due the high cost of this material and the limited performance and research data base available. Nevertheless, FRP has a wide range of applications as a construction material for new and existing structures, especially for strengthening.

Widespread research has been done on FRP as reinforcement for structural members. The desirability for GFRP usage as reinforcement to overcome the problem of corrosion in structural members reinforced with conventional steel rebars was the main concern of most investigators. The applications of GFRP are bridge decks, parking structures, MRI rooms, marine structures, and the strengthening of masonry buildings and concrete members to resist flexure and shear.

The potential of using GFRP as strengthening material on two-way slabs to increase the flexural and shear strength motivates the research that has been conducted at MUN by Ebead and Marzouk (2004).

Most of the previous investigations were conducted in beams and one-way slabs reinforced with GFRP. Very little research has been conducted in two-way slabs reinforced with GFRP as the main reinforcement. Some of the research on two-way slabs will be presented in the following section.

2.11 Previous Work on Two-way Slabs Reinforced with FRP

A total of 17 square slabs, 1000 mm in dimension, were tested by Matthys and Taerwe (2000 b) for punching resistance of concrete members reinforced with FRP grids. The slabs were cut from one-way slabs that had the following geometric properties : 1000 mm width, 120 or 150 depth, a span of 4 m, and a total length of 4.5 m. Originally, the slabs were tested in a four-point one-way bending experiment by Matthys and Taerwe (2000 a). As a result, the specimens were already cracked and showing between 3 to 5 cracks on the tension side.

Matthys and Taerwe's slabs were divided into three series according to the reinforcement types; series 1 was reinforced with steel used as reference slabs, series 2 was reinforced with different types of carbon FRP (CFRP) grids, and the third series was reinforced with a hybrid type of FRP comprising both glass and carbon fibers. All tested slabs were made with normal strength concrete except for one, made with high strength concrete.

The test results were presented in terms of ultimate load, failure mode, punching cone shape, and deflections. The experimental results, the ultimate load, were verified with different codes of expression for the ultimate punching capacity. The punching capacity according to CEB-FIP Model Code 1990 (MC90), Eurocode 2 (EC2), the Japanese Society of Civil Engineers (JSCE) (Recommendation 1997), and ACI 318-95 were calculated and compared to the ultimate load obtained from the experiments. In order to obtain comparable results to the experiment results, the investigators suggested a modification for the reinforcement ratio, and this modified reinforcement ratio is:

$$\rho \frac{E_r}{E_s}$$

where,

ρ = the reinforcement ratio

E_r = the FRP modulus of elasticity

E_s = the steel modulus of elasticity

The same modification has been recommended earlier by the JSCE in 1997.

Matthys and Taerwe also adopted and modified existing models to calculate the ultimate shear capacity for the tested slabs. The following modifications were introduced to the Hallgren (1996) and Menétrey (1996) models to account for the different physical properties of the FRP:

1. Implement the elastic behavior for the FRP in the model
2. Ignore the dowel action
3. Take the radius of the punching cone as 1.8d
4. Take the modified reinforcement ratio as $\rho\frac{E_r}{E_s}$

In conclusion, Matthys and Taerwe strongly recommended that the modified reinforcement ratio be used in the ultimate load calculations for concrete members reinforced with FRP, which accounts for the lower FRP modulus of elasticity, though it does not consider the lower bond properties of the FRP.

Banthia et al. (1995) tested four concrete slabs that were $600\times600\times75$ mm in dimension to study the behavior of concrete slabs reinforced with a fiber-reinforced plastic grid. Three slabs reinforced with FRP grids (NEFMAC, manufactured by Shimizu Corporation, Japan) were compared to a similar slab reinforced with conventional steel reinforcement. Normal strength, high strength and normal strength concrete with fiber were used to manufacture the slabs. The FRP grid had a tensile strength of 1200 MPa and an elastic modulus of 100 GPa based on the manufacturer specifications. The test results

were presented in terms of load-displacement curves and energy and load-reinforcement strain plots.

Banthia also verified the experimental results with existing codes equations, and concluded in this study that no significant changes for the codes equation were needed. Also, the use of the fiber reinforced concrete improved the ultimate carrying capacity and energy-absorption capability of the tested slabs.

El-Ghandour et al. (2002) tested a total of eight slabs in a two-phase experimental program. The normal concrete two-way slabs tested were reinforced with CFRP and GFRP, and CFRP shear reinforcement were used in two slabs. In the first phase of the experimental program, problems of bond slip and crack localization were encountered. To overcome these problems, the authors increased the reinforcement ratio.

A model to predict the shear capacity of two-way slabs reinforced with FRP was proposed and verified. ACI 318-95, ACI 440-98, and BS 8110 punching shear equations were modified to account for the difference in FRP properties. Also a strain limit of 0.0045 was recommended by the researcher as the maximum strain for reinforcement in the proposed model for shear capacity calculations.

El-Ghandour applied the strain approach proposed by Clarke (1996) and the stress approach combined with BS 8110 (1985) shear capacity equations to calculate the shear capacity for reinforced concrete two-way slabs reinforced with FRP. The two different

approaches used by the investigator resulted in lower and upper bound solutions, and thus the researcher proposed a modification to the strain approach.

The investigator proposed a correction factor to the equivalent steel area calculated as per the strain approach equal to 1.8, and thus the equivalent steel area used in the calculation can be obtained using the following equation

$$A_s = A_{FRP}(E_{FRP}/E_s)(\phi_E) \qquad (2.47)$$

where

A_s = equivalent area of steel

A_{FRP} = area of FRP

E_{FRP} = FRP modulus of elasticity

E_s = steel modulus of elasticity

$\phi_E = (\varepsilon_{FRP}/\varepsilon_y) = 1.8$ = correction factor

El-Ghandour suggested a strain limit of 0.0045 for the GFRP and used 0.0025 for the yield strain for the steel according to the BS 8110 (1985) to obtain the correction factor. Even though the modified model predicted the shear capacity for the tested slabs with good agreement with the experimental results, the 0.0045 strain limit for the FRP had no experimental evidence to provide justification for its use.

Ospina et al. (2001) carried out an experimental program to investigate the punching shear behavior of two-way slabs reinforced with GFRP. The experimental program consisted of four slabs; two slabs were reinforced with GFRP, one with GFRP 2-D grid (NEFMAC) and one with traditional steel. Mechanical end anchorage was provided to prevent any premature bar slippage.

The investigator presented a comprehensive investigation on the implementation of FRP reinforcement in slab construction. The main variables were the slab reinforcement material, the type of the reinforcement mat, and the flexural reinforcement stiffness.

Based on the load-deflection behavior, the strain in the tension reinforcement and the bar force gradients, the investigator concludes that the punching failure in FRP reinforced slabs was affected by the elastic stiffness of the FRP mat and its bond characteristics. The researcher also found that tension stiffening affects the behavior of GFRP reinforced slabs.

Ospina examined the existing code design provisions (ACI 318 and BS8110) and equations that were recently proposed by other investigators (Matthys and Taerwe 2000b and El-Ghandour et al. (1999). The author concludes that the equation proposed by Matthys and Taerwe (2000) provided the best estimation for the punching capacity of two-way slabs reinforced with FRP.

The investigator also proposed a rational model to calculate the punching capacity for two-way slabs reinforced with FRP. The model was modified from the strip model originally proposed by Alexander and Simmonds (1992) for steel reinforced slabs.

Rashid (2004) investigated the performance of GFRP bars as the main reinforcement for two-way slabs. A total of nine interior slabs, including a reference slab reinforced with conventional steel bars, were constructed and tested at the structural laboratory at Memorial University of Newfoundland (MUN). The investigation's main variables were the reinforcement ratio, concrete strength, and slab depth. The influence of high strength concrete on the punching strength of the GFRP reinforced slabs was investigated.

The test results reveal that normal strength concrete two-way slabs reinforced with GFRP exhibit higher deflection, greater crack width and lower punching loads compared to similar slabs with traditional steel bars. The investigator concludes that increasing the concrete strength or the slab depth improves the performance of the tested slabs; however, only two slabs made with high strength concrete were tested. That was enough motivation to carry out the current investigation, to obtain a better understanding of the behavior of high strength concrete two-way slabs reinforced with GFRP.

Rashid adopted and modified a rational model originally proposed by Marzouk and Hussein (1993) for two-way slabs reinforced with traditional steel bars. Some limitations in the original model due to the assumed failure geometry were eliminated and the GFRP properties were incorporated into the modified model.

The same modeling assumptions were used to describe the slab behavior, the failure mechanism and the failure criteria. The main assumptions of the original model were kept unchanged, and thus the modified model produced good predictions of the punching capacity of slabs reinforced with GFRP.

A simple and reliable model was presented by Dimitrios (2007) for the punching shear strength analysis of slabs reinforced with GFRP bars or grids based on shear-moment interaction. The model was originally developed by the investigator to calculate the shear capacity of reinforced concrete slabs with conventional steel rebars.

In the analysis of the steel reinforced slabs, the punching failure load is calculated using the following equation:

$$V_u = m.v_c.b_p.X.\cot\theta \qquad (2.48)$$

where the limiting shear stress in the compression zone is given by

$$v_c = 0.27 f_{cu}^{2/3} \qquad (2.49)$$

where, m represents a coefficient equal to 1.00 and 0.80 for normal weight and lightweight concrete, respectively.

θ = the angle of failure of the fracture cone surface, taken as 30 degrees

b_p = a larger control perimeter recommended by BS 8110-97 to account for the concrete interlock and the steel dowel action, and is given by

$$b_p = 4c + 12d \qquad (2.50)$$

where,

c = is diameter side or the column width

d = the effective depth of the slab

The combined neutral axis depth X of the slab is calculated as

$$X = \frac{2X_s X_f}{X_s + X_f} \qquad (2.51)$$

where,

X_s = is the neutral axis depth of the shear section

X_f = is the neutral axis depth of the flexural section

In the case of the GFRP, the investigator concludes that the calculations of the flexural neutral axis depth would be affected by the lower bond properties of the FRP reinforcement. The same observation was recognized by Ospina et al (2001). To

overcome the problem, Dimitrios et al. proposed a reduction factor of 45% of the FRP strain that was calculated assuming that the FRP has a perfect bond with the surrounding concrete by applying the equilibrium and compatibility conditions.

Chapter 3

3 Experimental Program

3.1 Introduction

This chapter describes in detail the experimental program carried out at the structural laboratory of Memorial University of Newfoundland (MUN) to investigate the behavior of high strength concrete (HSC) reinforced with glass fiber-reinforced polymer (GFRP) bars. The experimental program consists of the casting, testing and evaluation of six two-way slabs reinforced with GFRP bars and one reference specimen reinforced with traditional steel reinforcement.

The primary objective of this investigation is to develop a better understanding of the structural behavior of high strength concrete two-way slabs reinforced with GFRP, with a special focus on flexural cracking behavior. The effects of the clear concrete cover and the reinforcement percentage were considered in this program as major variables that

could affect cracking behavior. The specific test procedure, specimen details and materials used to carry out this research are presented in this chapter.

3.2 Materials

3.2.1 Concrete

The original mix design was developed at (MUN) (Marzouk and Hussein 1991) using type 10 Normal Portland Cement. In this investigation, the cement type used is Type 10E-SF-Normal Portland cement with silica fume at 8 % addition by weight, which complies with CSA A3000-03 Blended Hydraulic Cement GUb, 8SF. The target compressive strength is 70 MPa.

The mix design for high strength concrete used local material and Silica Fume Portland Cement, known commercially as HSF, and is produced by St.Lawrence Cement, Mississauga, Ontario. The mix also contained a low water-cement ratio (w/c) of 0.3, and water reducing admixtures were added to the mix. Also, a superplasticizer was added to the mix to enhance the workability. To delay the concrete setting and cement hydration to obtain a homogenous mix, a retarder was also used in the concrete mix.

The superplasticizer used in the mix is commonly known as EUCON 3 and it meets all the requirements of the ASTM C494 type F. It is comprised of an aqueous solution of sodium salt of poly-naphthalene sulfuric acid used as a superplasticizer for concrete. It is usually used to enhance the workability of the concrete without affecting the strength.

The superplasticizer helps to control the hydration rate of the cement to maintain optimum fluidity over time. It makes the concrete easier to handle without any segregation; it is possible to reduce the water cement ratio with the addition of superplasticizer and hence allow for the production of concrete with an increased compressive strength.

The water reducing admixture that was used to produce the high strength concrete in this experimental program is commercially known as EUCON DX. This is a strength increasing water reducing agent, which meets all the requirements of CSA A266.2 specifications for types WN and SN. It is an aqueous solution of hydroxyl-carboxilic acid and a catalyst that provides better hydration for cement.

The set retarding agent that was used in the mix is known as EUCON 727 admixture. This agent is used to enhance the compressive strength of the concrete by reducing water and to retard setting. It is a double metallo-organic salt derived from hydroxycarboxylic acid, that complies with CSA-A266.2 type R, RX and SR standards.

3.2.2 Mix Design

All of the seven test specimens were cast using high strength concrete produced at the concrete laboratory at MUN. The table below provides the mix proportions of the concrete used:

Table 3-1: High strength concrete mix proportions

Ingredients	High performance concrete
Cement (kg)	40
Coarse aggregate (kg)	107
Fine aggregate (kg)	65
Water (L)	12
Super plasticizer (ml)	1200
Water reducer (ml)	200
Retarding agent (ml)	40
Target Compressive strength, $f_c^{'}$	70 MPa

3.2.3 Mixing Procedure

In order to achieve the target strength, the following mix procedure was used:

- Charge 100% of coarse aggregate;
- Batch 100% of cement;
- Batch 100% of sand;
- Mix dry for 1-2 minutes in order to obtain homogeneous concrete mix;
- Mix for 5 minutes after adding 50% of estimated water with supper plasticizer (1200 ml);
- Mix for 3 minutes after adding 25% of water with water reducing agents and the retarder agent;
- Mix for 2-3 minutes with the rest of the water dose to target slump.

3.2.4 Reinforcement Properties

All six specimens tested in this study were reinforced with fiber glass reinforced polymer (GFRP), 16 mm, commercially known as Aslan 100 Vinly Ester Matrix GFRP Rebar. A tension test was performed to obtain the actual stress-strain relation for GFRP bars used in this current investigation. Only the modulus of elasticity was obtained from the tension test data.

The physical properties of GFRP bars are presented in Table 3-2.

Table 3-2: GFRP physical properties provided by the manufacturer

	Bar size (mm)	Cross Sectional Area (mm^2)	Nominal Diameter (mm)	Tensile Strength (MPa)	Modulus of Elasticity (GPa)
Manufacturer	16	217.56	15.88	655	40.8
Experiment	16	217.56	15.88	-	43.5

Figures 3-1 and 3-2 show the typical behavior of glass fiber reinforced polymer rebars in terms of the stress/ strain relationship.

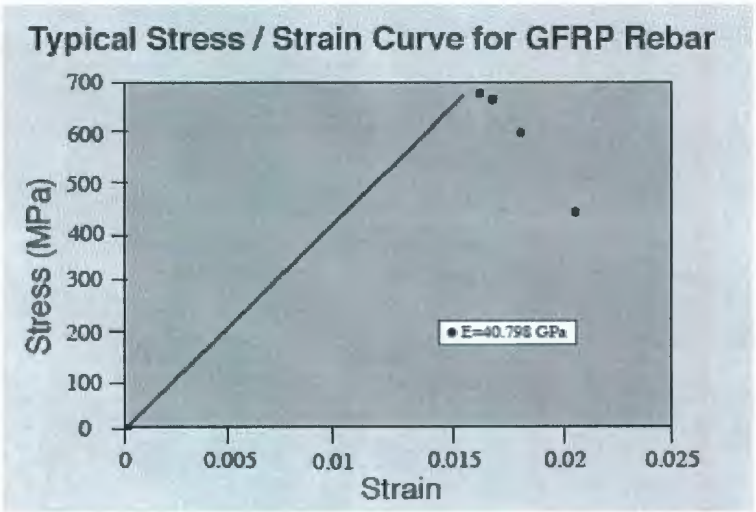

Figure 3-1: Stress-Strain curve for GFRP rebars provided by the manufacturer

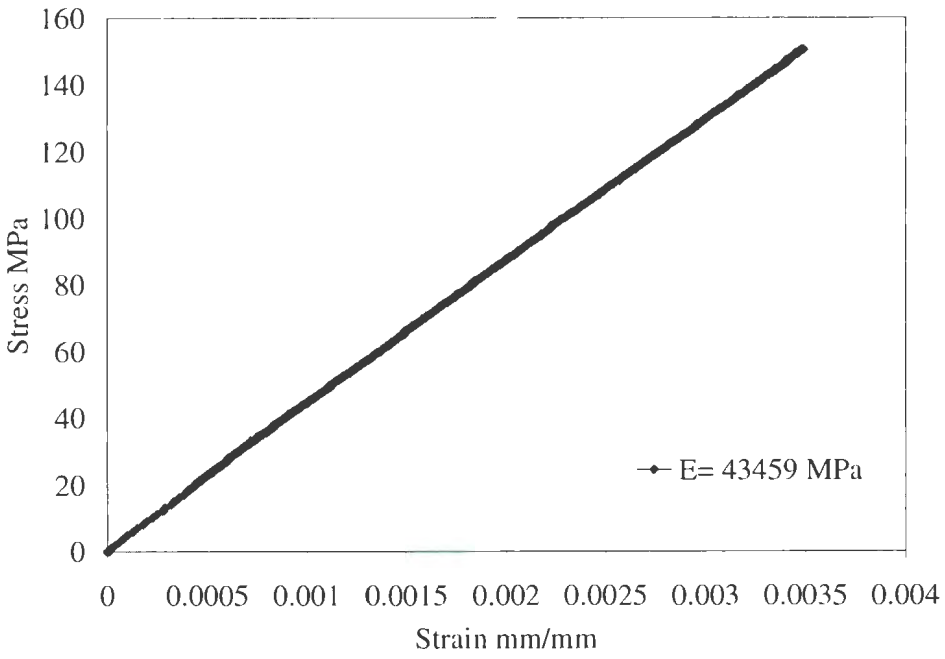

Figure 3-2: Stress-Strain curve for GFRP rebars test results

Based on the pullout test provided by the manufacturer, the maximum bond stress is 11.6 MPa. The bond stress is one of the most important factors affecting the cracking behavior of concrete members, especially in crack width calculations.

3.3 Details of Test Specimens:

A total of six specimens reinforced with GFRP, plus a reference steel reinforced slab, were tested in this investigation. The specimens were divided into two groups, whereby each group consisted of three specimens. The main variables considered in this investigation are the reinforcement ratio and the clear concrete cover.

The experimental program was divided into two series according to the variables considered to carry out this investigation, as mentioned earlier; the slabs in Series 1 have the same geometrical properties with different reinforcement ratios. The slabs in Series 2 have the same reinforcement ratio and different concrete clear covers. The reference slab was made of high strength concrete reinforced steel rebars, with the same reinforcement ratio and with identical geometrical properties.

All of the tested specimens were 1900×1900 mm slabs constructed and tested to failure in this study. All specimens were cast using high-strength concrete produced at the concrete laboratory (MUN), reinforced with GFRP rebars.

A reference slab reinforced with conventional steel rebars was constructed and tested to failure for comparison purposes. The details of all specimens were presented in the following table:

Table 3-3: Properties for all tested specimens

Specimen No	f_c' MPa	Slab thickness (mm)	Effective depth (mm)	Slab cover (mm)	Column width (mm)	Reinforcement ratio ρ %	Remarks
1-	66.8	150	110	30	250	1.0	
2-	62	150	110	30	250	1.2	
3-	64	150	110	30	250	1.5	
4-	64	200	160	30	250	1.2	
5-	70.06	200	145	45	250	1.2	
6-	67.58	200	135	55	250	1.2	
7-	70	150	135	30	250	1.2	Steel Ref slab

In this study, the balanced reinforcement ratio was calculated assuming that the crushing of concrete is the failure cause, using the following formula adopted from ISIS 2000. Figure 3-3 shows the strain stress distribution for concrete members reinforced with GFRP,

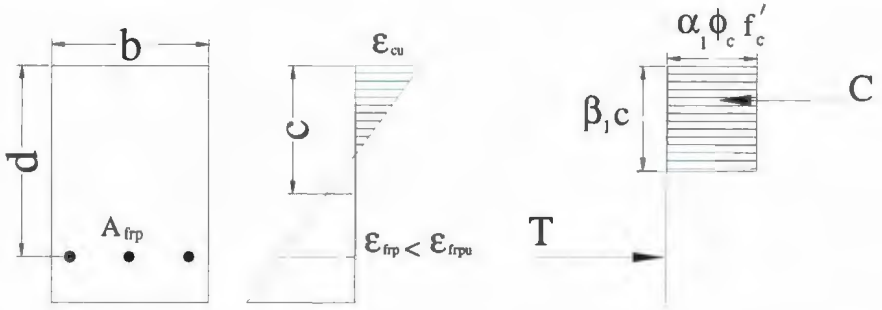

Figure **3-3**: Stress-Strain distribution at the ultimate (concrete crushing)

$$\rho_{bal} = 0.85\beta_1 \frac{f_c'}{f_{fu}} \left[\frac{\varepsilon_{cu}}{\varepsilon_{cu} + \varepsilon_{fu}} \right] \qquad (3.1)$$

where

ρ_{bal} = the reinforcement balanced ratio

f_c' = concrete compressive stress MPa

f_{fu} = FRP ultimate stress MPa

ε_{cu} = concrete ultimate strain

ε_{fu} = FRP ultimate strain

β_1 = stress block constant defined according to CSA A23-04, and it can be calculated by the following expression

$$\beta_1 = 0.97 - 0.0025 f_c' \qquad (3.2)$$

All of the tested specimens were designed to fail in punching shear; all slabs were over reinforced concrete members. To achieve this phenomenon, the following values were substituted in the above expression:

$\varepsilon_{cu} =$ 0.0035

$\varepsilon_{fu} =$ 0.018

$f_{fu} =$ 630 MPa

$f_c' =$ 70 MPa

The designed reinforcement ratio obtained is:

$\rho_{bal} = 1.2\%$

3.4 Test Set-up and Instrumentation:

A 10-ton crane was used to lift and install the specimens inside the loading frame and to remove them after testing. The loading frame used for testing was a large steel reaction frame. The slabs were rested vertically on the frame; rubber packing was installed between the specimens and the steel frame. The boundary condition in this case is a simply supported slab with the corner free to lift, which coincides with the selection of the isolated column-slab to represent the interior panel of a continuous slab.

A central manual-hydraulic jack, commercially known as ENERPAC Double-Acting, High Tonnage Cylinders, CLRG-30012, was used to apply the load in all tests. The capacity of the hydraulic jack that was used to carry the experimental program is 300 tons (600 kips), 0.305 m (12 inches) stroke and a maximum operating pressure of 69 MPa (10000 psi), see Figure 3.4.

LPDTs were used to record the deflection at the slab centers, and a total of five points besides the central deflection was measured from the distance that the ram traveled up the failure.

Electrical resistance strain gauges having a resistance of $120 \pm 0.3\%$ ohms were used to measure the variations of the concrete strains on the compression side; for the strain gauge locations, see Figure 3-5.

The specimens were loaded until two visible cracks appeared, and then the test was stopped to install LPDTs, which were used as crack gauges. These LPDTs were placed on the tension face of the slab in order to record the crack width; for the crack gauge locations, see Figure 3-6.

Similarly, a total of five strain gauges were installed and glued to the main reinforcement. Strain gauges 1 to 4 were installed on the main reinforcement; however, strain gauge 5 was installed on the transverse reinforcement. For all tested specimens, the locations of

the strain gauges were exactly the same; for the reinforcement strain gauge locations, see Figure 3-7.

The electronic strain gauges, LPDTs and the load reading were connected to a computerized data acquisition system. The measurements were recorded for all experiment results using LabVIEW software version 8, and the scanning rate was taken as one reading every second for all tested specimens. All data obtained was saved to a personal computer.

Figure 3-4: Test setup and Data acquisition system

3.5 Test Procedure

The slabs were placed on the testing frame, and the load was first applied up to 45 kN (10 Kips) then released to make sure the slab edges were completely resting on the frame. The load was then applied gradually using a manual-hydraulic jack up to the cracking load; the tests were stopped immediately after the appearance of visible cracks to install crack gauges. Crack gauges were installed and glued to the tension surface in order to measure crack width.

The load continues up to failure in intervals of 45 kN (10 Kips). For each load interval, the cracks were mapped and photographed as shown in Figure 3-8.

All of the strain gauges on the concrete, GFRP, and LPDTs, as well as the load readings, were connected into the data acquisition system, which scanned readings at a rate of one reading for every second interval.

This procedure was repeated in all tests up to the failure of the test specimens, and all data was recorded and stored in a personal computer.

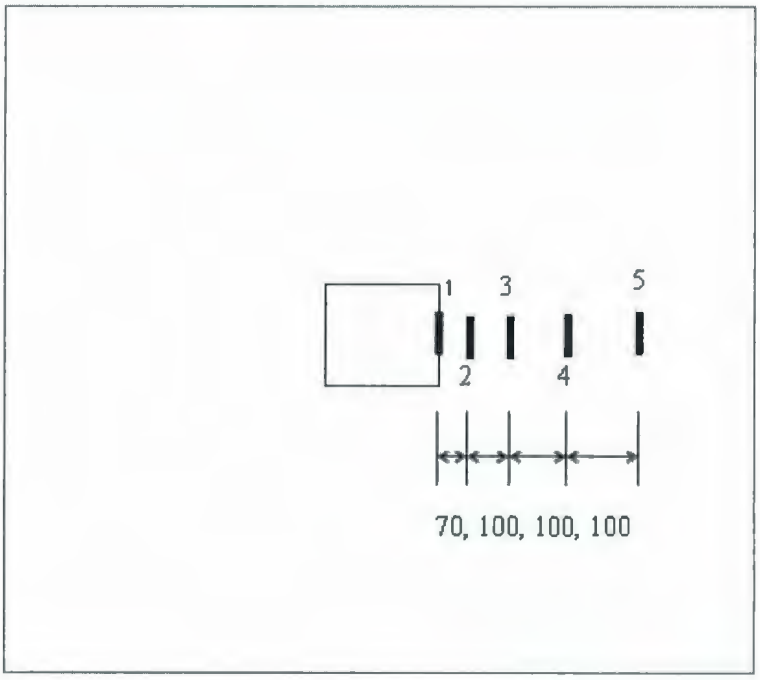

Figure 3-5: Concrete strain gauges arrangement

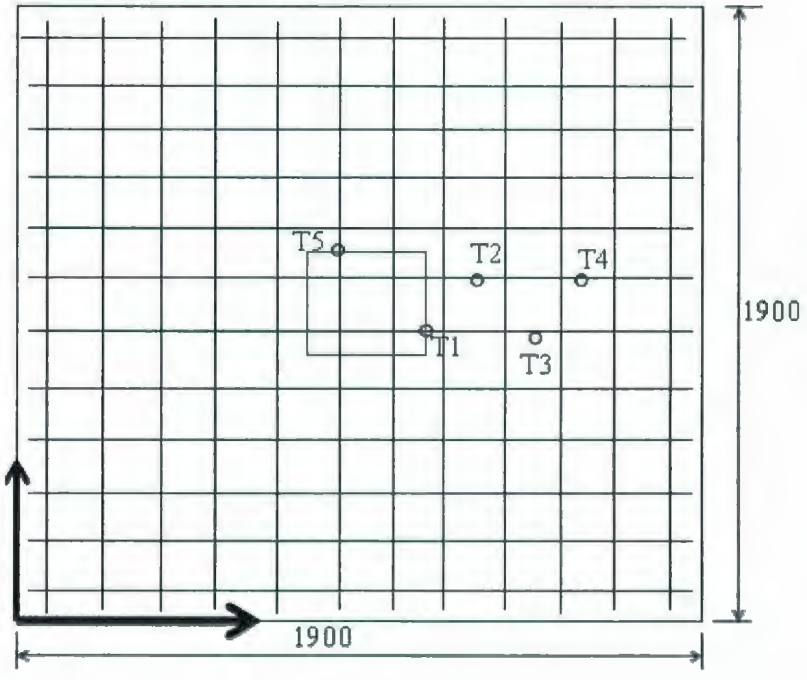

Figure 3-6: GFRP strain gauges arrangement used in all specimens

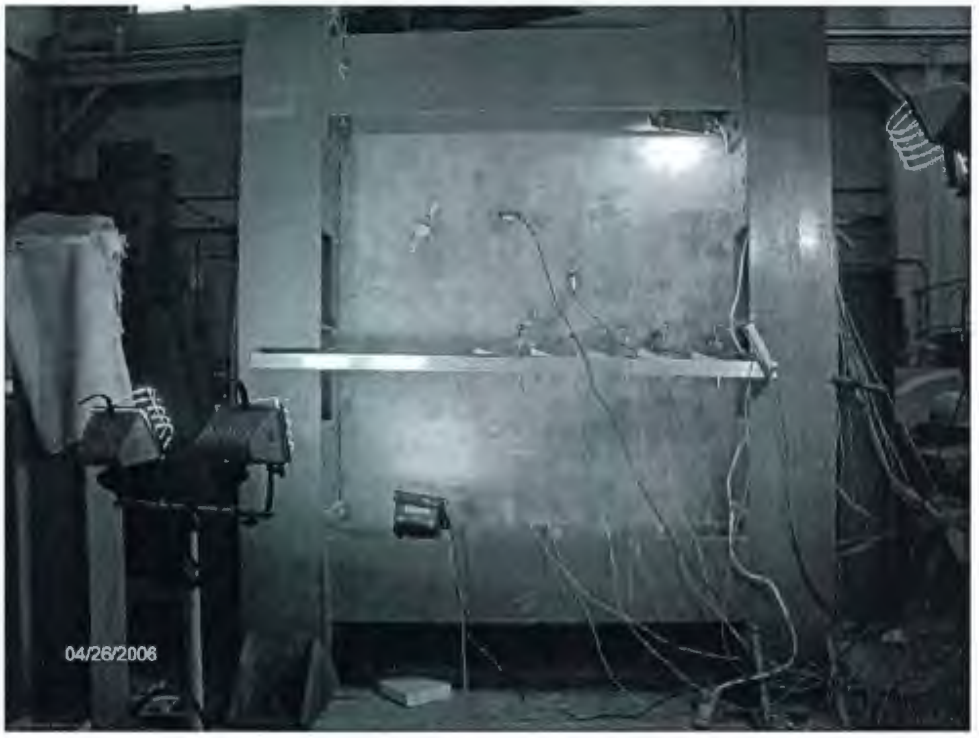

Figure 3-7: Crack gauge locations

Figure 3-8: Crack mapping

Chapter 4

4 Test Results and Discussion

4.1 Introduction

The test results and observations obtained from the experimental program are given in this chapter. Six high strength GFRP reinforced slabs were divided into two groups. The influences of the reinforcement ratio and the clear concrete cover on the behaviour of two-way slabs reinforced with GFRP bars were examined. The behaviour of the slabs are presented in terms of the load-deflection relationship at service load and ultimate load, the concrete strains, GFRP reinforcement strains, crack patterns and failure modes. Due to the large quantity of experimental data, only representative results are shown in this chapter.

4.2 Strains in Slab:

4.2.1 Concrete Strains:

In general, the concrete strains in the tangential direction were higher than those in the radial direction. The tangential direction represents the direction parallel to the column face and the radial direction represents the direction perpendicular to the column face. Concrete strain gauges in the radial direction were mounted at different locations on the compression side of the slabs, as explained in the previous chapter. Therefore, the maximum concrete strain in the radial direction was considered and measured on the compression surface of the slabs at distances of around 50 to 450 mm, 100 mm apart, from the middle of the column face. The concrete strains were much lower than $3500\mu\varepsilon$, which is the recommended crushing strain limit according to CSA-A23.3 (CSA, 2004).

The radial concrete strain profiles at different load levels are shown in Figure. 4-1 for Specimen 4 of Series 2 of the test slabs. The highest strain in each diagram shows the radial strain distribution at or close to the ultimate load. The maximum radial concrete strain generally developed at a certain distance very close to the column face. The strains then dropped quickly with an increase in the distance from the slab centre. This phenomenon was more pronounced in slabs with a higher reinforcement ratio and slab depth. This observation was also reported in some of the tests on high strength concrete slab-column connections by Hallgren (1996).

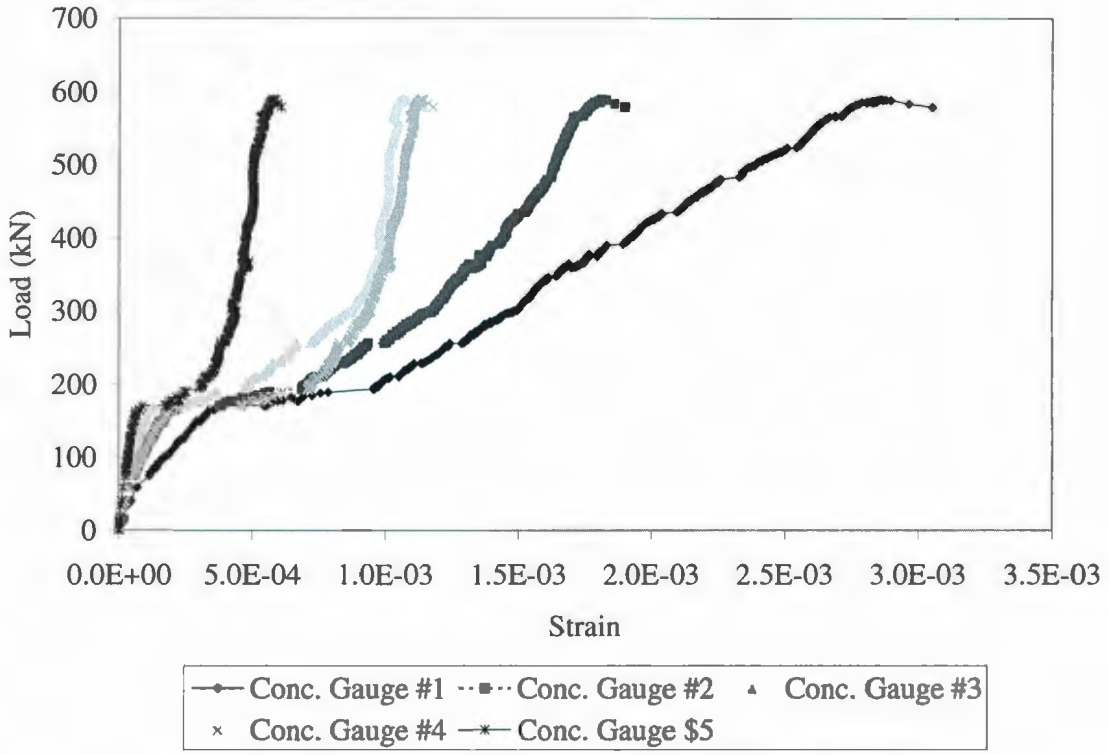

Figure 4-1: Concrete Strain vs Load Specimen 4 Series 2

4.2.2 Reinforcement Strains:

The strains in the reinforcement were measured at different locations. The maximum strains occurred around the column perimeter and the values are reported. The recorded maximum strain in the GFRP bars was 7076 με in Specimen 2 of Series 1, which had a 1.2% reinforcement ratio and 150 mm slab depth. This value is lower than the ultimate tensile strength of GFRP bars, around 16000 με. Based on the reinforcement strain values provided by the manufacturer of the GFRP, there was no rupture of the GFRP bars in any of the test slabs.

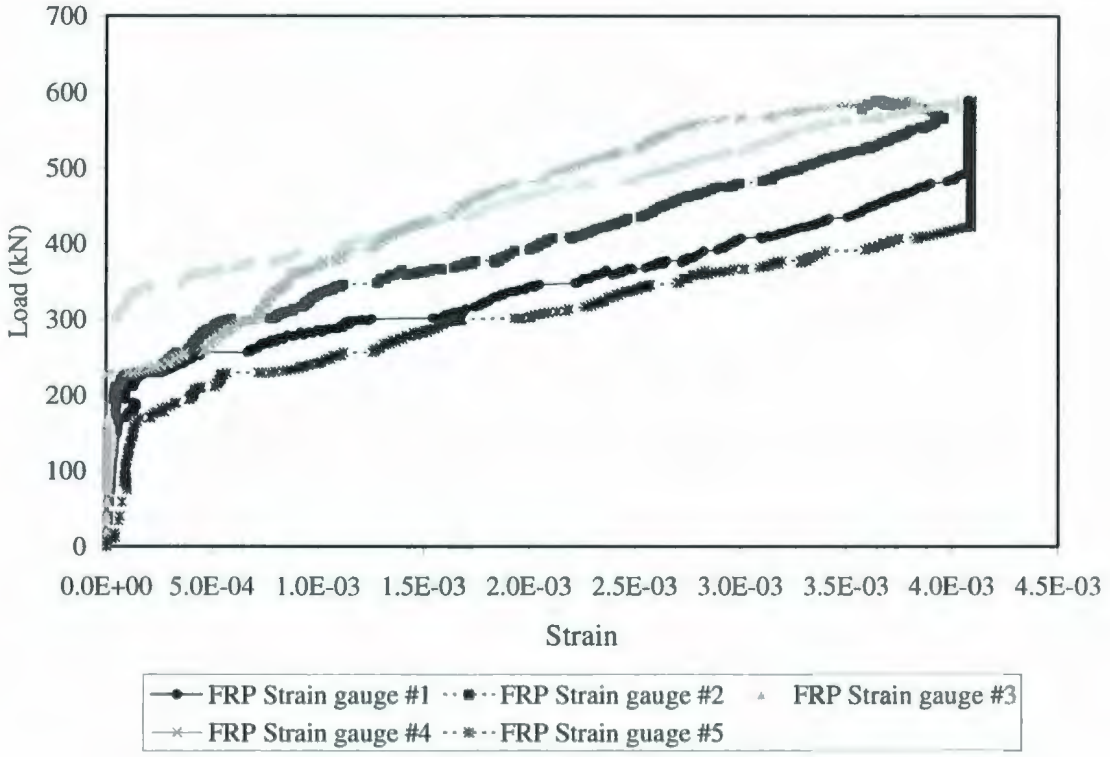

Figure 4-2: FRP Strain vs Load Specimen 4 Series 2

Figure 4-2 shows the relationship between the load and the reinforcement strains just below the column stub. The lowest curve in each diagram shows the radial strain distribution at or close to ultimate load. According to those figures, the higher reinforcement ratio and the higher slab depth led to a steeper load-reinforcement strain response; however, it also resulted in a decrease of the maximum reinforcement strains. The higher concrete strength not only resulted in a stiffer load-reinforcement strain response but also a higher ultimate reinforcement strain.

The reinforcement strain of the GFRP bars was significantly affected by the cracking of concrete. Reinforcement is assumed to carry all of the tensile force at the cracks; however, concrete would continue to carry the tensile load between the cracks through bond between the reinforcement and the concrete; this is called tension stiffening. As Figure 4-3 shows, the GFRP strain was linear before cracking and dramatically changed after the cracking in a non-linear manner affected by the gauge location and the crack width.

The tension stiffening effects of the concrete on the slab reinforcement could be assessed using the concave parts of the load-strain curves as suggested by Hallgren (1996). This phenomenon is very important in understanding the behaviour of GFRP reinforced slabs and requires further investigation.

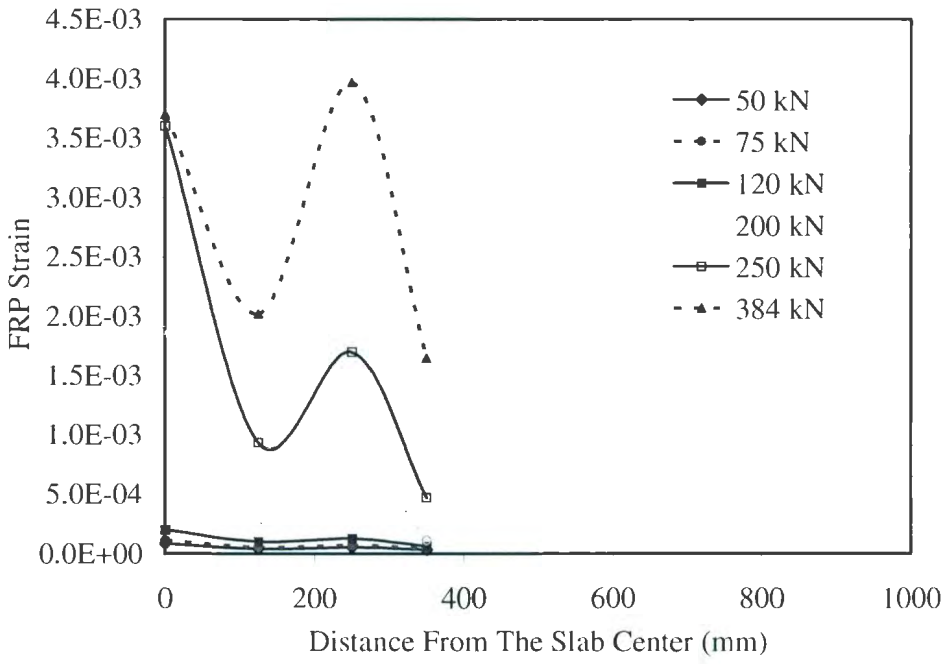

Figure 4-2: GFRP Strain Profile Specimen 3 Series 1

4.3 Load-deflection Characteristics:

The central load-deflection relationship was obtained from the LPDTs placed at the centre of the slab. The load deflection curves are shown in Figures 4-4 and 4-5 for both series. At the time of testing, the load was paused at certain intervals to map the cracks. When the system was put on hold, the load's readings were decreased slightly due to the relaxation of the slab's internal stresses. Thus, the load deflection graphs are not very smooth. However, this will not affect the slab's capacity.

The load-deflection curve of the GFRP reinforced slabs consisted of two linear characteristic portions with an initial crack formation, showing a completely different behavior than the steel reinforced slabs. The tested slab load-deflection characteristics are similar to previous normal strength concrete slabs reinforced with GFRP bars (Rashid, 2004). The slope of the load-deflection curve was normally steep before the formation of the first crack. This indicates the higher stiffness of the uncracked slab.

As the applied load was increased, the initial cracks formed and the slab experienced a slight gradual loss in stiffness at this transition stage. At the end of the transition stage, the stiffness of the slab decreased dramatically compared to that in the uncracked stage. Afterwards, the slope of the load-deflection curve was almost constant and started to decrease close to failure as shown in Figure 4-6.

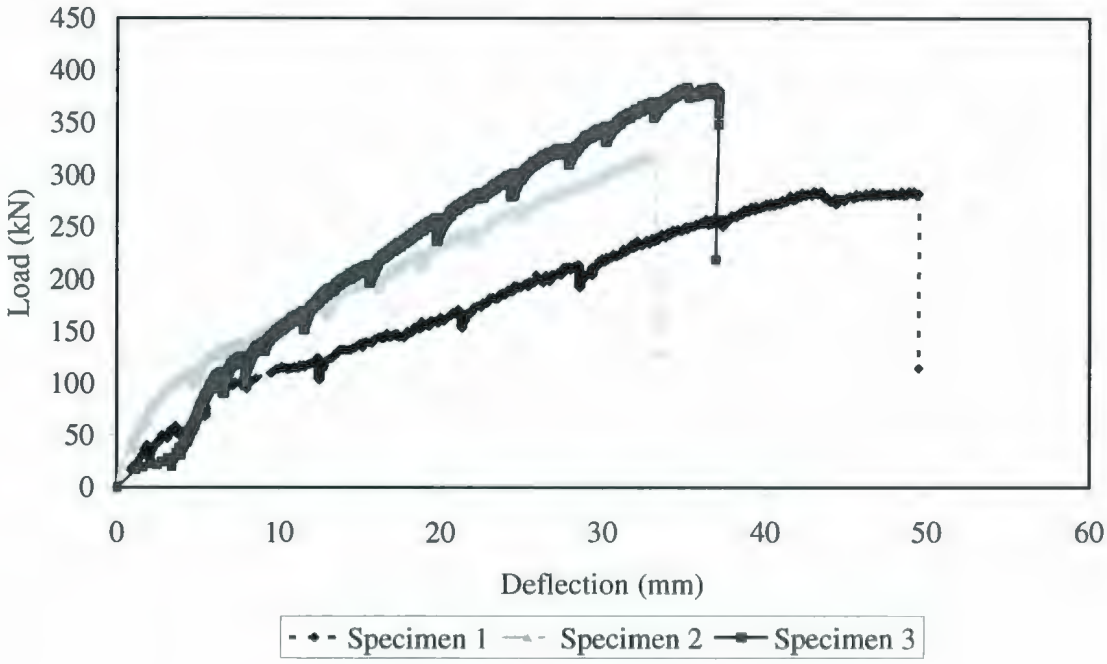

Figure 4-4: Load-Deflection Curves Series 1

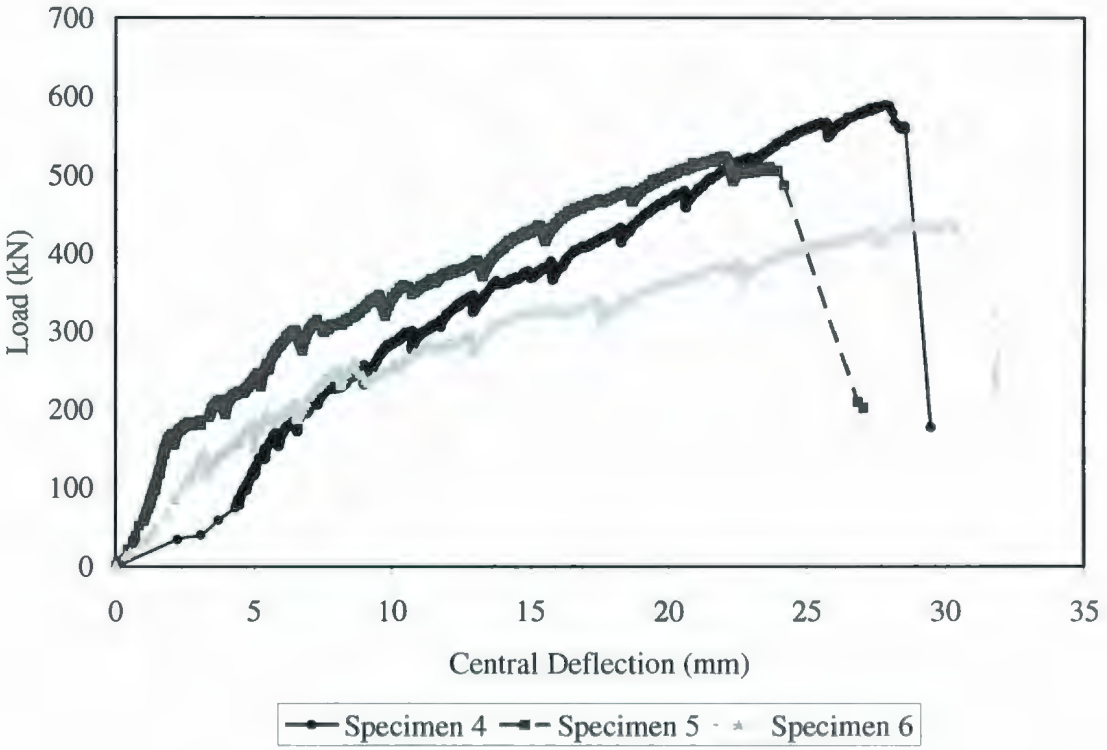

Figure 4-5: Load-Deflection Curves Series 2

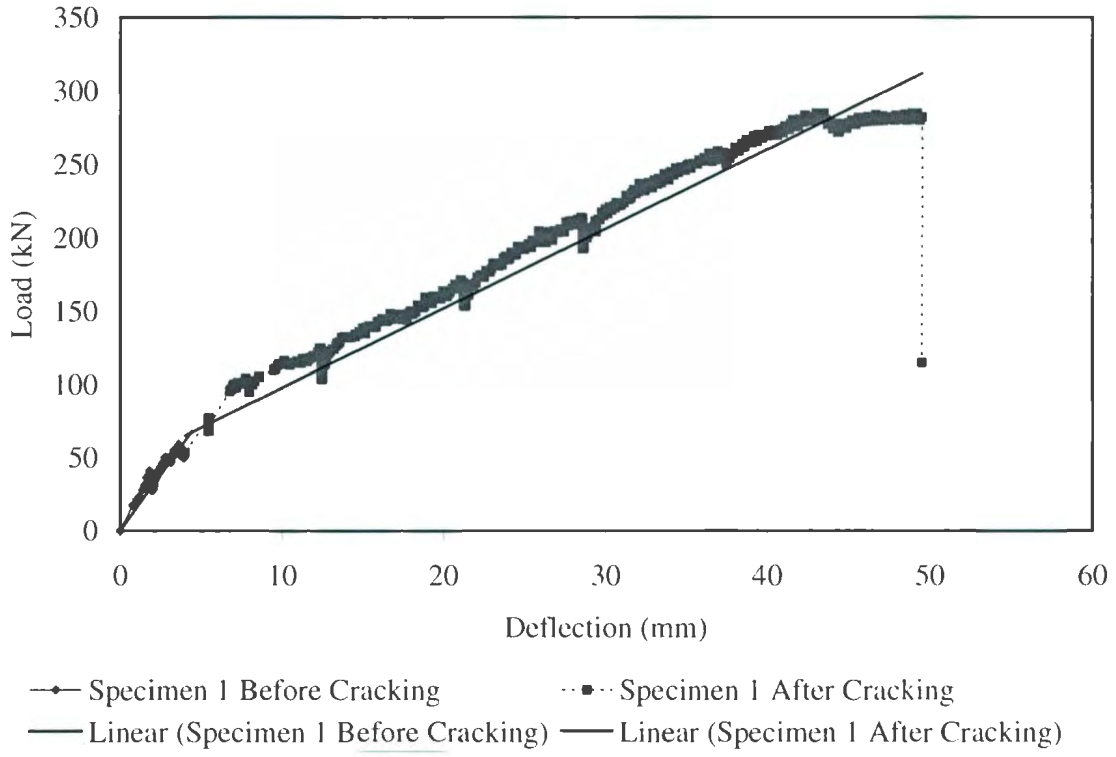

Figure 4-6: Load vs. Central Deflection Specimen 1

The deflection profiles shown in this chapter are similar for all the tested slabs; two specimens' results, one from each series, are shown in Figures 4-7 and 4-8. The deflection profile curves show acceptable deflections within the serviceability limit, and the service load is represented by the third curve in both graphs. The slabs showed excessive deflection after cracking, which indicates the lower stiffness of the cracked slabs.

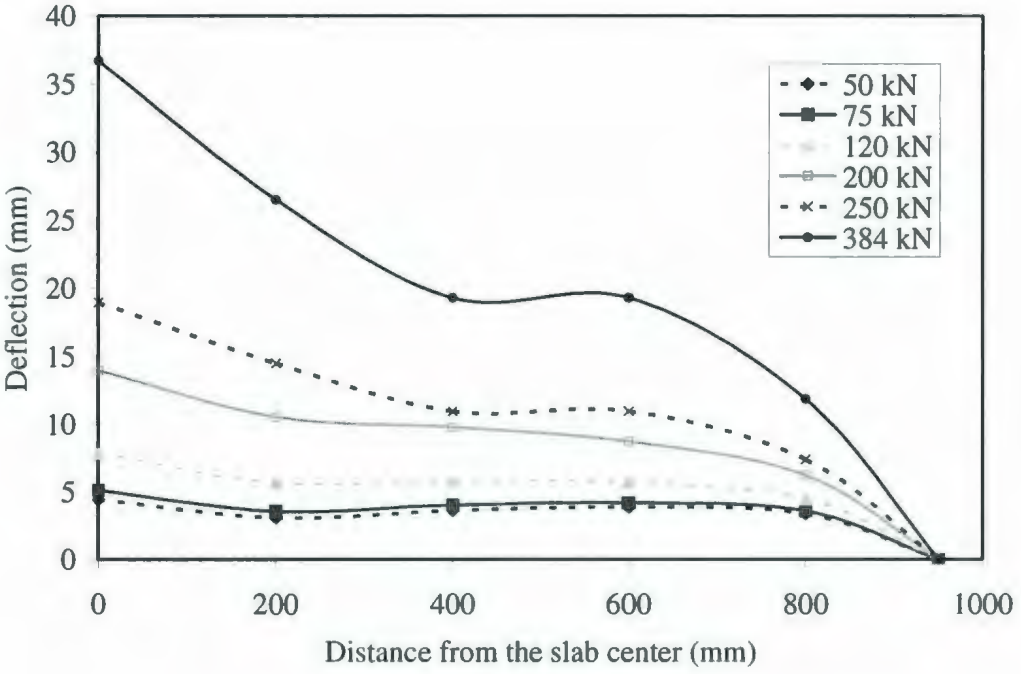

Figure 4-7: Typical Deflection Profile Series 1 (Specimen 3)

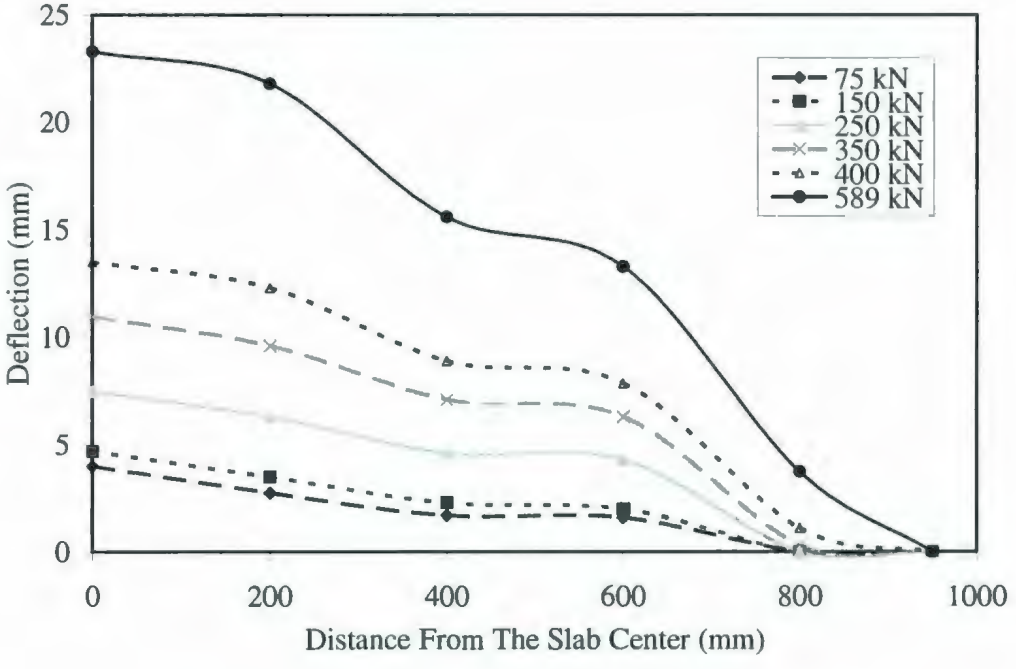

Figure 4-8: Typical Deflection Profile Series 2 (Specimen 4)

The load- deflection curve can indicate the failure mode for the slab, as defined by Marzouk and Hussein (1991). In the load-deflection graphs shown above, a positive slope up to the failure load is indicated, and the failure appears suddenly. This phenomenon is a clear sign of punching shear failure; this confirms the fact that all the slabs were designed to fail under punching shear, as explained in the experimental program.

The stiffness of the slabs in Series 1 increases as the reinforcement ratio increases. Observation of the experiment shows that, for Series 1, the slabs with a lower reinforcement ratio deflected more, showing more ductility. When increasing the slab thickness, as in Series 2, the slab stiffness shows an increase that is accompanied by less deflection and higher section capacity.

The effect of the slab thickness and the clear concrete cover can indicate that the higher the thickness of the slab the higher the stiffness. However, more ductility was recorded for the slab that has the same reinforcement ratio and different thickness, as shown in Figure 4-9.

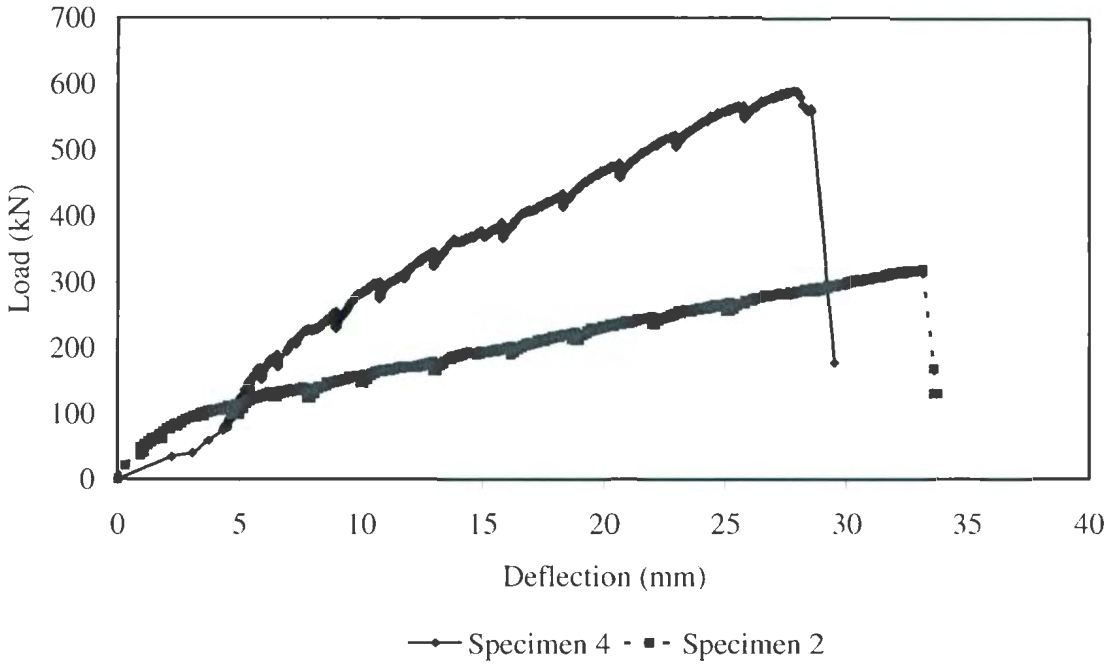

Figure 4-3: Load-Deflection Curves Specimen 2 vs Specimen 4

4.4 Crack Width Measurements:

The first crack formed in the slabs at a load ranging from 50 to 192 kN (11 to 45 Kips), which is 18 to 39% of the ultimate load as shown in Table 4-1. The crack width was measured using LPDTs as crack width measurement gauge, as mentioned previously. The slab was initially loaded, and as soon as hair cracks started to appear, the loading was stopped and crack gauges were glued to the slabs' tension side. At each load increment, the cracks were recorded and mapped, and pictures were taken to monitor the cracks' progress spacing measurement.

The accuracy of the measurements improved as the cracks started to widen after the end of each loading step. The load that corresponds to the first visible crack is tabulated in Table 4-1. The maximum recorded crack width at each load increment was observed around the column circumference.

The values of the crack width at service loads, w_s and the ultimate loads, w_u are also reordered in Table 4-1. The load-crack width curve seems to develop in a similar manner as the load-deflection relationship for all the tested specimens. The largest measured crack width approached 4.22 mm and was obtained from Specimen 1, the slab with the least reinforcement and thickness.

Table 4-1: Cracking characteristics of the test slabs

Specimen No	Service Load (kN)	Crack Width @ Service Load w_s (mm)	Deflection @ Service Load (mm)	First Crack Load (KN)	Deflection @ First Crack (mm)	Max. Crack Width w_u (mm)
1-	114	0.3766	09.200	50.00	3.942	4.2126
2-	154	0.4544	09.487	100.00	4.821	2.8340
3-	150	0.4170	07.867	120.00	7.867	1.1813
4-	340	0.4677	12.776	172.00	6.594	2.0753
5-	339	1.0247	10.537	192.00	4.231	2.5190
6-	256	0.5557	08.545	169.00	4.991	2.4929

4.5 Serviceability:

ACI 318-02 specifies the serviceability criteria in terms of the deflection and crack width for steel reinforcement specimens as follows:

1. A serviceability deflection limit of $l/180$, where l is the member span.

2. A crack width limit of 0.4 mm. It is generally accepted that stresses in the steel reinforcement should be around 0.6 f_y at the service loads. This would correspond to a strain of approximately 1200 micro-strains ($\mu\varepsilon$) for grade 400 steel.

These criteria are set to control the width of the crack and to limit it to a value of approximately 0.4 mm. ISIS (2001) recommends that the strain at service loads for GFRP reinforced beams or one-way slabs, ε_f should not exceed 2000μE. Table 4-1 shows the service loads, P, the crack width, w, and the service deflection, at a strain of 2000 μE for the test slabs.

The service load of the test slabs were in range of load 114 to 340 kN that corresponded to 2000 micro strains. The values of the service loads reported were at the range of 28% of the ultimate strain reported for Specimen 2, reinforced with ρ_b, to 50% for the other specimens.

The service deflections varied from 8.55 to 12.78 mm. As shown in Table 4-2, the corresponding crack widths at the service load were in the range of 0.38 to 0.56 mm. These values satisfy the cracking requirements at the service loads recommended by ACI committee 440 (2003). ACI 440.1 R-03 recommendations state that the maximum crack width of GFRP reinforced members could be about 1.5 to 1.7 times the value allowed for steel reinforced members (0.6 - 0.7 mm).

The service load of the GFRP reinforced slabs is very sensitive to slab depth. The average service load of the low depth slabs was about 45% lower than that of the high depth slabs. The reinforcement ratio had little influence on the serviceability of the slabs of Series 1.

4.6 Ultimate Capacity:

Table 4-2 shows the ultimate load, P, and the corresponding ultimate deflection for the test slabs. A comparison of the ultimate capacity of slab Specimen 1 and the reference slab, having the same geometry, reveals that using GFRP bars dramatically decreases the capacity. The ultimate load of the GFRP slab was 47% lower than the reference specimen ultimate capacity; the maximum deflection of the GFRP slab was 55% higher than the deflection of the reference slab. This behavior can be easily explained by the lower modulus of elasticity of the GFRP.

The test results reveal that reinforcement ratio has a slight effect on the load carrying capacity of the GFRP reinforced slabs. Ignoring the small variation of the concrete strength of the two Series tested, it can be seen that increasing the reinforcement ratio increased the ultimate load-carrying capacity of slabs of Series 1 by 12% and 37% when the reinforcement ratio increased by of 25% and 50%, respectively, over the slab of Specimen 1 designed with reinforcement ratio of 1%. The ultimate deflection decreased as the reinforcement ratio was increased. A significant decrease of 48% of the ultimate deflection was observed in the GFRP concrete slabs when the reinforcement ratio was increased by 25%.

The slabs of Series 2 have a constant reinforcement ratio of 1.2% and different concrete covers, whereby the clear concrete covers were 30, 45 and 60 mm. Specimens 5 and 6 in Series 2 show decreases of 15% and 35% of the ultimate carrying capacity compared to Specimen 4. From this observation, one can conclude that the clear concrete cover has an inverse effect on the slabs' carrying capacity.

On the other hand, the effective slab depth had a significant effect on the ultimate capacity. With an increase of the effective slab depth from 150 to 200 mm, the load carrying capacity of the slab specimen 4 in Series 2 increased by 85%, combined with a decrease in the ultimate deflection of 23%, compared to Specimen 2 in Series 1; see Figure 4-9.

Table 4-2: Deflection characteristics of the test slabs

Series No	Experiment No	Ultimate Load (kN)	Ultimate Deflection (mm)
1	1	282	46.000
	2	319	33.128
	3	384	36.765
2	4	589	29.500
	5	487	24.216
	6	437	30.173

4.7 Stiffness, Ductility and Energy Absorption Characteristics:

As mentioned earlier, the stiffness of a slab represents the amount of load needed to produce a unit displacement at the centre of a slab. The initial stiffness K_i is the tangential value of the slope of the load-deflection curve at the uncracked stage. The cracked stiffness K_{cr} is calculated as the average tangential value of the slope of the load-deflection curve after the transition stage has ended.

The values of K_t and K_{cr} are tabulated in Table 4-3. From the table, it is apparent that the slabs had a stiffer response before and after cracking when the reinforcement ratio and the slab depth were increased. Among all variables, the changing of the slab depth yielded the most prominent influence on the stiffness.

Ductility is traditionally defined as the ratio of the deflection at the ultimate load to that at the yield load for structures with traditional steel reinforcement. Ductility also describes the deformation ability of a structure from the service limit state to the ultimate limit state. Since GFRP bars do not exhibit any yield characteristics, a service load strain could be used instead of the traditional definition. ISIS (2001) recommends an allowable strain at service load of $2000\mu\varepsilon$. Thus, this value is adopted to define the ductility index for the test slabs.

The values of the ductility indexes of all test slabs are summarized in Table 4-3. The results show that the ductility of the GFPR reinforced slabs is considerably affected by the reinforcement ratio and the slab effective depth. The ductility of slabs in Series 1 decreased by 45% and 63% when the reinforcement ratio was increased by 25 and 50 %, making clear that the reinforcement ratio seems to have a strong influence on the ductility.

Table 4-3: Stiffness, ductility, energy absorption

Series No	Experiment No	K_t kN/mm	K_{cr} kN/mm	Ductility index Δ_u/Δ_y	Energy Absorption kN.mm
1	1	21.204	5.845	12.7	7173
	2	25.910	7.495	6.9	6042
	3	31.988	9.464	4.67	8184
2	4	39.414	18.882	4.23	10332
	5	46.563	21.20	5.54	8382
	6	42.067	21.25	4.52	8501

The clear concrete cover has a slight effect on the ductility index; in Series 2, the ductility index increased by 30% and 7% when the clear concrete cover increased from 30 mm to 45 mm and 60 mm, respectively. On the other hand, the slab thickness decreased the ductility index by 40% when the slab depth increased from 150 mm to 200 mm.

The energy absorption capacity is defined as the area under the load-deflection curve. The values of the energy absorption are shown in Table 4-4. The energy absorption capacity of the GFRP reinforced slabs increased as the reinforcement ratio was increased.

A comparison of slabs Specimen 1 and Specimen 3 in Series 1 indicates that the energy absorption capacity increased by approximately 14% as the reinforcement ratio was increased by 50%. The energy absorption capacity slightly decreased with increasing of the slab effective depth.

A comparison of slabs Specimens 4, 5 and 6 of Series 2 shows that there was an 18% decrease in this capacity when the clear concrete cover was increased. The effect of the slab thickness on the energy absorption capacity is clearly noticeable; an increase of 71% was experienced when the slab thickness was increased from 150 mm to 200 mm.

4.8 Cracking and Failure Characteristics:

The developing cracks were traced on the test slabs as the load was applied. The first cracks were observed along lines parallel to the horizontal reinforcement passing through the column stub on the tension surface of the slabs. These cracks were followed by the formation of similar cracks in the vertical direction. As the load was increased, cracks running roughly around the column circumference were formed, followed by the first diagonal crack that reached the corner of the slabs.

Normally, yield-line cracking patterns occur in a steel reinforced slab due to the yield characteristics of the steel reinforcement. However, as for the GFRP specimens, when the

load reached approximately 60% of the ultimate load of the GFRP reinforced slabs, the diagonal cracks reached all four corners and a pattern similar to flexural yield-line patterns clearly formed, especially for the slabs with low reinforcement ratio and high strength concrete.

As the load increased to failure, there were few new cracks appearing on the surface of the slab. Approaching the ultimate load, some audible sounds were heard for all test slabs. This could be due to the separation of the flexural reinforcement mesh from the surrounding concrete at that point. Spalling was observed in all of the tested slabs. As the ultimate load was reached, a punching cone developed for all the slabs.

The crack patterns at failure are shown in Figure 4-11 to Figure 4-15. Within the outline of the punching cone at failure, the crack patterns of the GFRP reinforced slabs exhibited a pattern that vaguely matched the layout of the GFRP bars, while the crack patterns of the reference slab closely matched the layout of the steel bars.

Figures 4-11 to 4-15 show the crack patterns of the tested slabs of Series 1 and 2. The formation of orthogonal cracks matched the reinforcement mesh and the yield line crack pattern in all slab of Series 1. This observation reveals that bar spacing has a significant effect on the formation of the crack patterns and the development of the flexural behaviour of the slab.

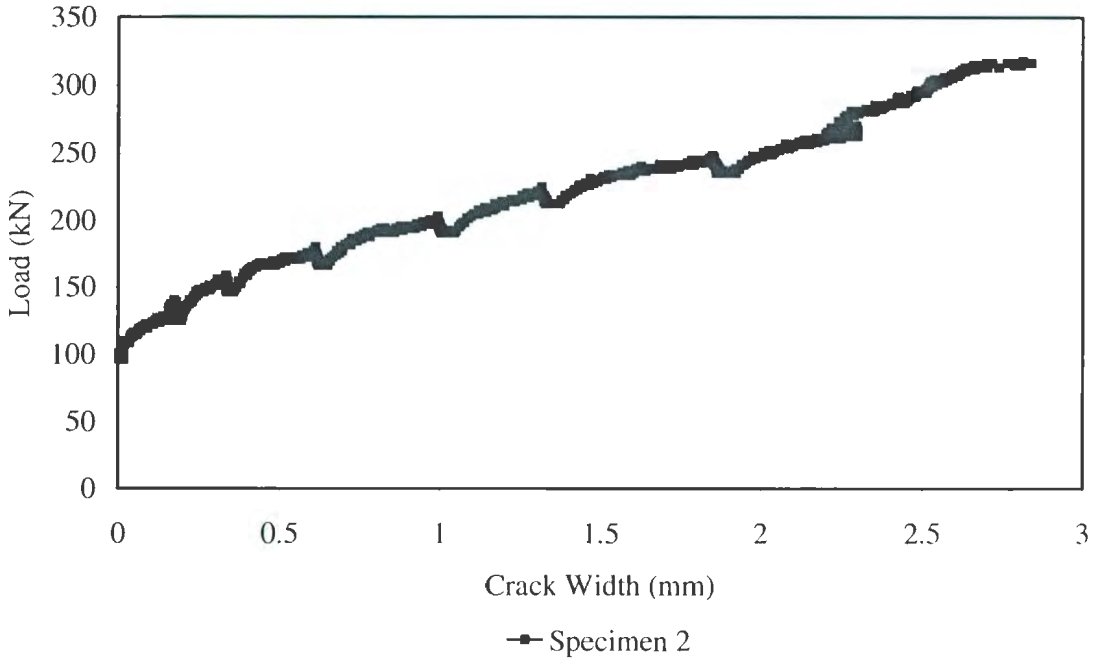

Figure 4-4: Load vs. Crack Width Specimen 2 Series 1

4.9 Failure Modes:

The failure modes of any reinforced two-way slab can be divided into two main modes, as defined by Marzouk and Hussein (1990). The first mode is the flexural failure mode that represents the exhaustion of the flexural capacity of the slab at failure and the yield of the steel or bond slip failure.

Figure 4-5: Crack pattern of Specimen 1

Figure 4-6: Crack pattern of Specimen 2

Figure 4-7: Crack pattern of Specimen 4

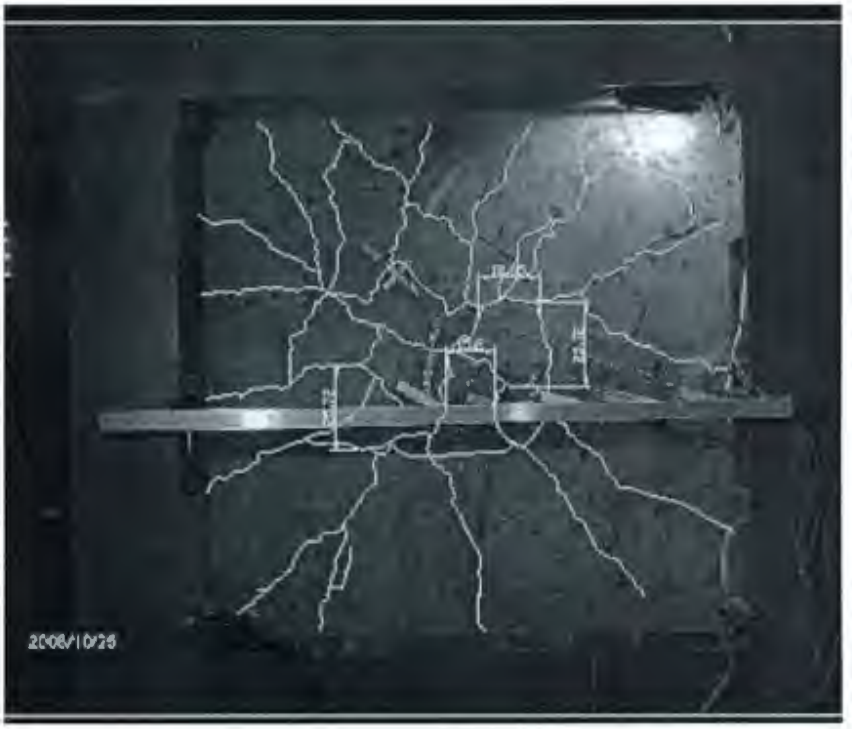

Figure 4-8: Crack pattern of Specimen 5

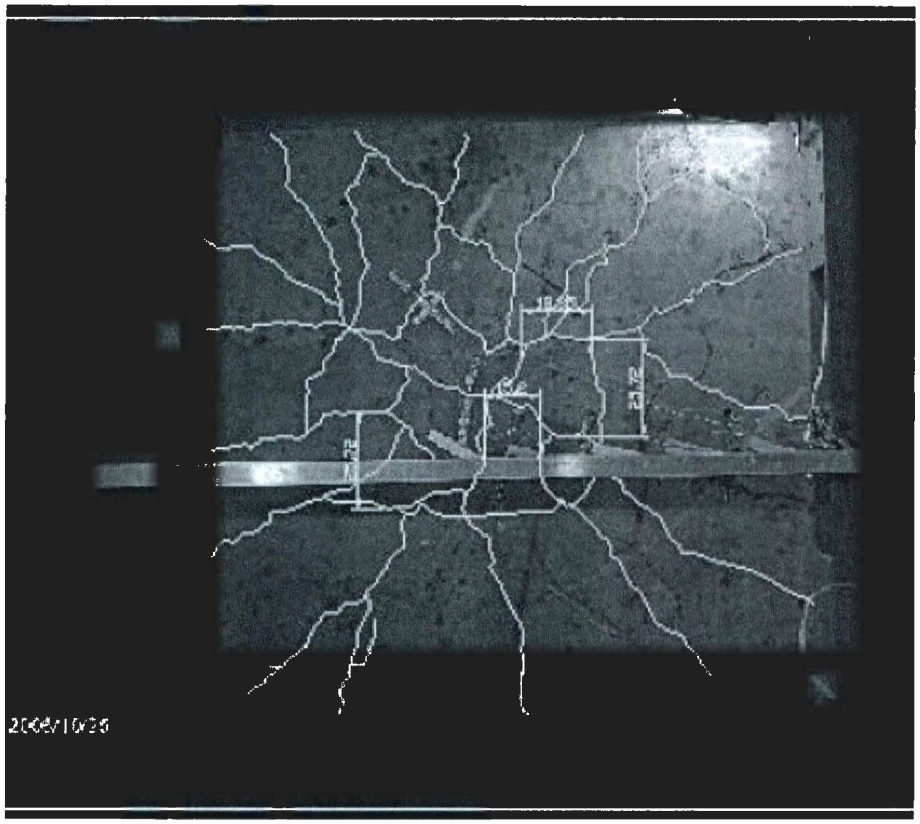

Figure 4-9: Crack pattern of Specimen 6

This flexural mode of failure should not occur in GFRP reinforced slabs due to the code recommendation that all GFRP flexural members should be over-reinforced (ISIS 2001; ACI 440.1R-03). On the other hand, flexural failure could also occur as a result of concrete crushing that is characterized as a flexural failure in compression. This compression flexure failure is allowed by the code for GFRP reinforced members.

The second mode of failure in a two-way slab is the punching shear failure mode that is triggered by the diagonal tension cracks developing inside the concrete around the column vicinity prior to the rupture of the reinforcement or crushing of the concrete.

Punching shear failure can be also subdivided into two types based on ductility and crack patterns. One type would be defined as a ductile punching failure or the flexural punching failure. The pronounced flexural behaviour in terms of yield-line crack patterns and the gradual load-deflection development can be observed in this type of failure. Nonetheless, the slab would fail before its flexural capacity is reached. The second type is the pure punching failure that leads to localized crack patterns and a sudden failure.

In the current study, punching cones were formed in all slabs without clear evidence of concrete crushing at the compression side. Also, no rupture of the GFRP bars was observed. This indicates that punching shear failure occurred in all slabs. However, the reference slab with steel reinforcement failed in flexure. On the other hand, the GFRP reinforced slabs showed a ductile punching failure.

The cracks in the tested slabs matched the reinforcement layout, and in particular, in the punching cone. This could be attributed to the small bar spacing of slabs. In all of the tested slabs, the cracks formed in a fashion similar to a yield-line crack pattern mechanism, and few localized cracks were observed.

Typically, as the ultimate load was reached, the slab started to fail due to the column penetrating through it. The strains in the GFRP bars did not reach the ultimate strain value, and therefore, the GFRP bar did not rupture. The strain readings from the concrete gauges on the compression side indicated that the concrete did not reach the crushing strain limit of approximately 0.0035.

However, a crack was observed around the column on the compression surface of slabs. It is difficult to differentiate whether the crack was formed because of flexure compression failure or due to the column punching through the slab. The same observation was reported by Hussein and Rashid (2004) for two-way slabs reinforced with GFRP bars, and was also reported by Hussein and Zhang (2006) for two-way slabs reinforced with CFRP.

4.10 Performance Evaluation of using High-Strength Concrete for GFRP Reinforced Slabs:

In the following section, the results of two slabs tested in the present investigation will be compared to the results of two slabs from previous research. GS2, a normal strength concrete slab reinforced with GFRP, was tested by previous investigators (Rashid, 2004). NS, a normal strength concrete slab reinforced with conventional steel, was tested by Marzouk and Ebead (2004). Both specimens were constructed and tested at MUN's structural laboratory.

The compared slabs have the same geometry and reinforcement ratio, but were reinforced with different reinforcement types (GFRP and Steel) and have different concrete compressive strengths (High and Normal); see Table 4-4. Only Specimen 2 in Series 1 had a slightly higher reinforcement ratio of 1.2%, compared to NS a normal strength slab reinforced with steel.

Table 4-4: Deflection characteristic of the reference slabs, and energy absorption

Title	f_c' MPa	ρ %	Reinforcement Type	Ultimate Load (kN)	Max.Deflection (mm)	Energy Absorption kN.mm
Specimen 1	66.8	1.00	GFRP	282	46.00	7173
Specimen 2	62	1.2	GFRP	319	32.128	6024
Reference Slab	70.0	1.00	STEEL	603	35.00	12128
GS2*	35.0	1.05	GFRP	218	38.00	5886
NS**	36.0	1.00	STEEL	420	24.50	5950

*Rashied (2004)
**Ebead and Marzouk (2004)

A normal strength concrete slab with a steel ratio of 1.00% provided an ultimate load of 603 kN and 24.75mm deflection. When normal strength concrete slab was reinforced with the same rate of 1.00% of GFRP, the ultimate load was only 218 kN and 38mm

deflection; when high strength concrete was used with GFRP at the same reinforcement ratio, the slab ultimate load capacity improved to 282 kN and the maximum deflection increased to 46mm. When the reinforcement ratio was increased to 1.2% with high strength concrete, the ultimate load capacity improved to 319 kN and the maximum deflection decreased to 32mm.

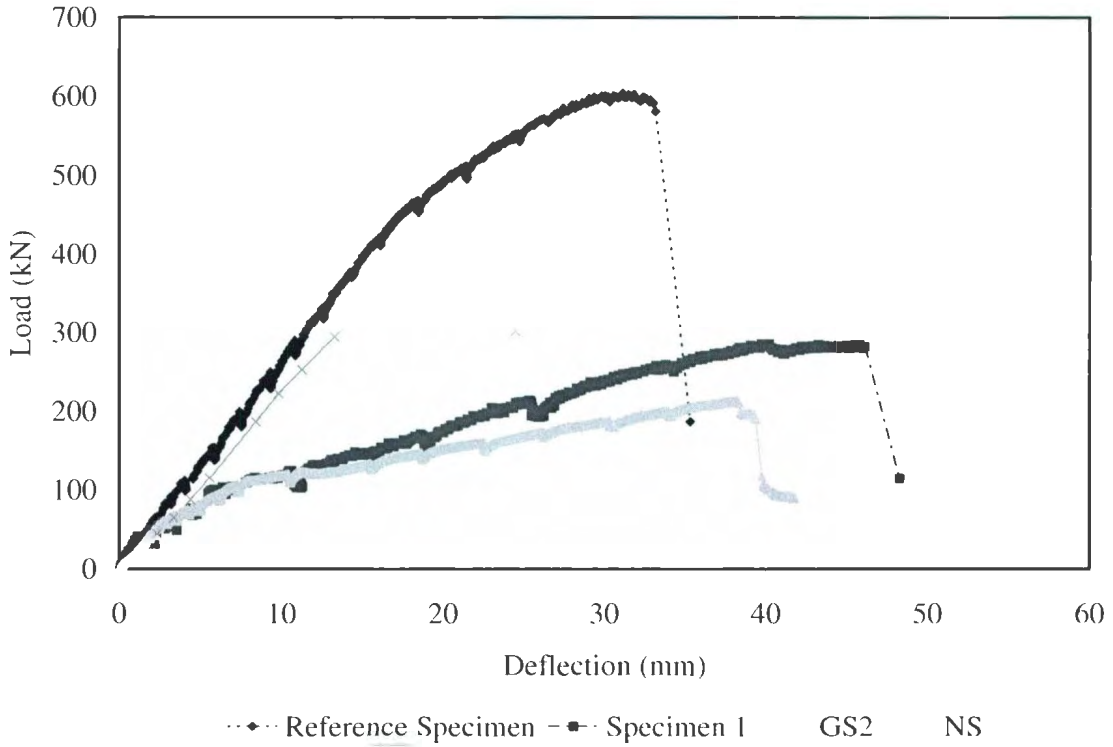

Figure 4-10: Load-Deflection Curves Reference Slab, Specimen 1, NS, and GS2

The ultimate load capacity was lowered from 603 kN to 218 kN when GFRP was used as the main reinforcement instead of conventional steel. However, for Specimen 1, when high strength concrete slab that reinforced with GFRP from the current study was used, the ultimate load increased to 282 kN from 218 kN for the normal strength concrete slab.

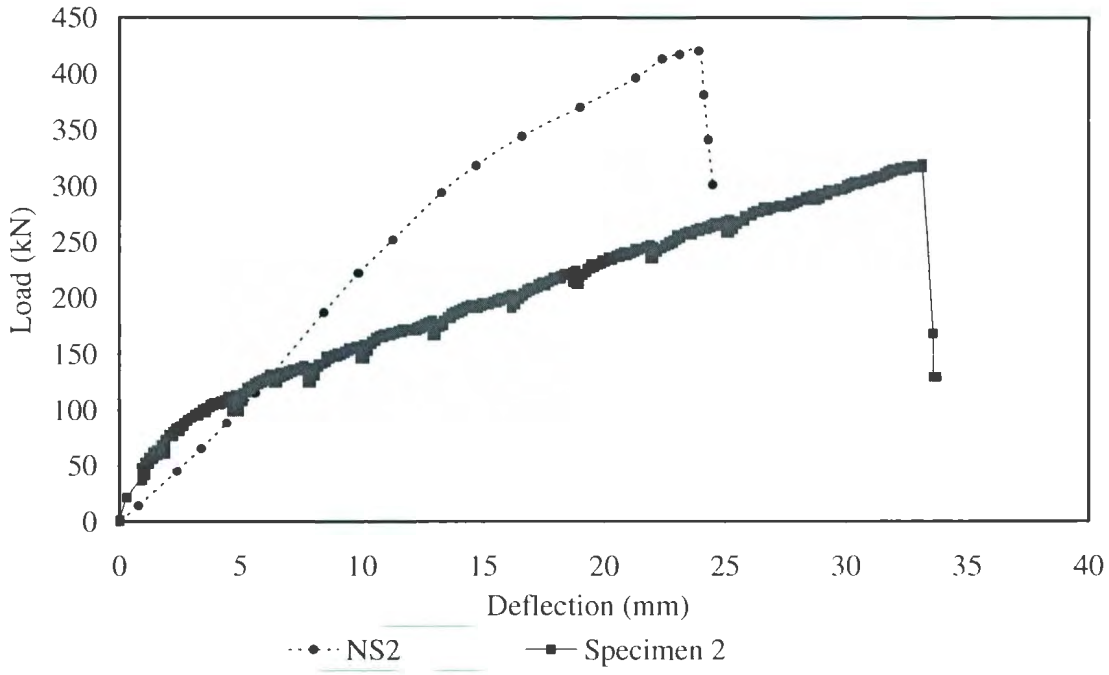

Figure 4-11: Load-Deflection Curves Specimen 2 and NS

When the reinforcement ratio increased to 1.2% for GFRP with the use of high strength concrete, the ultimate load carrying capacity is improved further as recorded, with Specimen 2 reaching 319 kN.

The ultimate capacity of Specimen 2 is comparable with the NS slab; the reduction in the ultimate load was only 30%, and the maximum deflection of Specimen 2 was more than NS by 35%. However, the energy absorption was the same for both specimens. The failure mode was punching shear for both specimens, though it was more ductile for the specimen reinforced with GFRP.

Therefore, it can be concluded that in order to achieve a good structural performance comparable with a normal strength slab reinforced with steel, high strength concrete with a higher GFRP reinforcement ratio is recommended.

Chapter 5

5 Numerical Investigation

5.1 Introduction:

The main objective of this chapter is to develop a cracking model for two way plates reinforced with GFRP under flexure loads and to verify the experimental results. A total of seven slabs were tested at MUN's structural lab. The results of all the tested slabs were analyzed and presented in the previous chapter.

The cracking behavior of the high strength two-way slabs reinforced with GFRP rebars is one of the main objectives of this research. A modified expression for the crack spacing and crack width formula is recommended to compensate for the differences in GFRP physical properties. In this chapter also, a finite element model using ABAQUS (version 6.5) was used to verify the load deflection response.

5.2 Crack Width and Crack Spacing Calculation Procedures:

The formation and evolution of cracks due to imposed tension or flexure for GFRP reinforced concrete members is conceptually similar to that in steel-reinforced members. However, major differences are expected due to GFRP's lower stiffness and brittle nature. This reflects in the bond behavior of GFRP and on concrete's tension stiffening effect. In this study, only flexure cracking will be considered.

5.2.1 Crack Spacing Calculations:

To calculate crack spacing, this study adopts the formula used for concrete members reinforced with conventional steel rebars, according to the Canadian Standard Association S 474-04 clause 9.3.5, and the same expression was previously recommended by NSF, the Norwegian Standards Association, NS 3473E (1992).

The average crack spacing, s_m, of cracks normal to the reinforcement shall be calculated using the following equation:

$$s_m = 2(c + 0.1s) + k_1 k_2 d_{bc}' h_{ef}\, b/A_s \qquad (5.1)$$

where,

c = concrete cover mm

s = bar spacing of the outer layer of the bars, mm

d_{be} = equivalent bar diameter of the outer layer of the bars

h_{ef} = effective embedment thickness taken as shown in Figure 5-1

b = width of the section

A_s = area of reinforcement within the effective embedment thickness

k_1 = coefficient that characterize the bond properties of the reinforcement

k_2 = coefficient that account for the strain gradient

The above expression addresses the most important variables considered to affect the cracking behavior of the reinforced concrete members agreed upon. The factors that have the most influence on the cracking behavior, according to scientists and engineers, are the clear concrete covers, the reinforcement ratio and the bond stresses.

The above expression can be divided into two terms, where the first part of the equation takes into account the clear concrete cover and the reinforcement ratio reflected in the bar spacing, assuming a perfect bond condition, and the second term addresses the bond effect on the cracking behavior, assuming a bond slip condition.

As mentioned earlier, the equation has been used successfully to calculate the mean crack spacing for concrete members reinforced with conventional steel rebars. In order to be

used in calculating the mean crack spacing for concrete members reinforced with GFRP as the main reinforcement, some modifications were applied to the second term to compensate for the difference of GFRP's physical properties, as compared to steel rebars.

The effect of the bond on the behavior of reinforced concrete members was recognized by Ospina et al. (2001) and Dimitrios (2007), and their studies resulted in the application of a 45% reduction for the bond value calculated, assuming a perfect bond condition.

In ongoing research at Memorial University of Newfoundland, Sabrah et al. (2007) recognized the effect of lower bond properties on reinforced concrete panels tested under direct tension. With strong experimental evidence, Sabrah et al. (2007) concludes that the effective tension zone for a GFRP bar is only 3 to 3.5 times the bar diameter. The tension zone, as defined and recommended by the present codes of practice for concrete members reinforced with traditional steel, is 7.5 times the bar diameter.

The effective embedment thickness for concrete members reinforced with steel, as defined by the Canadian Standard Association CSA 474-04, is shown in Figure 5-1. To compensate for the lower bond properties of GFRP, the effective embedment area was reduced to 40% of the value calculated, assuming a perfect bond condition.

The recommended modification was obtained by dividing the effective tension zone for the GFRP bars by the one for steel rebars, when the effective tension zone for GFRP was

taken as 3 times the bar diameter, which leads to the modification adopted and used in the crack spacing calculation in the present investigation.

For simplicity of calculation, the product of the constants k_1 and k_2 is taken as 0.1, according to the Canadian Standard Association CSA 474-94.

The analytical procedure to calculate the mean crack spacing of FRP slabs consists of the following steps:

1. The effective embedment thickness would be calculated as per Figure 5-1, and then the aforementioned reduction to 40% would be applied.
2. The constant k_1 and k_2 are taken as 0.1
3. The aforementioned modification and simplification to equation would be incorporated (5.1)

Thus, the new equation for FRP slabs is:

$$s_m = 2(c + 0.1s) + 0.04 d_{be}' h_{ef}\, b/A_s \qquad (5.2)$$

Comparison between calculated using the above mentioned equation and measured mean crack spacing is presented in Table 5-1.

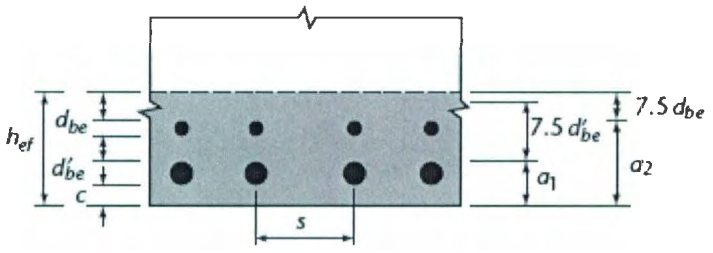

Figure 5-1: The effective embedment thickness

5.2.2 Crack Width Calculations for GFRP Reinforcement:

The current expressions used in calculating the crack width for concrete members are merely empirical in nature. The majority of design provisions to calculate crack width in members with FRP are based on modifications of statistical models made according to the Gergely-Lutz equation. The new expression by ISIS M04-00 (2001) suggests calculating crack width for members reinforced with FRP using the following equation:

$$w = 11\times10^{-6}\sigma_{frp}K_b\frac{h_2}{h_1}\sqrt[3]{d_c A} \qquad (5.3)$$

where,

w = the crack width at the tensile face of the beam, mm

E_s = modulus of elasticity of the steel, MPa

σ_{frp} = stress in the tension FRP reinforcement at location of the crack, MPa

h_2 = the distance from the extreme tension surface to the neutral axis, mm

h_1 = the distance from the centroid of tension reinforcement to the extreme tension surface, mm

d_c = concrete cover measured from the centroid of tension reinforcement to the extreme tension surface, mm

A = effective tension area of concrete surrounding the flexural tension reinforcement, having the same centroid as that reinforcement, divided by the number of rebars, mm^2

K_b = a bond coefficient, taken as 1.0 for FRP bars with bond properties similar to those of steel, greater than 1.0 for FRP bars with inferior bond quality, and less than 1.0 for FRP bars with superior bond qualities.

The Canadian Standard for the design of FRP-reinforced concrete structures, CSA S806-02, controls crack widths by limiting a factor, z, which is defined as

$$z = K_b \frac{E_s}{E_f} \sigma_{fr} \sqrt[3]{d_c A} \qquad (5.4)$$

where,

σ_{frp} = stress in the tension FRP reinforcement at location of the crack, MPa

E_s = modulus of elasticity of the steel, MPa

E_f = modulus of elasticity of the FRP, MPa

d_c = concrete cover measured from the centroid of tension reinforcement to the extreme tension surface, mm

A = effective tension area of concrete surrounding the flexural tension reinforcement and having the same centroid as that reinforcement, divided by the number of rebars, mm^2

K_b = a bond coefficient, taken as 1.2 for FRP bars with bond properties similar to those of steel

The maximum values recommended by the CSA S80602 for z are 45000 and 38000 N/mm, for interior and exterior exposure, respectively, and K_b is a bond coefficient equal to 1.2 for FRP bars with bond properties similar to steel deformed bars.

These z values are equivalent to maximum allowable crack widths of about 1.5 times greater than those allowed for both interior and exterior exposure conditions by CSA A23.3-04 for the design of steel-reinforced concrete members. The increase in the allowable crack width limits for FRP-reinforced concrete members has been driven by the superior corrosion resistance of FRP reinforcement.

In this investigation, the tension chord model was modified to account for the lower bond properties of the GFRP used as main reinforcement.

5.2.3 Modified Tension Chord Model:

This model is set up in terms of a simple yet complete formulation of the deformation process undergone by a reinforced concrete member by integrating the actual steel and concrete strains between cracks. Earlier formulations of the procedure were presented by Leonhardt (1977). Concepts from these procedures constitute the basis of the crack width calculation design rules for reinforced concrete members in CEB/FIP MC 90. The model has been lately the subject of considerable refinement and simplification by Sigrist and Marti (1994), Alvarez (1998), and Marti et al. (1998), who adopted the "Tension Chord Model" name.

One major feature of the tension chord model is the bond-slip constitutive relationship for steel. Acknowledging that the exact distribution of stresses in concrete and steel is not of primary interest, as long as the resulting steel stresses and overall member strains reflect governing influences and match experimental data, Marti et al. (1998) use a rigid perfectly plastic bond-slip relationship with a stepped descending branch that depends on the yielding of steel.

Since the amount of slip in steel-reinforced concrete members is not significant at service load levels, CEB/FIB MC90 proposes a rigid-perfectly plastic bond-slip relationship for the serviceability design of steel-reinforced concrete members:

$$\tau_b = 1.8 f_{ctm} \qquad (5.5)$$

where,

f_{ctm} = defined as the mean tensile strength of concrete

τ_b = bond stress, MPa

The model assumes that if the concrete stresses between cracks under maximum crack spacing conditions reach f_{ct}, a new crack will form midway between those spaced at s_{max}. As a result, the mean crack spacing in the stabilized crack formation stage is bounded by the following limits:

$$(s_{min} = \frac{s_{max}}{2}) \leq s_m \leq s_{max}$$

or

$$0.5 \leq \lambda = \frac{s_m}{s_{max}} \leq 1.0$$

where,

λ = a parameter introduced by Marti et al. (1998)

s_m = mean crack spacing, mm

s_{max} = maximum crack spacing, mm

The mean crack spacing is

$$s_m = \lambda s_{max} = \frac{\lambda f_{ct} \phi_b}{2\tau_{b0}} \left[\frac{1-\rho_s}{\rho_s} \right], \; 0.5 \leq \lambda \leq 1.0 \qquad (5.6)$$

s_m = mean crack spacing, mm

ϕ_b = bar diameter, mm

f_{ct} = concrete tensile strength, MPa

ρ_s = reinforcement ratio

τ_{bo} = bond stress, MPa

The tension chord model overcomes this problem by assuming that the mean crack width in the stabilized cracking stage can be calculated as

$$w_m = s_m(\varepsilon_{sm} - \varepsilon_{cm}) \tag{5.7}$$

where s_m is the mean crack spacing, ε_{sm} is the mean steel strain, both at the given load level, and ε_{cm} is the mean concrete strain at the end of the single crack formation phase. Based on the concrete stress distributions,

$$\varepsilon_{cm} = \frac{\lambda}{2}\frac{f_{ct}}{E_c} \tag{5.8}$$

That leads to

$$w_m = s_m\left[\varepsilon_{sr} - \frac{\lambda}{2}\frac{f_{ct}}{E_s}\frac{(1+\rho_s(n-1))}{\rho_s}\right] \tag{5.9}$$

The above equation evaluates crack width at the reinforcement level. In slabs reinforced with traditional steel, however, the cracks that matter are those at the tension face. These crack widths can be obtained by multiplying the same equation by $\left[\frac{h - x_d}{d - x_d}\right]$, where x_d is the neutral axis depth.

Implementing the tension chord model to high strength concrete two-way slabs reinforced with GFRP as the main tension reinforcement to calculate the crack width at the service load level, the expression used in this study is as follows:

$$w_m = s_m\left[\varepsilon_{sm} - \frac{\lambda}{2}\frac{f_{ct}}{E_c}\right] \qquad (5.10)$$

where,

E_c = the modulus of elasticity of the concrete.

f_{ct} = the concrete tensile strength, MPa

The mean crack spacing s_m is calculated as mentioned previously.

f_{ct} = defined as the concrete tensile strength computed according the following formula:

$$f_{ct} = 0.3\left(f_c'\right)^{2/3} \qquad (5.11)$$

The service load limit for GFRP reinforcement has been defined in the previous chapter, which corresponds to the reinforcement strain limit of $2000\times10^{-6}\ \varepsilon_f$.

To account for concrete tension stiffening, the following term is introduced to the formula that is used to calculate crack width;

$$\frac{\tau_b s_m}{\phi_b E_f} \qquad (5.12)$$

where,

τ_b = bond stress, MPa

s_m = the mean crack spacing, mm

E_f = the modulus of elasticity for the reinforcement, MPa

ϕ_b = bar diameter, mm

To account for the lower bond properties of FRP, a reduction to 40% is recommended to equation (5.12). Applying the aforementioned modification to the calculated bond strength and incorporating equation (5.12) into expression (5.10) to account for the tension stiffening effect, the new expression used to calculate the crack width at the reinforcement level for GFRP slabs is as follows:

$$w_m = s_m\left[\varepsilon_{sm} - \frac{0.4\tau_b s_m}{\phi_b E_f} - \frac{\lambda}{2}\frac{f_{ct}}{Ec}\right] \qquad (5.13)$$

where,

τ_b = bond stress, MPa

s_m = the mean crack spacing, mm

E_f = the modulus of elasticity for the reinforcement, MPa

ϕ_b = bar diameter, mm

E_c = the modulus of elasticity of the concrete.

f_{ct} = the concrete tensile strength

ε_{sm} = the mean steel strain

Finally, the crack on the concrete tension face is calculated by multiplying the expression above by the factor, $\left[\frac{h - x_d}{d - x_d}\right]$

The characteristic crack width should be calculated according to the formula below:

$$w_k = 1.7 w_m \qquad (5.14)$$

The above equation was used to calculate the crack width at the serviceability limit state and compared to those ones measured at the laboratory. Table 5-2 shows the results obtained using the formulas mentioned above compared with the laboratory results.

Table 5-2: Crack width calculation results and comparison

Specimen No	f_c' (MPa)	f_{ct} (MPa)	E_c (MPa)	Crack width calculated (mm)	Modified crack width (mm)	Crack width ISIS 2001 (mm)	Crack width Measured (mm)	Modified/ Measured	ISIS 2001/ Measured
1	66.80	4.94	37E3	0.342	0.473	0.56	0.377	1.26	1.48
2	62.00	4.70	35E3	0.327	0.453	0.53	0.454	1.00	1.17
3	64.00	4.80	36E3	0.289	0.403	0.50	0.417	0.97	1.19
4	64.00	4.80	36E3	0.307	0.392	0.42	0.468	0.84	0.90
5	70.06	5.10	37E3	0.426	0.604	0.60	1.025	0.59	0.58
6	67.58	4.98	37E3	0.418	0.664	0.82	0.556	1.2	1.47
Average								0.97	1.13

Table 5-1: Crack spacing calculations results and comparison

Specimen No	Specimen width (mm)	Concrete cover (mm)	Effective reinforcement area	Number of bars	Bar diameter (mm)	Reinforcement spacing (mm)	Effective Depth (mm)	Effective Depth reduced (mm)	Crack Spacing (mm) calculated	Crack Spacing (mm) measured	Crack Spacing (calculated/ Measured)
1	1900	30	2179.51	11	15.88	167.00	164.98	65.99	184.76	175	1.06
2	1900	30	2575.78	13	15.88	141.00	164.98	65.99	165.50	167	0.99
3	1900	30	3170.19	16	15.88	115.00	164.98	65.99	145.81	148	0.99
4	1900	30	3764.60	19	15.88	96.80	164.98	65.99	132.25	157	0.84
5	1900	45	3368.33	17	15.88	108.00	179.98	71.99	176.09	218	0.81
6	1900	60	2972.06	15	15.88	123.00	194.98	77.99	223.78	214	1.05
Average											0.95

5.3 Ultimate Load Calculations:

The ultimate load capacity of the high-strength two-way slabs reinforced with GFRP was verified with a finite element model using ABAQUS version 6.5.1.

5.3.1 Finite Element Analysis:

The lack of research and numerical models that describe the behavior of High-strength concrete reinforced with Fiber-glass reinforced polymer (GFRP) is the primary motivation of this study.

The nonlinear analysis of Reinforced-Concrete (RC) slabs represents an inherently complex problem caused by the following factors:

i) Nonlinear relationships of concrete and reinforcement.

ii) Cracking of concrete.

iii) Imperfect bond between reinforcement and concrete.

The experimental measurements from High-Strength Concrete and reinforcing bars tested in the laboratory were incorporated into a plasticity-based material model implemented in a finite element analysis code. The analysis is based on a smeared crack model, where

constitutive calculations are performed independently at each integration point of the finite element model.

5.3.2 Geometric Modeling:

One quarter of the slab is modeled due to geometrical and loading symmetry with an 8×8 mesh using an 8-node quadrilateral shear flexible element (thick shell) with six degrees of freedom at each node. A 2×2 reduced Gaussian integration rule is used over the element plane, and nine Simpson-type integration points are used through the thickness of the concrete slab.

5.3.3 Material Modeling:

A plasticity-based concrete constitutive model using a simple form of yield surface written in terms of the first two stress invariants is used for both materials. The model adopts the classical concepts of plasticity theory: strain rate decomposition into elastic and inelastic strain rates, elasticity, yield, flow, and hardening. The post cracking behavior is assumed based on the brittle fracture concept of Hillerborg et al. (1976), where the fracture energy is required to form a unit area of crack surface. The adopted material model is described in full detail by ABAQUS 6.5.

Cracking dominates the material behavior in the case of the tensile state of stress. A crack detection plasticity surface is used to determine the location of the crack and the orientation of the crack. The analysis is based on the smeared crack model, where constitutive calculations are performed autonomously at each integration point of the finite element model.

Once the concrete has cracked, three phenomena are evident. Namely, aggregate interlock, dowel action, and tension stiffening. Shear friction accounts for the transfer of the shear forces across a crack. As the crack width increases, the contact area of the concrete on the two sides of the crack decreases. Thus, the shear forces transferred by the aggregate interlock or the shear friction mechanism decreases.

In reinforced concrete structures, reinforcement that crosses the cracks tends to prevent the cracked pieces from separating (bond), and thus enhances the aggregate-interlock mechanisms. Moreover, any movement of cracked pieces of concrete parallel to the crack causes the reinforcement crossing the crack to transfer shear forces by dowel action. On the other hand, due to the bond effect, concrete is still capable of carrying tensile stresses in the concrete after the formation of primary cracks. As the load increases, more secondary cracks appear and tensile stresses in the concrete are related gradually.

The smeared crack model imagines the crack region to remain as a continuum but switches its initial isotropic properties over to an orthotropic medium with orthotropic properties on crack initiation. The two aspects of crack behavior that have received most

attention are the possibility of the crack changing orientation during propagation and tension stiffening.

Tension stiffening does play an important role in filling in the deflection curve by cutting out sharp stiffness drops associated with the initiation of cracking. The stiffness reflects the presence of regions of uncracked concrete as well as the cracked ones in the domain of integration. In the vicinity of the crack, the bond is completely destroyed and the tension stiffening should essentially disappear; the figure below presents the tension stiffening model used in this study.

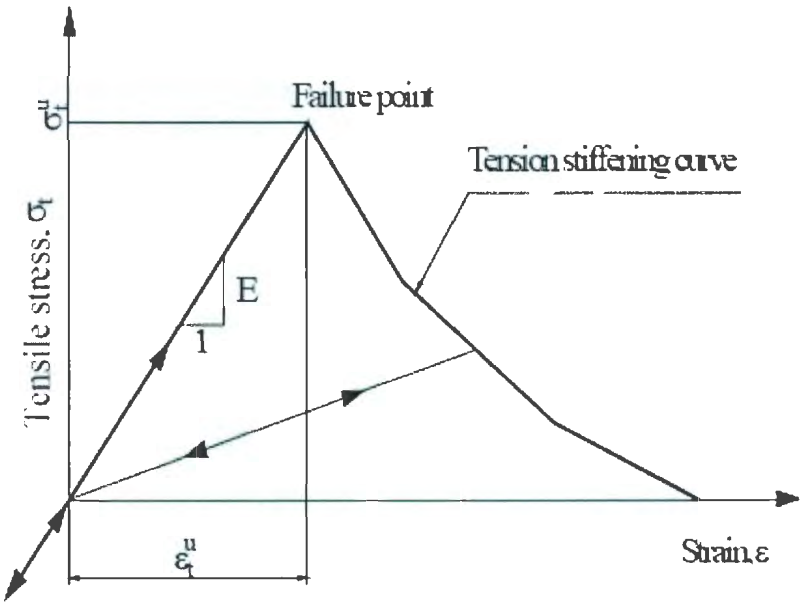

Figure 5-2 Tension Stiffening Model

5.3.4 Finite Element Analysis Assumptions:

The analytical program was carried out using ABAQUS 6.5.1 (2003) finite element program. The material properties of high-strength concrete implemented in the analysis were taken from the experimental data of an experimental program of ongoing research on high strength concrete reinforced with GFRP at Memorial University of Newfoundland.

The cylinder concrete compressive strength f_c' values used in this study were obtained from experimental data obtained at Memorial University of Newfoundland's laboratory. The concrete modulus of elasticity is calculated using the expression below:

$E_c = 4500\sqrt{f_c'}$, based on CSA-A23.3-04(Cl.8.6.2.2).

The mechanical properties of the GFRP as main reinforcement are given below:

Table 5-1: Summary of GFRP properties

Material	Bar Diameter (mm)	Area (mm^2)	Elastic Modulus (GPa)	Yield Stress (MPa)	Ultimate Stress (MPa)
GFRP	15.88	198	40.8	-	600

In finite element modeling, the smeared crack model of ABAQUS 6.5.1 (2003) was used. The material model adopted for this study was explained earlier, and the post failure for high strength concrete is modeled with the tension stiffening model shown in Fig 5-2, which allows the user to define the strain- softening- behavior for cracked concrete.

One quarter of the slab was modeled, due to the geometrical symmetry, and loaded in the transverse direction incrementally up to failure. The boundary condition of the simple support slab was represented by spring elements allowing the free corner to lift after loading.

GFRP rebars were modeled as reinforcement layers embedded in the concrete element; these layers are embedded in the concrete and located at the centerline of the actual reinforcing bars in the slabs. The layers are smeared with a constant thickness that is equal to the area of each bar multiplied by the number of bars used in each direction divided by the slab width. The GFRP, as the main reinforcing bars, were assumed to behave in a linearly elastic manner up to the failure stress, which is the ultimate tensile strength shown in Table 5-3.

The Riks algorithm is used to effectively obtain the static equilibrium solution for unstable response encountered in concrete due to concrete cracking in tension. The Riks algorithm is based on an attempt to step along the equilibrium path (the load-displacement curve) by prescribing the path (arc) length along the curve to be traversed in each increment, with the load magnitude included as unknown.

A real time monitoring of the central node that represents the tested slabs central deflection was maintained for all tested specimens, and the nonlinear behaviour of the concrete from the deflected path of the central node can be clearly noticed

Spring elements were used on the slabs edges to simulate the simply supported boundary conditions. The resultant deflected shapes obtained using the model coincides with the experimental ones in terms of the central deflection and the slabs' corners lifting up.

5.3.5 Results of the Finite Element Analysis:

The results obtained using the finite element model were ultimate load, maximum deflection, and principle stresses.

Due to the symmetry of the slab geometry and loading, the principle stresses obtained were the same in both directions, a typical two-way slab response with the same reinforcement spacing in both directions. The principle stresses are presented as stress contour.

The ultimate load and maximum deflection results obtained using FEM were presented in Table 5-4 and compared to the results obtained from the experiments. The maximum

principle stresses and the load-deflection curves for all tested specimens are presented in Figures 5-3 to 5-8.

The load-deflection curves obtained using the finite element model followed the same trend as the experimental ones. However, the transition zone between the uncracked and cracked specimen was very smooth on the FEM results. The difference between the FEM and experimental results can be easily explained, due to the use of the smeared crack constitutive model in this analysis, which results in a situation where the cracking point is not exactly identified.

Table 5-2: Finite element results and comparison

Specimen No	Load (KN)		Deflection (mm)		FEM/Experimental	
	FEM	Experimental	FEM	Experimental	Load	Deflection
1	292	282	32.56	48.00	1.04	0.68
2	340	319	34.00	33.13	1.07	1.03
3	412	384	34.00	36.77	1.08	0.92
4	620	589	20.34	29.50	1.05	0.69
5	516	487	21.00	24.22	1.06	0.87
6	468	437	25.30	37.20	1.07	0.68

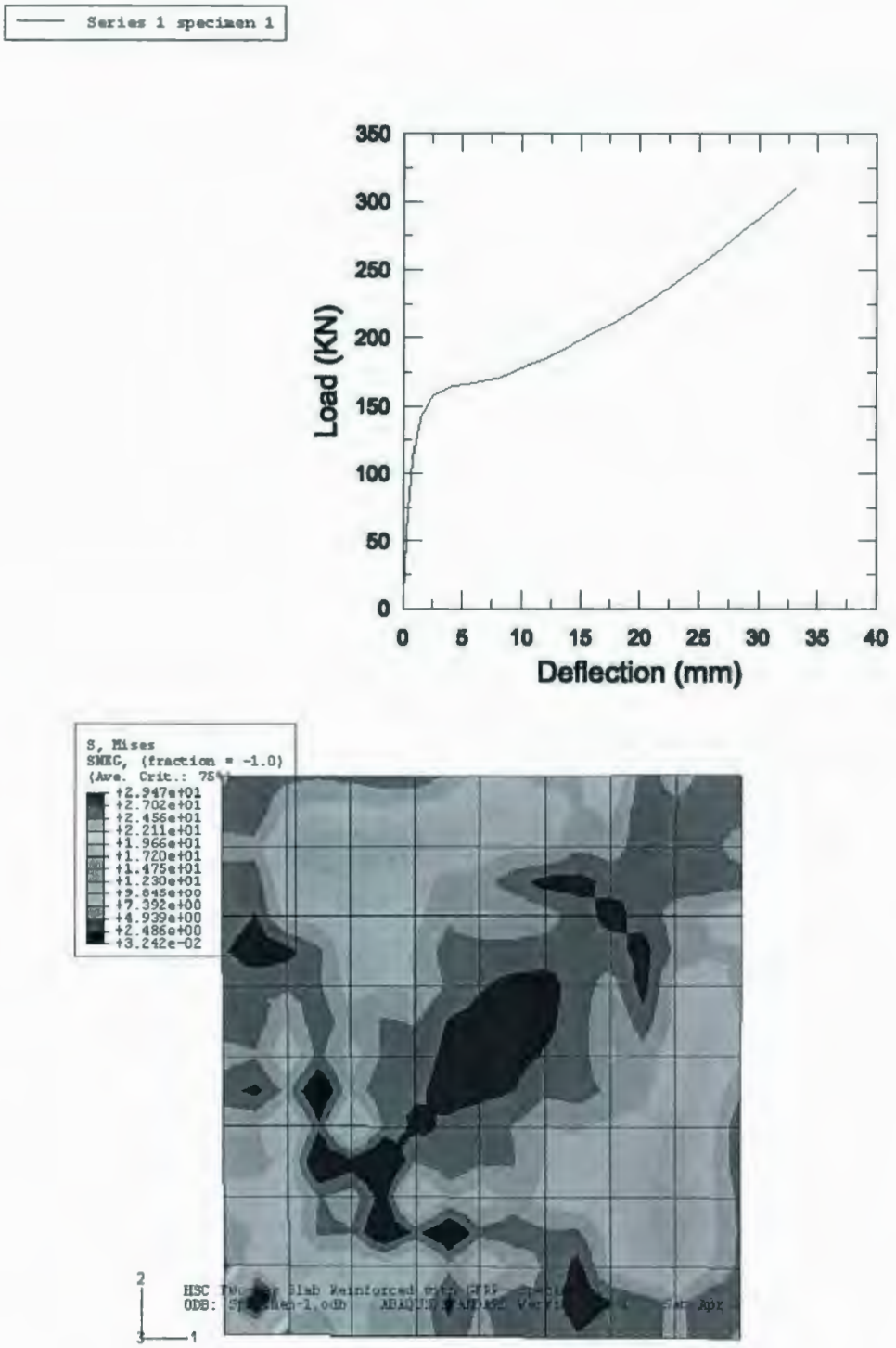

Figure 5-3: FEM results Specimen 1

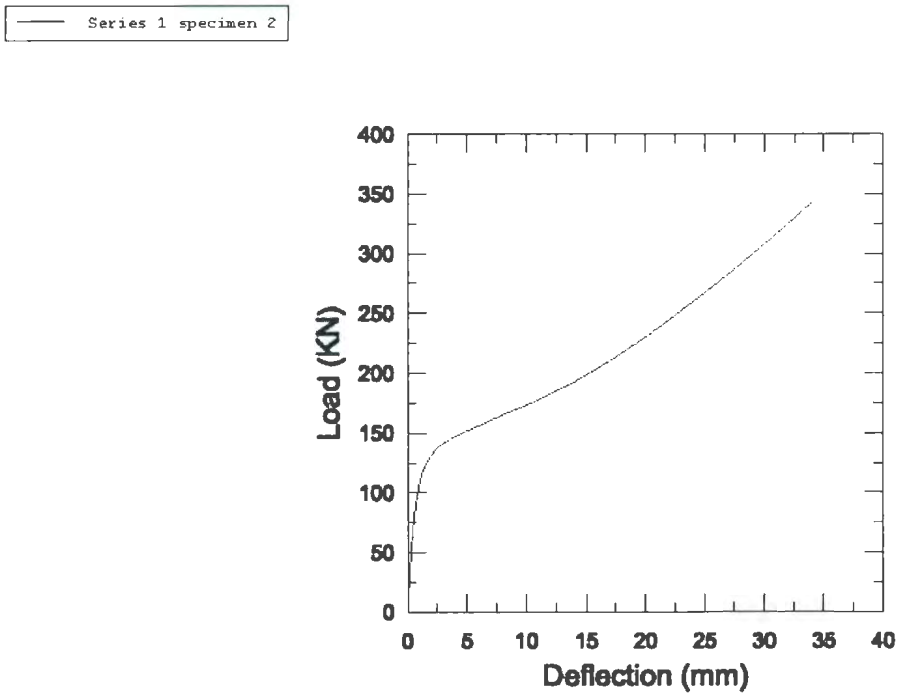

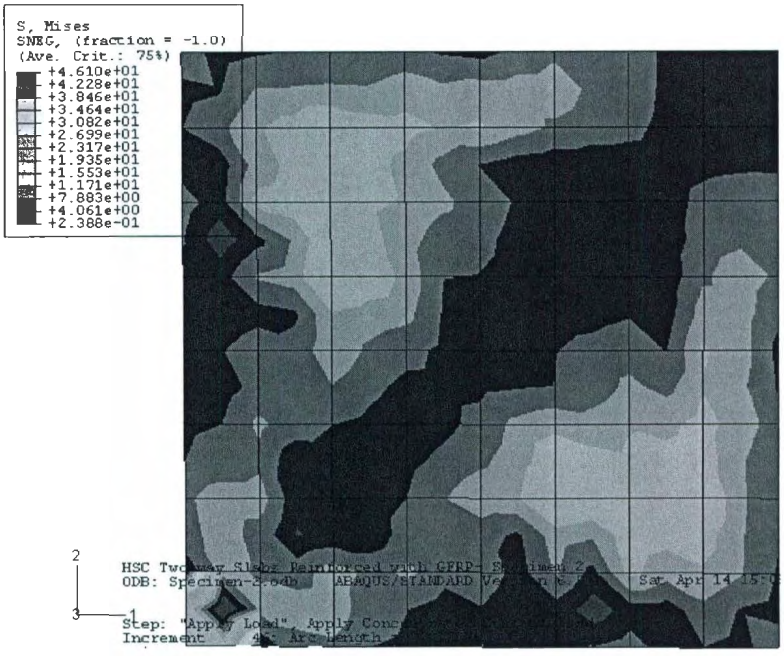

Figure 5-4: FEM results Specimen 2

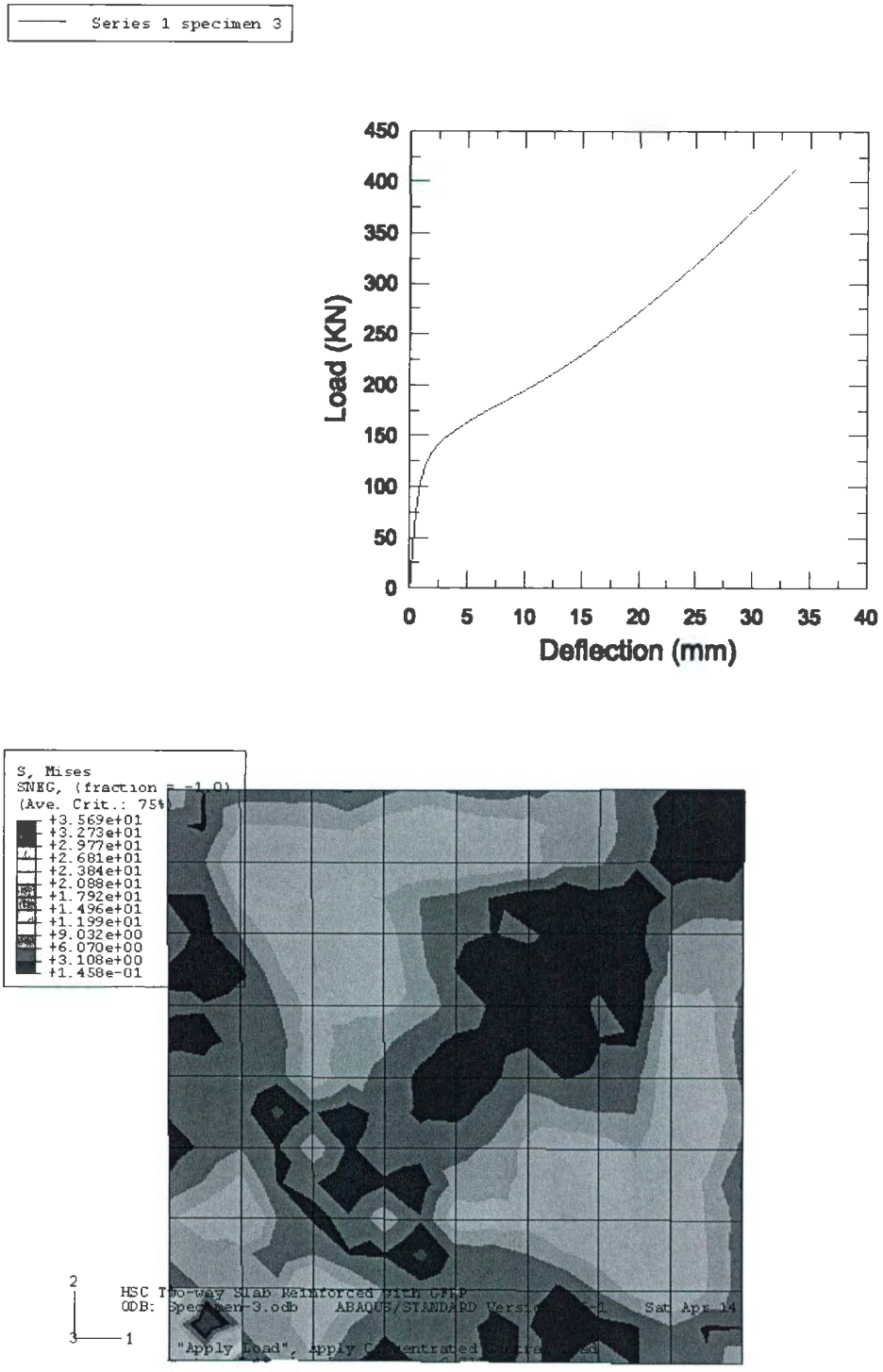

Figure 5-5: FEM results Specimen 3

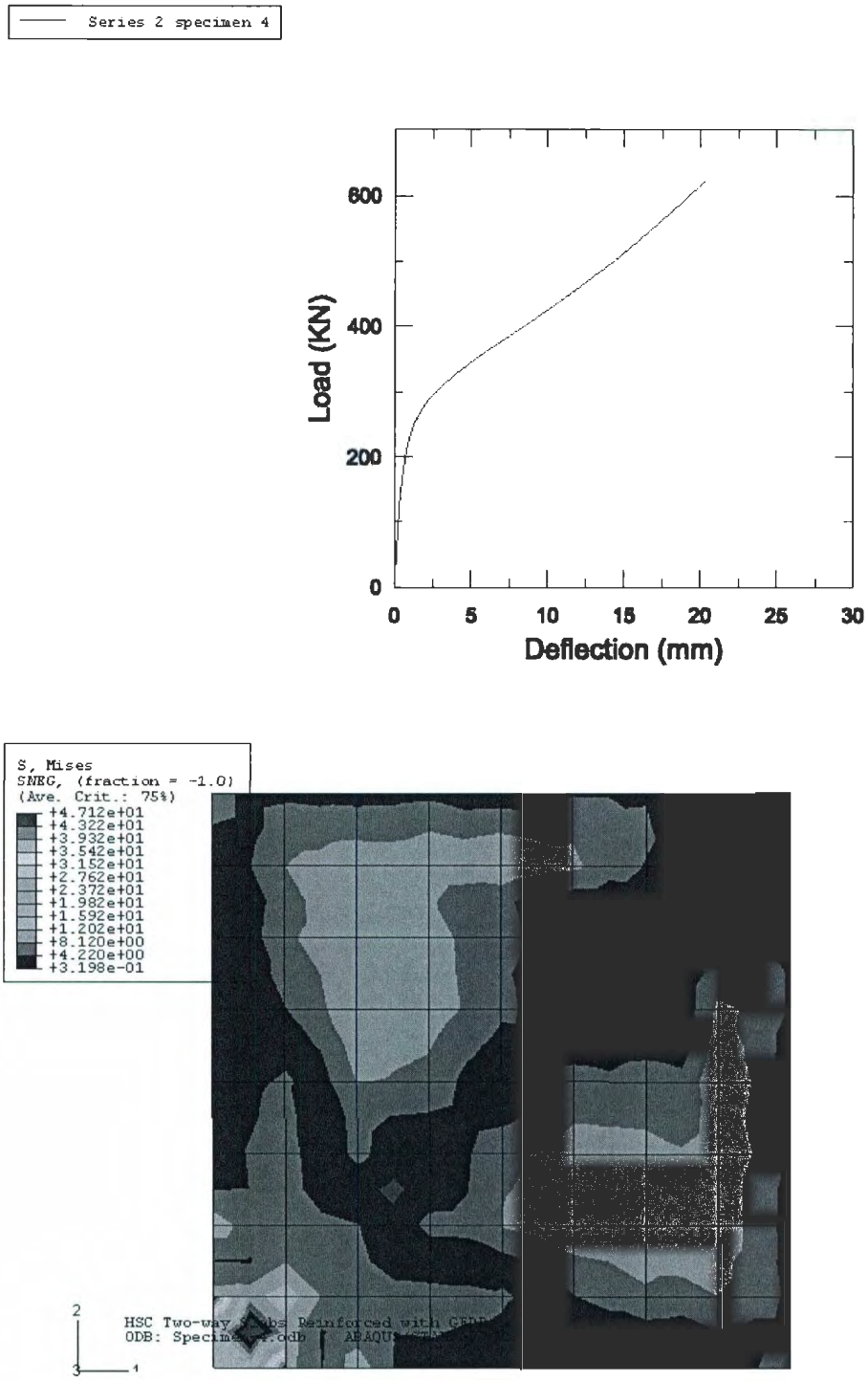

Figure 5-6: FEM results Specimen 4

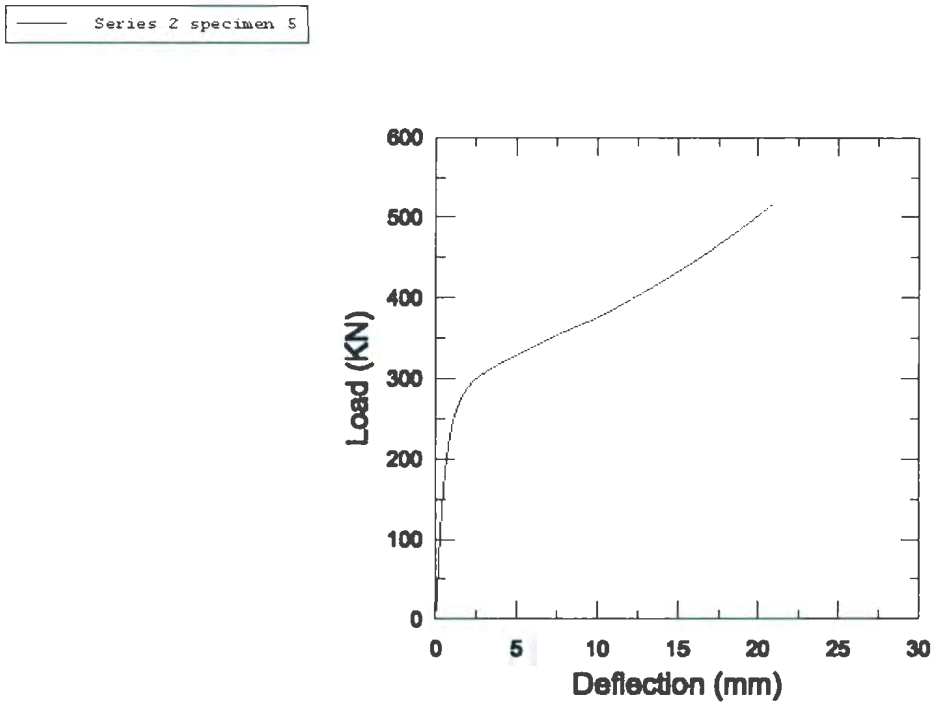

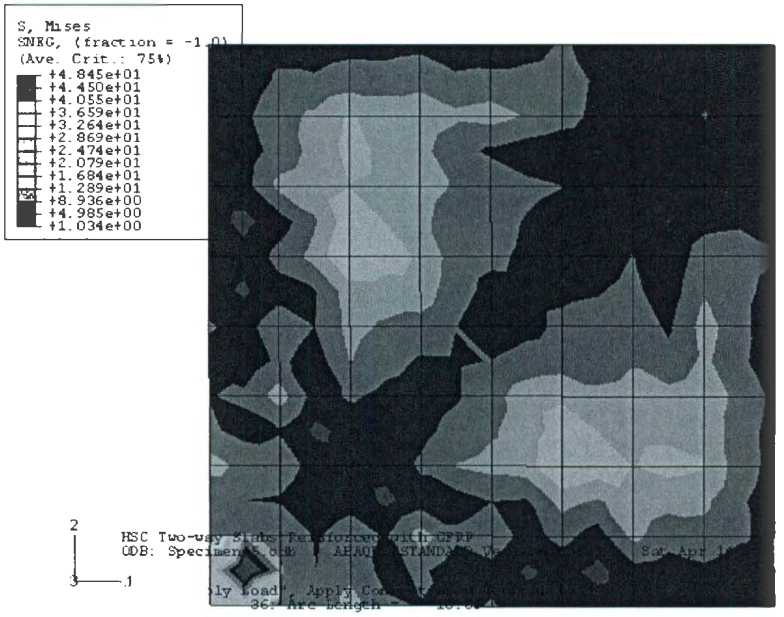

Figure 5-7: FEM results Specimen 5

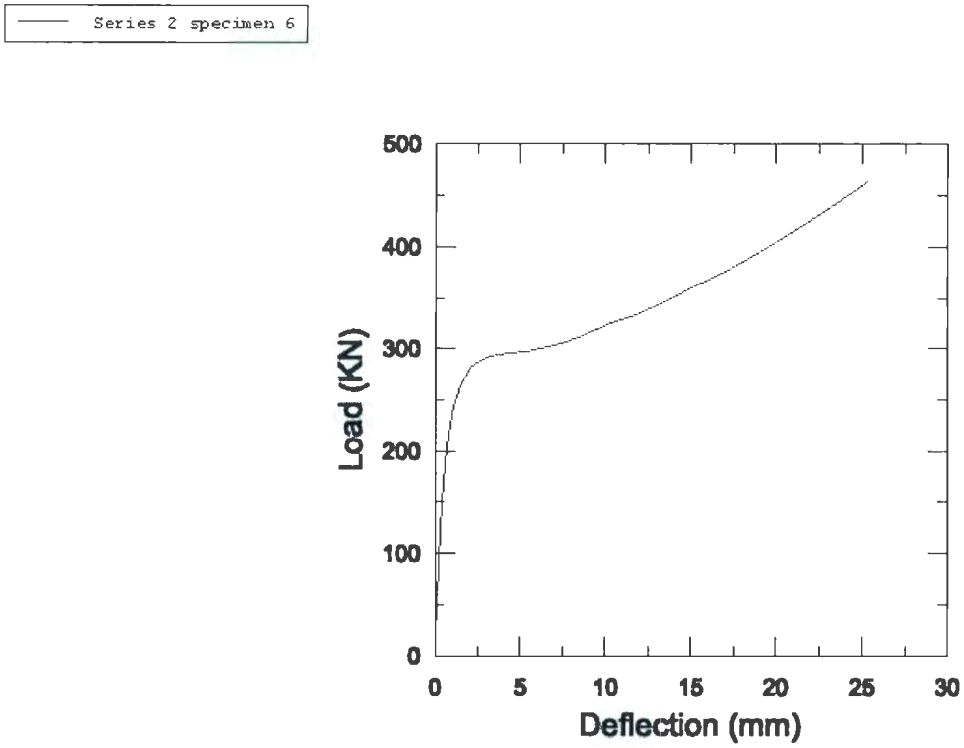

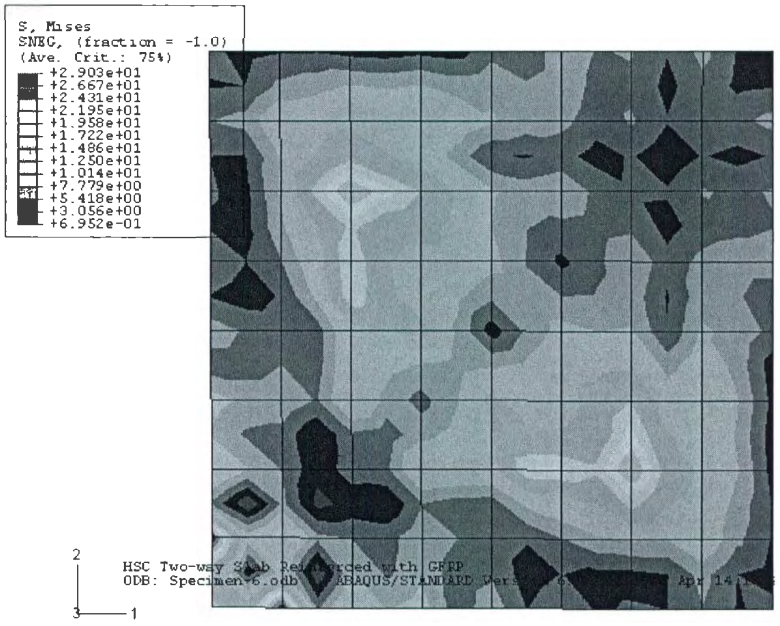

Figure 5-8: FEM results Specimen 6

In the following section, the test results obtained using the finite element analysis are compared to the experimental results and presented in terms of load-deflection graphs, as per Figures 5-9 and 5-10. The load-deflection curves obtained using the finite element model follow the same trend as the experimental ones that are bilinear in nature.

The finite element model estimated the load-deflection response with fairly good agreement. The model slightly over-estimated load deflection response for all slabs, especially before cracking; however, the model was in agreement with the experimental results.

The principle stress contours presented above are close to failure, and the maximum stresses were recorded around the columns, which indicates that the column penetrated the slab at failure.

Based on the comparison of the finite element model predictions to the experimental results presented in Table 5-4, the finite element model estimated the ultimate capacity and the maximum deflection of the high strength concrete two-way slab with reasonable accuracy with the experimental results. Therefore, it can be concluded that FE analysis can be used with confidence to predict the behavior of such slabs.

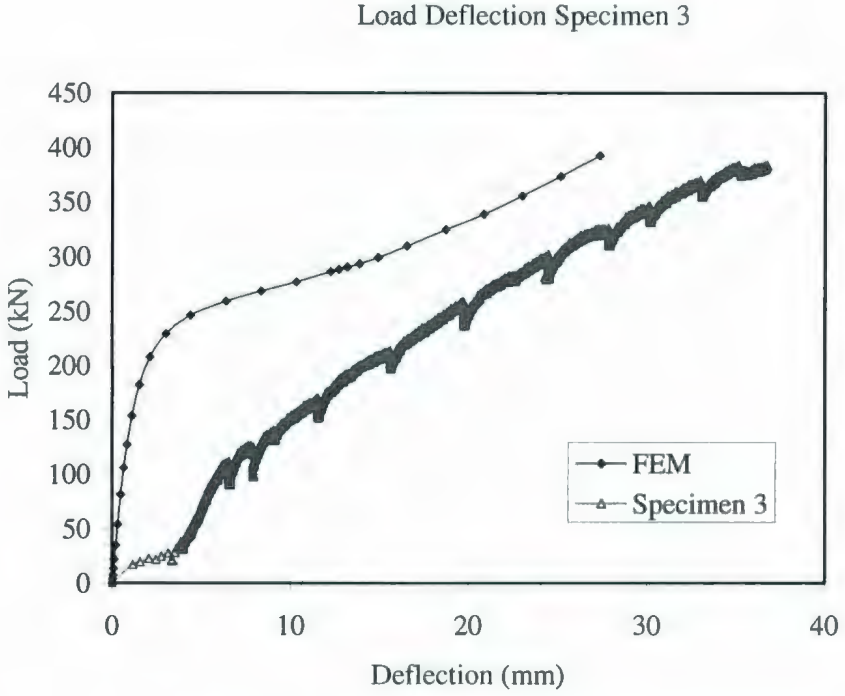

Figure 5-9: Load-Deflection relationship Specimen 3

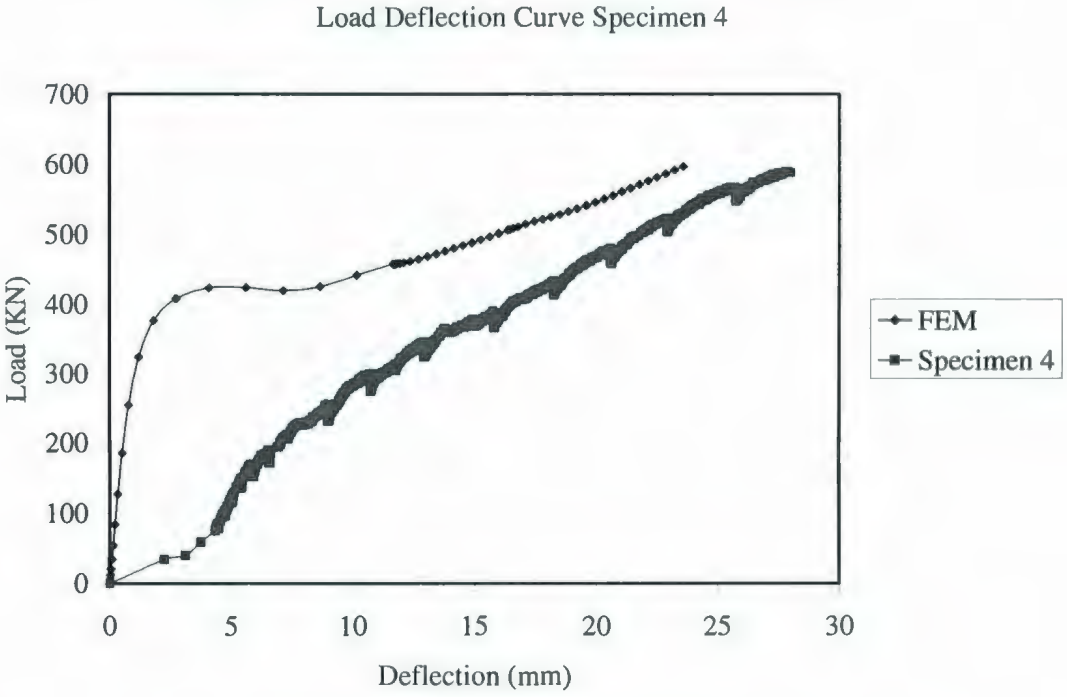

Figure 5-10: Load-Deflection relationship Specimen 4

Chapter 6

6 Summary and Conclusion

6.1 Summary:

A comprehensive experimental and theoretical investigation on high strength concrete slabs reinforced with GFRP is presented. The research work is divided into two main phases: experimental and numerical investigations.

The experimental investigation was conducted on the flexural behavior of high strength two-way slabs reinforced with GFRP, with an emphasis on cracking behavior. The experimental work was focused on the effect of the reinforcement ratio and concrete clear cover on the structural and cracking behavior of high strength two-way slabs reinforced with GFRP.

The numerical investigation consisted of two parts. The first part was on the development of modified expressions to calculate crack width and spacing. The second part was

devoted to adopting a finite element model that can predict the structural behavior in terms of the slab's ultimate capacity and maximum deformation.

6.2 Behavior of Two-way Slabs Reinforced with GFRP:

Due to the different mechanical properties of GFRP and conventional steel rebar, the flexural behavior of two-way slabs reinforced with GFRP is completely different than those reinforced with steel rebars.

As expected, the use of GFRP lowered slab ultimate carrying capacity by 47% and increased maximum slab deformation by 55%, when it is compared with a slab made of high strength concrete and conventional steel reinforcement.

The load deflection curve of the slab reinforced with GFRP is bilinear in nature, and completely different than the steel reinforced slabs. The first line represents the stiffness of uncracked slab. The second line corresponds to the stiffness of the cracked section. There is a smooth transition between the two lines, which indicates that the slabs do not completely or suddenly lose their uncracked stiffness once the first crack is formed. Increasing the reinforcement ratio resulted in increasing the load ultimate load carrying

capacity of the slab, the slab stiffness, and on the other hand, increasing the reinforcement ratio, which resulted in a lower maximum deflection

Increasing the reinforcement ratio from 1% to 1.5% increased the ultimate load from 280 to 385 kN. Therefore, an increase of 50% in the reinforcement ratio resulted in a 37% increase in the ultimate load carrying capacity of the slab. Increasing the concrete clear cover resulted in lowering the load carrying capacity and the maximum deflection for the tested slabs. Increasing the concrete clear cover from 45 to 60 mm decreased the ultimate load by 35%.

The service load for the tested slabs ranges between 114 to 340 kN, which is about 28 to 50% of the ultimate load recorded. The corresponding deflection for the service loads recorded range from 8.55 to 12.78 mm. All the recorded deflections satisfy the requirements for the serviceability limit state of the existing codes.

The service load cracks were measured and recorded for all tested slabs, as per the code definitions for the service load. The values of the crack widths measured were in the range of 0.38 to 0.56 mm. These values satisfy the cracking requirements at the service loads recommended by ACI committee 440 (2003). ACI 440.1 R-03 recommendations state that the maximum crack width of GFRP reinforced members could be about 1.5 to 1.7 times the value allowed for steel reinforced members (0.6 - 0.7 mm).

Service load is very sensitive to slab depth, and so increasing slab depth from 150 mm to 200 increased the service load by 50%. The reinforcement ratio had no influence on the service load.

The results indicate that the ductility of the GFPR reinforced slabs is considerably affected by the reinforcement ratio and the slab effective depth. The ductility of slabs in Series 1 decreased by 45% and 63% when the reinforcement ratio was increased by 25 and 50 %, indicating that reinforcement ratio has a strong influence on ductility.

The clear concrete cover has a slight effect on the ductility index. In Series 2, the ductility index increased by 30% and 7% when the clear concrete cover increased from the usual 30 mm cover to 45 mm and 60 mm, respectively. On the other hand, an increase in slab thickness decreased the ductility index by 40% when the slab depth increased from 150 mm to 200 mm.

The energy absorption capacity increased by approximately 14% as the reinforcement ratio was increased by 50%. The energy absorption capacity slightly decreased with increasing of the slab effective depth. Increasing the slabs clear concrete cover inversely influenced the energy absorption capacity. As the slab cover increased by 50%, there was an 18% decrease in this capacity.

GFRP strain was measured and reported from the tested slabs, showing a typical elastic behavior up to the failure; however, the strain variation can be divided into two segments before and after cracking. The maximum strains occurred around the column perimeter.

The recorded maximum strain in the GFRP bars was 7076με in slab specimen 2, Series 1, which had a 1.2% reinforcement ratio and 150 mm slab depth. This value is 44% less than the ultimate tensile strength of GFRP bars, which is approximately 16000με. Based on the reinforcement strain values provided by the manufacturer, there was no rupture of the GFRP bars in any of the test slabs.

The maximum concrete strain recorded on the compression side of all tested slabs has never reached the crushing concrete strain, nor were any signs observed during the experiments indicating that the phenomenon had occurred.

For all GFRP specimens, when the load reached approximately 60% of the ultimate load of the GFRP reinforced slabs, the diagonal cracks reached all four corners and a pattern similar to flexural yield-line patterns clearly formed, especially for the slabs with low reinforcement ratio and high strength concrete. The orthogonal crack formation for all tested slabs followed the reinforcement spacing, thus the rebar spacing considerably affected crack patterns for high strength concrete two-way slabs reinforced with GFRP.

As expected, all tested slabs failed in punching shear, as designed. At failure, there were no signs of reinforcement rapture or concrete crushing.

The use of high strength concrete slab reinforced with GFRP provided good structural performance, providing the use of a high reinforcement ratio that exceeds that used for steel reinforcement.

6.3 Cracking Behavior of Two-way Slabs Reinforced with GFRP:

The cracking behavior was typical in nature for two-way slabs, except that they were wider for slabs reinforced with GFRP. The first crack was formed along the middle third of all tested slabs; the maximum crack width measured in this experimental investigation was 4.12 mm.

The effect of the reinforcement ratio was evident on the cracking width, since increasing the reinforcement ratio resulted in a reduced crack width. The maximum recorded crack width of the entire tested specimen was measured for the specimen with the lowest reinforcement ratio.

The cracking behavior of the tested slabs was typical in nature, since cracking started with the first crack formed at the middle third of the slabs orthogonal cracks appeared first, then the diagonal cracks formed later. When the load reached 60% of the maximum load, the diagonal cracks reached the slabs corners, forming a typical yield line pattern.

The crack width slightly changed with the applied load up to point where no new cracks were formed and the cracked section was stabilized. Then, the applied load was increased and combined with an increasing of the crack width. Increasing the concrete clear cover affected the crack width in such a way that, as the concrete cover is increased, the crack width is also increased.

The GFRP strain was showing a linear increase up to the cracking, and then the change in the GFRP strain was dramatically changed. It is worth mentioning that the distribution of the GFRP strain after cracking was dependent on where the crack was formed.

6.4 Numerical Verifications for Crack Width and Crack Spacing:

A rational model was adopted and modified, accounting for the different mechanical properties of the GFRP to predict the crack width for two-way slabs. A reduction to 40% of the calculated bond strength was incorporated to the original model equation, and thus

the new formula used in this investigation to calculate the crack width at reinforcement level is:

$$w_m = s_m \left[\varepsilon_{sm} - \frac{0.4\tau_b s_m}{\phi_b E_f} - \frac{\lambda}{2} \frac{f_{ct}}{Ec} \right]$$

The model was verified against the results of the current experimental program. The modified model estimated the crack width with excellent agreement with the experiment results.

The adopted model slightly under-estimated the crack width in the case of higher concrete clear covers, because the model was originally developed for members with regular cover.

For crack spacing verification, an expression was adopted and modified to account for the lower bond properties of the GFRP, and the modified equation estimated crack spacing for high strength two-way slabs reinforced with GFRP in good agreement with the experimental results.

The following equation was used to calculate the mean crack spacing in this investigation:

$$s_m = 2(c + 0.1s) + 0.04 d_{be}^{'} h_{ef}\ b/A_f$$

The aforementioned equation was modified from its original format in the following manner:

- A reduction to 40% for the calculated tension zone, assuming a perfect bond condition
- The constants k_1 and k_2 were taken as 0.1

Finite element is powerful tool in numerical analysis that can be used to verify the ultimate load and maximum deformation. The results obtained using the finite elements model include the principle stresses, the ultimate load, and the maximum deflection.

The principle stresses obtained show symmetry in both directions, which is a typical two-slab response. The ultimate load and maximum deflection obtained were used in verification of the experimental results, and the model shows a fairly good agreement with the experimental results.

6.5 Code Limitations and Crack Width Calculations:

The code of practice CSA S806-02 and ISIS 2000 design manual define the limit state serviceability for concrete members reinforced with FRP with strain limit of 2000με , and the experimental results measured for the crack width were within the code limitations.

In conclusion, ISIS 2001 recommendations for crack spacing, crack width, and service load limit are in good agreement with the experimental results obtained in this investigation.

For crack width calculation, the code CSA S806-02 adopts the Gergely-Lutz equation. The code equation slightly over estimated the crack width, and that can be easily explained due to the empirical nature of the equation that the code uses.

6.6 Conclusion:

The research focused on investigating the flexural behavior for high strength two way slabs reinforced with GFRP, with considerable concern for the serviceability limit state. In conclusion, the behavior of high strength two-way slabs reinforced with GFRP was

satisfactory within the serviceability limits and provisions of the existing codes, providing the use of a higher ratio than steel.

A numerical model and related expressions were modified to calculate crack width and crack spacing to account for the lower modulus of elasticity and bond properties for the GFRP rebars. The modified adopted model estimated crack width and crack spacing with excellent agreement with the laboratory results; however, GFRP bars should not be used for concrete members with a high clear concrete cover.

A finite element model was adapted and modified to predict the structural behavior of GFRP two way slabs in terms of the load-deflection relationship. The modified ABAQUS model was very successful in predicting the behavior within a satisfactory limit.

6.7 Recommendation for Future Research:

1. More in depth investigation for the cracking behavior of high strength concrete two-way slabs reinforced with GFRP materials under long term loading (Creep and shrinkage).
2. Research on the behavior of reinforced concrete members reinforced with GFRP as main reinforcement under dynamic loads is essential.

3. More comprehensive studies on the bond relations of GFRP reinforcement and concrete and the dowel action of GFRP in two-way slabs is vital to developing a better understanding of the failure mechanism for such members.

References

1. ACI Committee 224R-01 "Control of Cracking in Concrete Structures" American Concrete Institute, Farmington Hills, Michigan, USA, 2001.

2. ACI Committee 318, "Building Code Requirements for Structural Concrete (ACI 318-89), American Concrete Institute, Farmington Hills, Michigan, USA, 1989.

3. ACI Committee 318, "Building Code Requirements for Structural Concrete (ACI 318-95), American Concrete Institute, Farmington Hills, Michigan, USA, 1995.

4. ACI Committee 440. 1R-03 "Guide for the Design and Construction of Concrete Reinforced with FRP Bars," American Concrete Institute, Farmington Hills, Michigan, USA, 2003, 42p

5. ACI Committee 318, "Building Code Requirements for Structural Concrete (ACI 318-99), American Concrete Institute, Farmington Hills, Michigan, USA, 1999.

6. ACI Committee 224 "Causes, Evaluation, and Repair of Cracks in Concrete Structures" ACI Journal May-June 1984, Report no. 2241.R-84, pp. 211-229

7. Alvarez, M. "Influence of Bond Behavior on the Deformation Capacity of Structural Concrete" Report No. 236, Institute of Structural Engineering, EHT, Zurich, August 1998

8. ASTM C494/C494M-05 "Standard Specification for Chemical Admixtures for Concrete' ASTM International, West Conshohocken, Pa.; 2005

9. Banthia, N., Al-Asaly, M., and Ma, S. "Behavior of Concrete Slabs Reinforced with Fiber-Reinforced Plastic Grid," Journal of Materials in Civil Engineering, ASCE, V. 7, No. 4, 1995, pp. 643-652

10. Beeby, A., W. "A study of Cracking in Reinforced Concrete Members subjected to Pure Tension" Technical Report 42.468, Cement and Concrete Association, London, 1972.

11. Beeby, A., W. "The Prediction of Crack Width in Hardened Concrete" Structural Engineering. 57A, No 1, 1979, pp. 9-17

12. Benmokrane. A., Tighiouart, B., and Chaallal, O. "Bond Strength and Load Distribution of Composite GFRP Reinforcing Bars in Concrete" ACI Materials Journal, V. 93, No. 3, May-June 1996, pp. 246-253

13. British Standards Institution "Structural Use of Concrete, BS8110: Part 1-Code of Practice for Design and Construction, British Standard Institution, London, 1985, 172 pp

14. Broms, B. B. "Crack Width and Crack Spacing in Reinforced Concrete Members" Journal of the American Concrete Institute, Proceedings V. 62, No. 10, Oct. 1965, pp. 1237-1255

15. Chaallal, O., and Benmokrane, B. "Pullout and Bond of Glass Fiber Rods Embedded in Concrete and Concrete Grout" RILEM Materials and Structures Journal, V. 26, No. 157, 1993, pp. 167-175

16. Comité Euro-International Du Béton-Fédération de la Précontrainte (CEB-FIP) (1990) "*CEB-FIP Model Code 1990 (MC-90), Design Code*" Comité Euro-

International Du Béton-Fédération de la Précontrainte (CEB), Thomas Telford Ltd., London, 1993, 437 pp

17. CSA Standards S806-00 "Design and Construction of Building components with Fiber-Reinforced Polymers" Canadian Standard Association, Toronto, Ontario, Canada, 2000, 177 p

18. CSA Standards A23.3-04 "Design of Concrete Structures" Canadian Standard Association, Toronto, Ontario, Canada, 2004, 220 p

19. CSA Standards S474-94 "Concrete Structures, Offshore Structures" Canadian Standard Association, Toronto, Ontario, Canada, 1994

20. CSA Standards S474-04 "Concrete Structures, Offshore Structures" Canadian Standard Association, Toronto, Ontario, Canada, 2004

21. CSA Standards CSA A266.2 "Chemical Admixture for Concrete" Canadian Standard Association, Toronto, Ontario, Canada, 1994

22. CSA A3000-03 "Cementitious Materials Compendium " Canadian Standard Association, Toronto, Ontario, Canada, 2004

23. Clarke, J. L. "Modification of Design Rules to Incorporate Nonferrous Reinforcement," Report No. 1, Sir William Halcrow & Partners Ltd.; 1996

24. Dimitrios, D. Theodorakopoulos, and Narayan Swamy "Analytical Model to Predict Punching Shear Strength of FRP-Reinforced Concrete Flat Slabs" ACI Structural Journal, V.104, No.3, May-June 2007, pp. 257-266

25. Ebead, U., and Marzouk, H. "Fiber-Reinforced Polymer Strengthening of Two-Way Slabs" ACI Structural Journal, V.101, No. 5, September-October 2004, pp. 650-659

26. Ebead, U., and Marzouk, H. "Tension Stiffening Model for Fiber-Reinforced R.C Two-Way Slabs" Materials and Structures, V. 38, No. 2, March 2005, pp. 193-2000

27. Ehsani, M. R, Saadatmanesh, H., and Tao, S. "Design Recommendations for Bond of GFRP Rebars to Concrete" Journal of Structural Engineering, March 1996, pp. 247-254

28. El-Ghandour, A. W., Pilakoutas, K., and Waldron, P. "Punching Shear Behavior of Fiber Reinforced Polymers Reinforced Concrete Flat Slabs: Experimental Study" Journal of Composite for Construction, ASCE, V. 7, No. 3, 2003, pp. 258-265

29. El-Ghandour, A. W., Pilakoutas, K., and Waldron, P. "New approach for the punching shear capacity prediction of FRP RC flat slabs" Proc., 4th Int. Symp. On Fiber Reinforced Polymers Reinforced Concrete Structures, FRPRCS-4, Baltimore, 1999, pp. 135-144

30. El-Ghandour, A. W., Pilakoutas, K., and Waldron, P. "Behavior of FRP flat slabs with CFRP shear reinforcement," Proc. 8th European Conf. on Composite Materials ECCM-8, I. Crivelli Visconti, ed., Naples, Italy, June, Vol. 2, pp. 399-406

31. Frosch, R. J. "Another Look at Cracking and Crack Control in Reinforced Concrete" ACI Structural Journal, V.96, No.3, May-June 1999, pp. 437-442

32. Gergely, P., and Lutz, L. "Maximum Crack Width in Reinforced Concrete Flexural Members" Causes, Mechanism, and Control of Cracking in Concrete, ACI Publication SP-20, 1968, pp. 87-117

33. Gilbert, R. I. "Time-dependent cracking and crack control in reinforced concrete structures", ACI International Special Publication SP225, Serviceability of Concrete, Editor F. Barth, Chapter 15, American Concrete Institute, Detroit, 2005, pp. 223-240

34. Hallgren, M. (1996). "Punching Shear Capacity of Reinforced High Strength Concrete Slabs". Doctoral Thesis, Department of Structural Engineering, Royal Institute of Technology, Stockholm, Sweden, 206pp

35. Hillerborg. A, Modéer, M., and Petersson "Analysis of Crack Formation and Crack Growth in Concrete by Means of Fracture Mechanics and Finite Elements" Cement and Concrete Research. Vol. 6, 1976, pp. 773-782

36. Hussein, A. (1990). "Behavior of Reinforced Concrete Slabs Made with High-Strength Concrete" M. Eng. Thesis, Faculty of Engineering and Applied Science, Memorial University of Newfoundland, St.John's, Newfoundland and Labrador, Canada, August, 145 pp

37. Hibbitt, K., and Sorensen" ABAQUS users manual (version 6.5.1)", Providence, R. I. Hibbitt, Kalrsson and Sorensen Inc, 2003

38. ISIS "Reinforcing Concrete Structures with Fiber Reinforced Polymers, Design Manual, No. 3" The Canadian Network of Center of Excellence on Intelligent Sensing for Innovative Structures, Winnipeg, Manitoba, Canada, 2001.

39. Institute of Building Research of the Japanese Ministry of Construction, BIR (1997). "Design Guideline of FRP Reinforced Concrete Building Structure" Journal of composites for Construction, ASCE, Vol. 1, No. 3, pp. 99-115

40. Japan Society of Civil Engineers, JSCE "Proceedings of the Third International Symposium on Non-Metallic (FRP) Reinforcement for Concrete Structures (FRPRCS-3)" Japan Concrete Institute, Sapporo, Japan, 1997, 1705p

41. Leonhardt, F. "Crack Control in Concrete Structure" IABSE Surveys, S-4/77, IABSE 3/1977, International Association for Bridge and Structural Engineering, Zurich, Switzerland, 1977.

42. Marti, P., Alvarez, M., Kaufmann, W., and Sigrist, V. "Tension Chord Model for Structural Concrete" IABSE 4/98, International Association for Bridge and Structural Engineering, Zurich, Switzerland, 1998, pp. 287-298.

43. Marzouk, H., and Hussein, A. "Experimental Investigation on the Behavior of High-Strength Concrete Slabs" ACI Structural Journal, V. 88, No. 6, November-December 1991, pp. 701-713

44. Marzouk, H. and Chen, Z. W. "Nonlinear Analysis of Normal- and High- Strength Concrete Slabs" CAN. J. CIV.ENG. Vol. 20 ,1993, pp. 696-707

45. Marzouk, H. and Chen, Z. W. "Finite Element Analysis of High-Strength Concrete Slabs" ACI Structural Journal, V, 90, No. 5, September-October 1993.

46. Marzouk, H. and Chen, Z. W. "Fracture Energy and Tension Properties of High-Strength Concrete" Journal of Materials in Civil Engineering, V, 7, No. 2, May, 1995

47. Matthys, S., and Taerwe, L. "Concrete Slabs Reinforced with FRP Grids. a: One-Way Bending," Journal of Composite for Construction, ASCE, V. 4, No. 3, 2000, pp. 145-153

48. Matthys, S., and Taerwe, L. "Concrete Slabs Reinforced with FRP Grids. b: Punching Resistance," Journal of Composite for Construction, ASCE, V. 7, No. 4, 2000, pp. 154-161

49. McGregor, J. G., Rizkalla, S. H., and Simmonds, S. H. "Cracking of Reinforced and Prestressed Concrete Wall Segments" Structural Engineering Report No. 82, University of Alberta, Edmonton, Alberta, Canada, 1980.

50. Nawy, E. G. and Neuwerth, G. E. "Fiber Glass as Main Reinforcement for Two-way Slabs, Plates and Beams" Engineering Research Bulletin No.56 (1976) Rutgers University (The State University of New Jersey)

51. Nawy, E. G., and Blair, K. W. "Further Studies on Flexural Crack Control in Structural Slab Systems. Cracking, Deflection and Ultimate Load of Slab Systems" SP-30, American Concrete Institute, Detroit, Michigan, 1971, pp. 1-42

52. Nawy, E. G. " Fiberglass Reinforced Concrete Slabs and Beams" , Journal of the Structural Division, ASCE, V 103, 1977, pp. 421-440

53. NSF, NS 3473E:1992 "Concrete Structures Design Rules" (Prosjektering av betongkonstruksjoner. Beregnings- og konstruksjonsregler) Norwegian Standards Association (NSF), Oslo, 1992

54. Ospina, C. E.; Alexender, S. D. B.; and Cheng, J. J. R. "Punching of Two-Way Concrete Slabs with Fiber-Reinforced Polymer Reinforcing Bars or Grids" ACI Structural Journal, V. 100, No. 5, Sept.-Oct. 2003, pp. 589-598

55. Ospina, C. E., Alexander, D. B., and Cheng, J. J. R. "Behavior of Concrete Slabs with Fiber-Reinforced Polymer Reinforcement" Structural Engineering Report NO. 242, Department of Civil Environmental Engineering, University of Alberta, Edmonton, Canada, 2001, 355p

56. Phillips, D. V., and Binsheng, Z "Direct tension tests on notched and un-notched plain concrete specimens" Magazine of Concrete Research, 1993, 45, No. 162 Mar., pp. 25-35

57. Rizkalla, S. H., Hwang, L. S., and El Shahawi, M. "Transverse Reinforcement Effect on Cracking Behaviour of R.C Members" CAN. J. ENG. Vol. 10 (1983), pp. 566-581

58. Rashid, M. "Behavior of Slabs Reinforced with GFRP Bars" Master Thesis, Faculty of Engineering, Memorial University of Newfoundland, St. John's, Canada, 2004.

59. Sabrah, T.B., Marzouk, H., and Hussein, A. "Cracking of GFRP-Reinforced Concrete Panels under Direct Tension", 8th International Symposium on Fiber Reinforced Polymer Reinforcement for Concrete Structures, Greece, 2007.

60. Sigrist, V., and Marti, P. "Ductility of Structural Concrete" A contribution Proceedings, Workshop on Development of EN 1992 in Relation to New Research Results and to the CEB-FIP Model Code 1990, Czech Technical University, Prague, 1994, pp. 211-223

61. Tastani, S. P., and Pantazopoulou. S. J. "Experimental Evaluation of the Direct Tension Pullout Bond Test" Bond in Concrete-from research to standards 2002, Budapest.

62. Zhang, Q., Marzouk, H., and Hussein, A. "A Preliminary Study of High Strength Concrete Two-Way Slabs Reinforced with Glass Fiber-Reinforced Polymers" Proceedings of the 33rd Annual CSCE General Conference, Canadian Society for Civil Engineering, June 2-4, 2005, Toronto, Canada.

63. Zhang, Q. "Behavior of Slabs Reinforced with CFRP Bars" Master Thesis, Faculty of Engineering, Memorial University of Newfoundland, St. John's, Canada, 2006.

Appendix A:

Input File for FEM Specimen 2

```
*Heading
 HSC Two-way Slabs Reinforced with GFRP- Specimen 2
** Job name: Specimen-2 Model name: Plate Model
*Preprint, echo=NO, model=NO, history=NO, contact=NO
**
** PARTS
**
*Part, name=Slab
*End Part
**
**
** ASSEMBLY
**
*Assembly, name=Assembly
**
*Instance, name=Part-1-1, part=Slab
*Node
*Element, type=S8R
*Nset, nset=L-X
  5,   6, 27, 28, 29,  30,  61,  63,  65,  88, 200, 203, 208, 210, 222, 224
 225,
*Elset, elset=L-X
  2, 50, 51, 54, 55, 62, 63, 64
*Nset, nset=L-Y
  3,   4,   6, 17, 18, 26,  43,  55,  56,  84,  87, 127, 132, 171, 173, 177
 181,
*Elset, elset=L-Y
  1, 2, 16, 18, 34, 35, 37, 39
*Nset, nset=Part, generate
  1, 225,   1
*Elset, elset=Part, generate
  1, 64,   1
*Nset, nset=_PickedSet7, internal
 16,
*Nset, nset=_PickedSet8, internal
 14,
*Nset, nset=_PickedSet9, internal
```

```
 12,
*Nset, nset=_PickedSet10, internal
 11,
*Nset, nset=_PickedSet11, internal
10,
*Nset, nset=_PickedSet12, internal
 21,
*Nset, nset=_PickedSet13, internal
 20,
*Nset, nset=Center
 6,
** Region: (Slab:Part)
** Section: Slab
*Shell Section, elset=Part, material=Concrete
150., 9
*Rebar Layer
X-X, 1.3, 1., -38., GFRP, 0., 1
Y-Y, 1.3, 1., -38., GFRP, 90., 1
*Element, type=Spring1, elset=Springs/Dashpots-1-spring
65, 16
*Spring, elset=Springs/Dashpots-1-spring
1
100.
*Element, type=Spring1, elset=Springs/Dashpots-2-spring
66, 14
*Spring, elset=Springs/Dashpots-2-spring
1
100.
*Element, type=Spring1, elset=Springs/Dashpots-3-spring
67, 12
*Spring, elset=Springs/Dashpots-3-spring
1
110.
*Element, type=Spring1, elset=Springs/Dashpots-4-spring
68, 11
*Spring, elset=Springs/Dashpots-4-spring
1
120.
*Element, type=Spring1, elset=Springs/Dashpots-5-spring
69, 10
*Spring, elset=Springs/Dashpots-5-spring
1
110.
*Element, type=Spring1, elset=Springs/Dashpots-6-spring
70, 21
```

```
*Spring, elset=Springs/Dashpots-6-spring
1
100.
*Element, type=Spring1, elset=Springs/Dashpots-7-spring
71, 20
*Spring, elset=Springs/Dashpots-7-spring
1
100.
*End Instance
**
*Nset, nset=Slab, instance=Part-1-1, generate
  1,  225,    1
*Elset, elset=Slab, instance=Part-1-1, generate
  1,  64,   1
*Nset, nset=_PickedSet20, internal, instance=Part-1-1
 18,
*Nset, nset=_PickedSet21, internal, instance=Part-1-1
 30,
*Nset, nset=Center, instance=Part-1-1
 6,
*Nset, nset="Loading Area", instance=Part-1-1
  1,  4,  5,  6, 85, 86, 87, 88
*Elset, elset="Loading Area", instance=Part-1-1
 2,
*End Assembly
**
** MATERIALS
**
*Material, name=Concrete
*Concrete
28.,      0.
37., 0.00025
45.,  0.0005
52., 0.00075
58.,   0.001
*Failure Ratios
 1.16, 0.04,   0.,   0.
*Tension Stiffening
1.,    0.
0., 0.004
*Elastic
35000., 0.15
*Material, name=GFRP
*Elastic
40800., 0.2
```

```
**
** INTERACTION PROPERTIES
**
*Surface Interaction, name=IntProp-1
1.,
*Surface Behavior, augmented Lagrange
**
** BOUNDARY CONDITIONS
**
** Name: BC-1 Type: Displacement/Rotation
*Boundary
_PickedSet20, 3, 3
** Name: BC-2 Type: Displacement/Rotation
*Boundary
_PickedSet21, 3, 3
** Name: BC-3 Type: Symmetry/Antisymmetry/Encastre
*Boundary
Part-1-1.L-X, YSYMM
** Name: BC-4 Type: Symmetry/Antisymmetry/Encastre
*Boundary
Part-1-1.L-Y, XSYMM
** ----------------------------------------------------------------
**
** STEP: Apply Load
**
*Step, name="Apply Load", nlgeom=YES
Apply Concentrated Central Load
*Static, riks
0.01, 1., 1e-05, , 1., Center, 3, 50.
**
** LOADS
**
** Name: Concentrated Central Load   Type: Concentrated force
*Cload
Center, 3, -85000.
**
** OUTPUT REQUESTS
**
*Restart, write, frequency=0
*Monitor, dof=3, node=Center, frequency=1
**
** FIELD OUTPUT: F-Output-1
**
*Output, field
*Node Output
```

```
CF, RF, U
*Element Output, directions=YES
E, S
*Contact Output
CDISP, CSTRESS
**
** FIELD OUTPUT: F-Output-2
**
*Node Output, nset=Center
U, UR, UT
**
** HISTORY OUTPUT: H-Output-2
**
*Output, history
*Node Output, nset=Center
CF3, U1, U2, U3
**
** HISTORY OUTPUT: H-Output-1
**
*Output, history, variable=PRESELECT
*End Step
```

Appendix B:

Punching shear capacity

The punching shear capacity of two-way slabs is calculated form the following expression:

$V_u = V_c + V_d$

where,

1. $Vc = V_{cc}\cos\theta$

V_d is the dowel contribution to the shear capacity which is ignored in this study.

$$V_{cc} = 4(X\cot\theta + D)\frac{X}{\sin\theta}f_r$$

2. $f_r = 0.6\sqrt{f_c'}$

3. $V_c = 4b_o X\cot\theta f_r$

where, b_o is the critical perimeter for punching shear = $4(\lambda d + D)$

$\lambda = 1.0$ for square columns

4. $$X = \frac{2X_s X_f}{X_s + X_f}$$

5. $$X_s = X_f = \frac{1.5\varepsilon_{cu}}{\varepsilon_{cu} + \varepsilon_{fu}}d$$

Thus,

6. $V_c = 4(d + D)X\cot\theta f_r$

Substitute

$f_c' = 64$ Mpa

$\theta = 29°$

D = 250 mm

d = 112 mm

Calculate f_r from equation-2

$f_r = 4.8$ Mpa

$X_s = X_f = 27.35$ mm

X = 27.35 mm

Finally,

$$Vc = 4(112 + 250) \times 27.35 \times \cot 30 \times 4.8 = 329 \text{ kN}$$

Flexural capacity

The flexural moment capacity of two-way slab can be calculated using yield line theory, originally developed for two-way slabs reinforced with traditional steel, however the principles were used here as follow:

1. $P_{flex} = 8M_b\left(\frac{s}{a-c} - 0.172\right)$

Where M_b is the radial moment capacity of slabs, s is the side dimension, and a is the side dimension between supports of slabs.

M_b for slabs reinforced with FRP is calculated as follow:

2. $M_b = bd^2\rho E_f \varepsilon_f\left(1 - \frac{0.5\beta X}{d}\right)$

3. $X = \left[-\varepsilon_{cu} + \left[\varepsilon_{cu}^2 + \frac{4\alpha\beta f_c'}{E_f\rho}\varepsilon_{cu}\right]^2\right]\frac{E_f d\rho}{\alpha\beta f_c'}$

4. $\varepsilon_f = \frac{d-X}{X}\varepsilon_{cu}$

Substitute

$\varepsilon_{cu} = 0.0035$

d= 112 mm

$f_c' = 64$ Mpa

$\alpha = 0.85 - 0.0015f_c' \geq 0.67$

$\alpha = 0.754$

$\beta = 0.97 - 0.0025f_c' \geq 0.67$

$\beta = 0.81$

$E_f = 40800$ Mpa

$\rho = 1.5\%$

Thus

$$X = \left[-0.0035 + \left(0.0035^2 + \frac{4 \times 0.754 \times 0.81 \times 64}{40800 \times 0.015} \times 0.0035 \right)^{1/2} \right] \times \frac{40800 \times 112 \times 0.015}{0.81 \times 0.754 \times 64}$$

X= 46.66 mm.

$$\varepsilon_f = \frac{112 - 46.66}{46.66} \times 0.0035 = 4.9 \times 10^{-3}$$

$$M_b = 1900 \times 112^2 \times 0.015 \times 40800 \times 0.0049 \left[1 - \frac{0.5 \times 0.81 \times 46.66}{112} \right]$$

$$M_b = 59.4 \text{ kN.m}$$

$$P_{flex} = 8 \times 59.4 \left[\frac{1900}{1840 - 250} - 0.172 \right]$$

$$P_{flex} = 486.115 \text{ kN.}$$

Comparing the above results with experiment 3 results

Failure Load = 384 kN

P(theoretical)/P(experiment) = 0.86